Dissipative Wave Propagation in Phononic Crystals and Metamaterials: Models and Analysis

by

Michael J. Frazier

B. S., Embry-Riddle Aeronautical University, 2009

M. S., University of Colorado, 2011

A thesis submitted to the

Faculty of the Graduate School of the

University of Colorado in partial fulfillment

of the requirements for the degree of

Doctor of Philosophy

Department of Aerospace Engineering Sciences

2015

This thesis entitled:
Dissipative Wave Propagation in Phononic Crystals and Metamaterials: Models and Analysis
written by Michael J. Frazier
has been approved for the Department of Aerospace Engineering Sciences

Professor Mahmoud I. Hussein

Professor Carlos A. Felippa

Professor Dale A. Lawrence

Professor Kurt Maute

Professor Todd W. Murray

Date

The final copy of this thesis has been examined by the signatories, and we find that both the content and the form meet acceptable presentation standards of scholarly work in the above mentioned discipline.

Frazier, Michael J. (Ph.D., Aerospace Engineering Sciences)

Dissipative Wave Propagation in Phononic Crystals and Metamaterials: Models and Analysis

Thesis directed by Professor Mahmoud I. Hussein

Through deliberate material and geometrical design of the internal structure, phononic crystals and metamaterials, collectively, phononic materials, elicit fundamental wave phenomena pertaining to acoustic/elastic systems. This unique ability among classical materials and composites has immediate engineering applications including vibration control in structures. Moreover, ongoing research has been directed toward technological improvements in communications, energy harvesting, and acoustic imaging as well as the proposal of new devices for acoustic cloaking, nondestructive super-resolution imaging, and even flow control. Periodicity, emerging from the spatial repetition of a representative structural element, the unit cell, is a characteristic feature of phononic materials and makes them accessible to Bloch's theorem for dynamic analysis. This analysis is central to predicting phononic material performance which inspires the previously stated applications. However, energy dissipation stemming from the damping mechanisms inherent to all materials is absent from much of the theoretical literature. This omission adversely affects the prediction of phononic material performance and foregoes damping as a potential design parameter/objective. In support of improved performance predictability and strategic material design with damping, this dissertation extends the analysis techniques originally developed in the context of dissipative vibration in damped structures to dissipative wave propagation in damped phononic materials.

The frequency band diagram summarizes much of the dynamic performance of phononic materials and, ultimately, phononic devices, visually separating propagating and non-propagating wave modes into distinct frequency regions denoted pass bands and band gaps, respectively. Accounting for the practical effects of energy dissipation on the acoustic/elastic waves improves the predictive capability of the band diagram and is one of the main thrusts of this dissertation. Both the material and excitation environment are considered. Viscous and viscoelastic type damping,

respectively, represent dissipation consistent with motion involving a fluid and the time-dependent behavior of polymers and metals. The dissertation shows the changes that occur in the band diagram, especially the size of the band-gap region, as the damping is tuned continuously from one damping type to another. Regarding the excitation environment, phononic structures may be subject to impact and harmonic loading. The dissertation investigates the distinctive response of free and prescribed waves to energy dissipation, with implications for phononic structures subject to impact and harmonic loading, respectively. Free waves dissipate energy over time while prescribed waves dissipate energy over the extent of phononic material/structure producing radically differing band diagrams for the same phononic material.

For cloaking and super-resolution imaging devices, performance is further linked to the properties of the underlying phononic material. No natural material or composite exhibits the negative density/modulus or anisotropic density required for their operation. However, over a narrow range of wave frequencies, these extraordinary properties emerge dynamically in phononic materials due to relative motion among the internal structure. This dissertation advances the discussion of phononic material performance by examining the changes undergone by the dynamic effective properties due to energy dissipation. In addition to the conventional dynamic effective density and modulus, a dynamic effective viscous damping constant is presented and provides a means of measuring damping beyond the low-frequency regime of the viscoelastic correspondence principle.

As an additional focus, this dissertation also considers damping as an objective of phononic material design. The results of the previous studies, in particular, that on free wave propagation in damped phononic materials, opened the door to design proposal for enhanced dissipation. The dissertation examines the effect of phononic material configuration on the overall material damping capacity, demonstrating the emergence of enhanced dissipation in phononic materials featuring localized resonating bodies as compared to those without. Such behavior, which in our work has been referred to as “metadamping”, provides a new strategy for the design of material systems that exhibit high levels of dissipation without sacrificing load-bearing capacity (stiffness) which is a feat beyond most traditional materials and composites.

Acknowledgements

I am grateful for the guidance provided by my research advisor, Prof. Mahmoud Hussein, for the interest and dedication he displayed to my advancement from student to scientist. I must also thank my colleagues in the Phononics Laboratory for providing both a congenial and scientifically stimulating atmosphere. I would especially like to thank Bruce L. Davis and Liao Liu, who welcomed me into the Laboratory, and Osama R. Bilal, who joined me on the graduate journey and accompanied me until its completion.

In addition, the financial support of the AGEP, GAANN, and NSF Graduate Research Fellowships for the duration of my graduate studies benefited the completion of the research contained within this dissertation.

Finally, to my parents, Clyde and Myra, who emphasized education and nurtured my interest in science from its earliest stages, and to the rest of my family who showed everlasting support, thank you.

Contents

Chapter

Tables

Table

Figures

Figure

Chapter 1

Introduction

1.1 Phononic Materials

The problem of vibration control is of central importance in many areas of civil, mechanical, and aerospace engineering. Seismic loading on buildings, noise from reciprocating machines, activation-induced oscillations in deployable space structures are a few examples. Often, vibration is undesirable for its adverse effects on the performance and integrity of a structural component or assembly. In the form of noise pollution, it may also be a source of personal discomfort. To address this problem, two solutions from structural dynamics are: (1) alter the frequency/intensity of the excitation source; (2) mitigate the effects of the excitation with the aid of external vibration absorbers or energy dissipating materials. However, if dynamic loading is inherent to the environment or the operation of the system, then the first option is nullified. The second option requires the modification of original designs with statically inessential components which, particular to energy dissipating materials, may diminish the overall load-bearing capacity. These provisional changes typically incur additional development costs. A third option that voids the limitations and drawbacks of the previous approaches is to internalize the function of vibration control and make it an inherent feature of the structure. However, advanced composites which, compared to their classical counterparts, may provide superior thermal, corrosion, toughness, and other attributes do not typically possess a vibration control capability beyond their constituents.

Phononic materials distinguish themselves from among classical materials and composites by the unique ability to manipulate acoustic/elastic vibrational waves. This is accomplished by

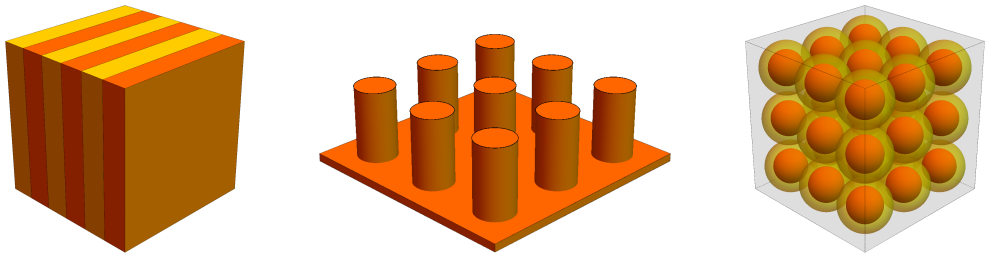

(a) 1D (b) 2D (c) 3D

Figure 1.1: Representative phononic materials with periodicity in multiple dimensions. The colors distinguish the homogeneous constituents of a composite.

deliberately structuring and arranging the material phases and/or geometry to take advantage of fundamental wave-material interactions, including interference and resonance. Due to these interactions, a phononic material is transparent to vibrational waves only over certain frequency bands, and becomes opaque in the intervening *band gaps* where wave propagation is forbidden. Figure 1.1 depicts examples of a phononic material in one, two, and three dimensions where a common feature is a material (Figs. 1.1a and 1.1c) or geometrical (Fig. 1.1b) periodicity described by a *unit cell*, the fundamental repeating element. Periodicity in addition to material makeup characterize the phononic material dynamics. Structures incorporating phononic materials are inherently capable of regulating vibration without the negative consequences of the aforementioned remedies.

As detailed later in the chapter, phononic materials are not restricted to vibration control applications. A theoretical understanding of the mechanics of wave propagation in phononic materials has led to many articles proposing improvements to current technologies – even overcoming previously accepted limits – and introducing new ones. However, the value of theoretical work lies in its predictive capability for which accounting for more of the relevant variables is beneficial. From a fundamental mechanics perspective, there is little consideration in the literature for material damping or the energy dissipation it engenders in vibrational waves. This situation is in contrast to the large structural dynamics literature aimed at developing phenomenological models of the different damping mechanisms for use in structural analysis. This dissertation extends the

models and analysis techniques originally developed in the context of damped vibration in finite structures to dissipative wave propagation in phononic materials. The overarching goals are not only to illuminate the effects of material damping on the wave propagation characteristics (thus, qualitatively reflecting observation and extending predictability), but also to explore damping in phononic material design. From an analytical perspective, material models may be lumped, continuous, or a combination of the two. In addition, there are a variety of damping models in concert with the complexity of dissipative mechanisms. In this dissertation, material models are largely lumped (or discretized), leading to ordinary differential equations of motion. The focus is on two linear damping models: viscous and viscoelastic (described in later chapters).

This chapter explains the theory underpinning the dynamic analysis of phononic materials, and then discusses typical results using a one-dimensional material model. Additional phononic material classifications are also scrutinized. Following a non-exhaustive literature review for orientation, the chapter closes with an overview of the remainder of the dissertation.

1.2 Unit Cell Analysis and the Dispersion Band Diagram

Phononic materials inherit their name from solid-state physics where, at the nanoscale, phonons, the quantized vibrations of a crystal lattice, influence the transfer of heat within solids [1]. In quantum mechanics, the time evolution of a cyrstal state follows the Schrödinger equation, a partial differential equation (PDE) with periodic coefficients and whose solutions are wave functions given by the one-dimensional Floquet theory [2] or three-dimensional Bloch theory [3]. The purview of this dissertation, however, is at larger scales where the unit cell comprises an artificial lattice and vibrational waves are associated with the propagation of elastic/acoustic (sound) waves. In one dimension, the relevant equation of motion is

$$\frac{\partial}{\partial x}\left[E(x)\frac{\partial u}{\partial x}\right] = \rho(x)\ddot{u}, \tag{1.1}$$

where u is the displacement from equilibrium, and the density $\rho(x)$ and Young's modulus $E(x)$ are functions reflecting the periodic quality of the phononic material. Apparently, the equation of

motion possesses the same mathematical properties as the Schrödinger equation, thus permitting the extension of Bloch theorem to vibrational waves in periodic media [4]. In this context, the one-dimensional Bloch solution is given by

$$u(x, \kappa, t) = \tilde{u}(x)\mathrm{e}^{\mathrm{i}\kappa x + \lambda t} \tag{1.2}$$

where the wave envelope is described by a wave number $\kappa = 2\pi/\ell$ (ℓ: the wavelength), characterizing the spatial frequency, and temporal parameter $\lambda = \mathrm{i}\omega$, with $\omega = 2\pi/T$ (T: the period), characterizing the temporal frequency. Although x is defined over the full space $-\infty < x < \infty$, following the periodicity of the medium as expressed by the lattice constant a, the amplitude function $\tilde{u}(x)$ is periodic on $x \in [0, a]$. As a consequence, the following relation holds

$$u(x + a, \kappa, t) = u(x, \kappa, t)\mathrm{e}^{\mathrm{i}\kappa a}, \tag{1.3}$$

and declares that the analysis of a *single* periodic element – the unit cell – yields the solution for all x. These conclusions generally apply to two- and three-dimensional problems.

Together, the Bloch solution and equation of motion formulate an eigenvalue problem with eigenfunctions $u(x, \kappa)$ corresponding to eigenvalues $\lambda(\kappa)$ (or $\kappa(\lambda)$ depending on the method). The eigenvalues constitute the *dispersion relations* which describe much of the nature of wave propagation in phononic materials including the speed of sound, the velocity of a wave packet, the energy velocity in the absence of dissipation, and, crucial to the problem of vibration control, the location of band gaps described in Sec. 1.1. For a one-dimensional phononic material similar to Fig. 1.1a, Fig. 1.2 provides a graphical illustration of the dispersion relations referred to as a *band diagram*.

In this case, the dispersion relation follows the $\kappa(\lambda)$-formulation, which yields a complex wavenumber $\kappa = \kappa_\mathrm{R} + \mathrm{i}\kappa_\mathrm{I}$ for a given frequency. To display both the real and imaginary components, Fig. 1.2 divides the κa-axis into right and left half-panes, respectively. While the value of κ_I is theoretically unbounded, the present $\kappa(\lambda)$-formulation limits $\kappa_\mathrm{R} \in [0, \pi/a]$ which, for one-dimensional problems, is the *irreducible Brillouin zone* [5]. The physical implications of a complex wavenumber are revealed through Eq. (1.2) where κ_R corresponds to the wave's characteristic

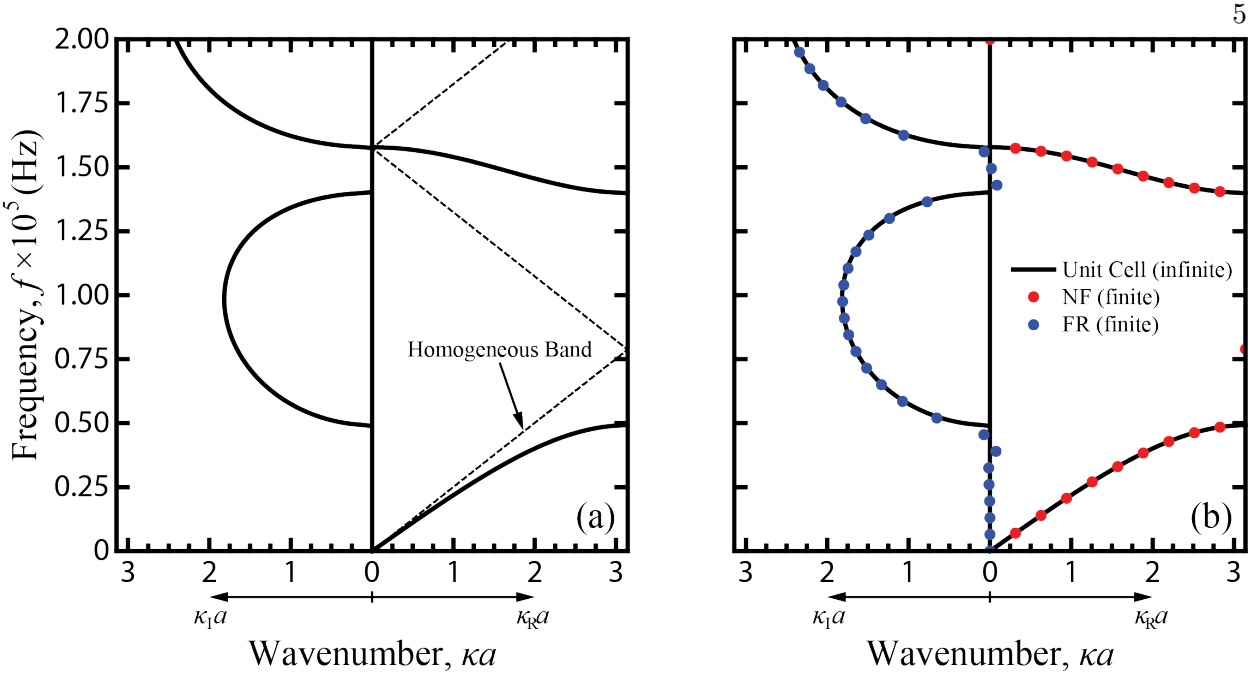

Figure 1.2: Dispersion band diagram for a one-dimensional, layered phononic material by unit cell analysis. (a) Superimposed is the frequency-wavenumber relationship of a homogeneous material with the volume-averaged properties of the phononic material. (b) Overlaid are the results derived from the natural frequency (NF) analysis and frequency response (FR) of a finite structure.

oscillations over space and κ_{I} describes the exponential decay of the wave amplitude. For the case of $\kappa_{\mathrm{R}} = 0, \pi/a$, the wave nodes are stationary, signifying a standing wave. Each of these scenarios is illustrated in Fig. 1.3 where the displacement profiles associated with three, nearly-equal frequencies in Fig. 1.2 are plotted at two instances in time. Figure 1.3a shows the displacement profile of the *propagating mode* at $f = 0.491 \times 10^5$Hz. The wave propagates through the phononic material such that a phase difference develops between the profiles at any two instances in time provided that the duration is not a whole-number multiple of the period, T. Figure 1.3b shows the displacement profile of the *evanescent mode* at $f = 0.492 \times 10^5$Hz, within the band gap. In addition to the spatial decay of wave amplitude corresponding to $\kappa_{\mathrm{I}} > 0$, the wave nodes remain stationary for all time following $\kappa_{\mathrm{R}} = \pi/a$. The special case of $(\kappa_{\mathrm{R}}, \kappa_{\mathrm{I}}) = (\pi/a, 0)$ occurs between $f = 0.491 \times 10^5$Hz and $f = 0.492 \times 10^5$Hz, and, as shown in Fig. 1.3c, results in neither wave propagation nor spatial decay in amplitude.

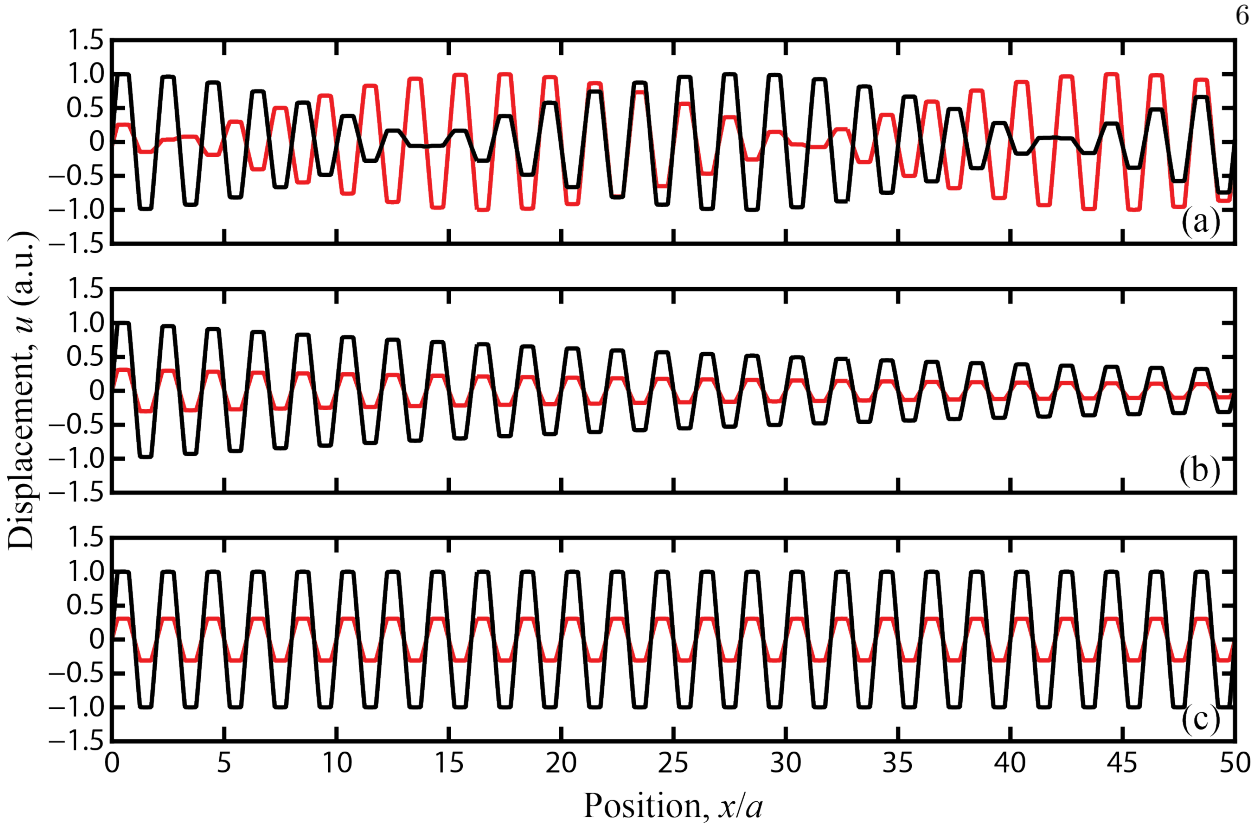

Figure 1.3: Displacement profiles of select modes of a one-dimensional phononic crystal with the dispersion given in Fig. 1.2. Snapshots taken at $t = 0$ (black curve) and $t = T/5$ (red curve). (a) Propagating mode at $f = 0.491 \times 10^5$Hz. (b) Evanescent mode at $f \approx 0.492 \times 10^5$Hz. (c) Special case of a standing, non-decaying mode $[(\kappa_{\mathrm{R}}, \kappa_{\mathrm{I}}) = (\pi/a, 0)]$ at $f \approx 0.491957568 \times 10^5$Hz.

In Fig. 1.2, it is apparent that the dispersion consists of distinct frequency regions for which κ is either real-valued or complex. Accordingly, in the κ_{R}-pane, the associated frequency bands describe vibrational waves capable of propagating through the phononic material similar to light through glass. However, in the band gaps, a complex wavenumber reflects an interference phenomenon that renders the phononic material opaque within these frequency regions. With proper engineering of the phononic material substructure, band gaps may be tuned in number, size, and location within the band diagram, demonstrating the potential and flexibility of native vibration control though phononic materials.

As illustrated in Fig. 1.2a, a homogeneous material is non-dispersive (i.e., ω is linearly proportional to κ with the speed of sound the constant of proportionality) and band gaps do not

exist. As $\kappa \to 0$, the lowest frequency band in the propagating pane also linearizes. Here, the wavelength is large in comparison to the phononic material substructure and experiences only the averaged properties, effectively homogenizing the material. In the long wavelength limit, the bands of the phononic material and its volume-averaged homogeneous counterpart coincide.

In this dissertation, a *material* is defined over the full space characterizing its periodicity. For example, the periodicity of Fig. 1.1a extends infinitely in the direction normal to its layering. Consequently, the dispersion is continuous, representing an infinite number of propagation modes. In contrast, a *structure* is finite in extent and, thus, possesses a limited set of vibration modes. Given that any implementation of a phononic design would necessarily be a finite structure, a connection between unit cell analysis and structural performance need be established [6, 7]. Figure 1.2b shows the same dispersion as in Fig. 1.2a overlaid with the results obtained from two typical structural analyses on a corresponding finite structure of ten unit cells. In the κ_{R}-pane, the discrete natural frequencies and wavenumbers of the free-free phononic structure show good agreement with the band structure which suggests a kinship. Increasing the number of unit cells in the structure will lead to more complete coverage. The response in the band gap is that of the unit cell alone. In the κ_{I}-pane, the spatial logarithmic decrement obtained from the frequency response of the phononic structure closely aligns with the band structure. Together, the natural frequencies and frequency response of the phononic structure solidify the relationship between the material analysis and the structure response. This is also verified through time simulations. Nevertheless, in obtaining a continuous dispersion from a unit cell analysis, the material perspective is the most comprehensive and efficient option.

1.3 Phononic Crystals and Metamaterials

As mentioned in Sec. 1.1, interference and resonance are the two mechanisms by which phononic materials exert control over vibrational wave propagation. These wave-material interactions also serve as a means of categorizing phononic materials into two subgroups: *phononic crystals* and *metamaterials*.

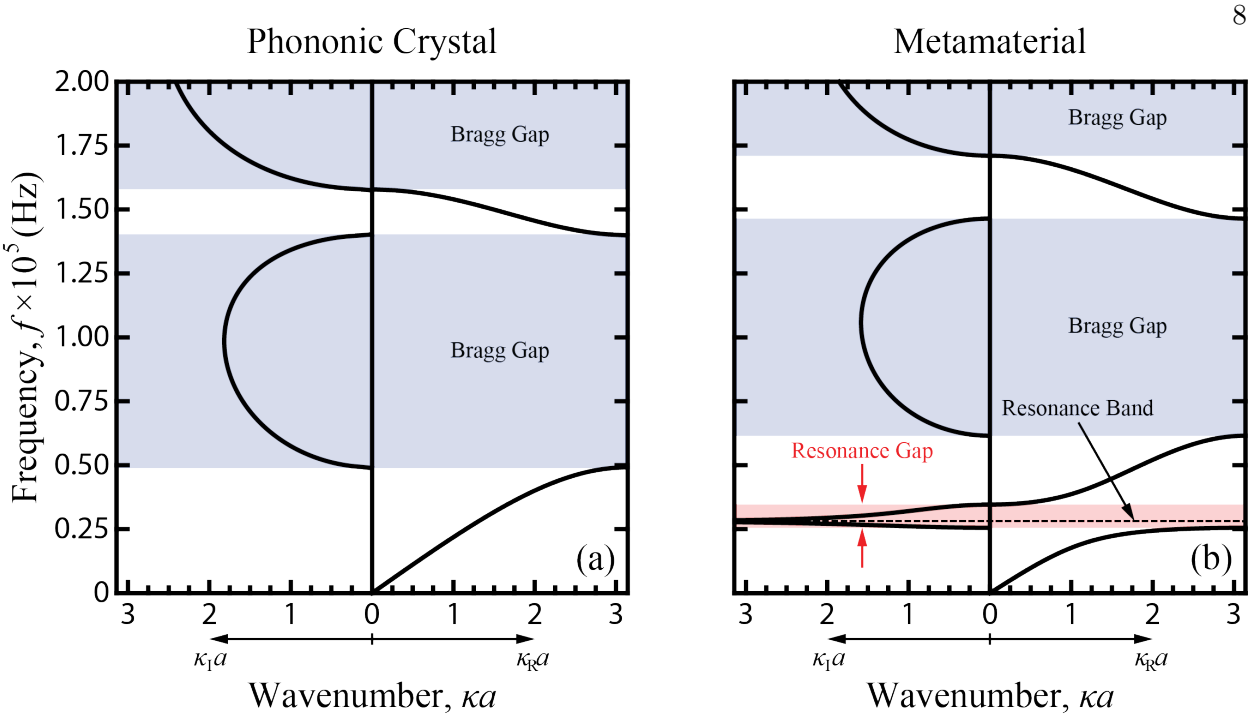

Figure 1.4: Dispersion band diagrams for a one-dimensional (a) phononic crystal with band gaps induced by Bragg scattering and (b) metamaterial featuring a resonance-induced gap before those of Bragg scattering.

Bragg scattering describes a process by which a light wave, upon passing through a crystal, is partially reflected at every plane of atoms. Depending on the spacing between planes, the reflected components may interfere with each other and the incident wave, forbidding wave propagation through the crystal. Similarly, the artificial atoms of phononic crystals (i.e., the material/geometrical constituents) interact with vibrational waves. In this context, the band gaps in the band diagram of a conventional phononic crystal are the result of the Bragg scattering effect. Figure 1.4a shows the same dispersion diagram as in Fig. 1.2 with the Bragg band gap frequency regions lightly shaded. A typical feature of Bragg band gaps is the *smooth* variation in κ_I over the relevant frequency range. Due to the dependency on constituent spacing, the size of phononic crystals with a band gap for low-frequency applications (i.e., at long wavelengths) may become impractically large.

Bragg scattering and interference effects also exist within metamaterials, leading to band

gaps in the dispersion band diagram. However, for metamaterials, the lowest gap is typically not the result of Bragg scattering, rather the result of a *local resonance* phenomenon [8]. Below the length scale of the background wavelength (i.e., subwavelength), the metamaterial possesses a resonating structure tuned to the background frequency. Consequently, a large fraction of the wave energy is transfered from the background and localized within the resonator. This coupling (or hybridization) opens a band gap before Bragg effects have the same result [9]. In Fig. 1.4b, a subwavelength resonator produces a resonance band that hybridizes with the lowest frequency band in Fig. 1.4a, splitting it in two with an intervening resonance gap. A typical feature of resonance gaps is the *piecewise-smooth* variation in κ_{I} over the relevant frequency range [10]. Also typical is the rapid plateauing of the lowest frequency band, representing the increasing mode localization. Unlike Bragg scattering, the resonance phenomenon does not depend on periodicity or constituent spacing (provided the resonators are not so close as to couple to each other). Thus, for low-frequency applications, metamaterial-based devices will have a smaller spatial profile than those of phononic crystals.

1.4 Advanced Applications

Composites, often modeled as periodic materials, have found widespread application in engineering. Motivated by the desire to know the frequency-dependent displacement and stress profiles in layered composites, early studies [4, 11, 12] exploited periodicity to apply Bloch theorem and simplify the analysis. Gupta [6] connected the natural frequencies stemming from the analysis of a periodic structure to the wave propagation characteristics obtained from the simpler unit cell analysis (as demonstrated in the previous section). Thus, the unit cell analysis may extend from periodic materials to the dynamic characterization of multi-storey buildings, aircraft fuselages, and other engineering structures possessing periodicity [13]. Tassilly [14], studying bending wave propagation in material periodic beams, proposed constructing periodic railway ties to take advantage of phononic band gaps for sound abatement. Indeed, as remarked throughout this chapter, the inherent vibration control capability of phononic materials has many engineering applications. However,

the utility of phononic materials extends beyond vibration isolation in structures to more advanced applications.

Phononic crystal waveguides are constructed by replacing the constituents along a path in the phononic structure with an alternate material. Appropriately designed, this defect creates a narrow band of propagating frequencies within the broad band gap of the underlying phononic crystal. The effect is that only waves within the defect band are able to propagate through the guide while the surrounding phononic material serves as a barrier. For waves outside the defect band, interference at the entrance to the waveguide acts as a "acoustic dam" to prevent propagation as if the waveguide were absent. Alone, the waveguide is a simple filter. Combining two such defects, Pennec *et al* [15] simulated the multiplexing/demultiplexing capabilities of a Y-shaped waveguide with each defect band tuned to a different frequency. Scaled to the relevant dimensions, the lower insertion loss (decrease in signal power from embedded device) of phononic filters compared to electric ones opens phononic crystals to signal processing and RF communications applications [16]. In addition, where current acoustic imaging methods balance resolution and penetration depth, waveguides allow for the decoupling of the transmitting/receiving element and the aperture size of an acoustic imaging device for deep high-resolution imaging in nondestructive testing [17]. Apart from waveguides, acoustic diodes for unidirectional wave propagation with communications and medical applications have also attracted the attention of researchers [18–20]. In addition, using phononic crystals, convex lenses for the focusing of sound has also been experimentally demonstrated [21]. Interestingly, Cervera *et al* [21] attributed the refractive capability of the acoustic lens to the increased effective density of phononic crystal due to the relative motion of the constituents. Remarkably, Yang *et al* [22] and Sukhovich *et al* [23] focused ultrasound using phononic lenses lacking any curvature (i.e., flat) utilizing an effective negative refraction property (not available from classical materials) predicted by attributes of the corresponding band diagram. However, material damping impacted the image quality. In each of these instances, an *effective* (i.e., global) material property emerges from local wave-material interactions.

The prefix "meta-" (meaning "beyond") is associated with materials that, through deliber-

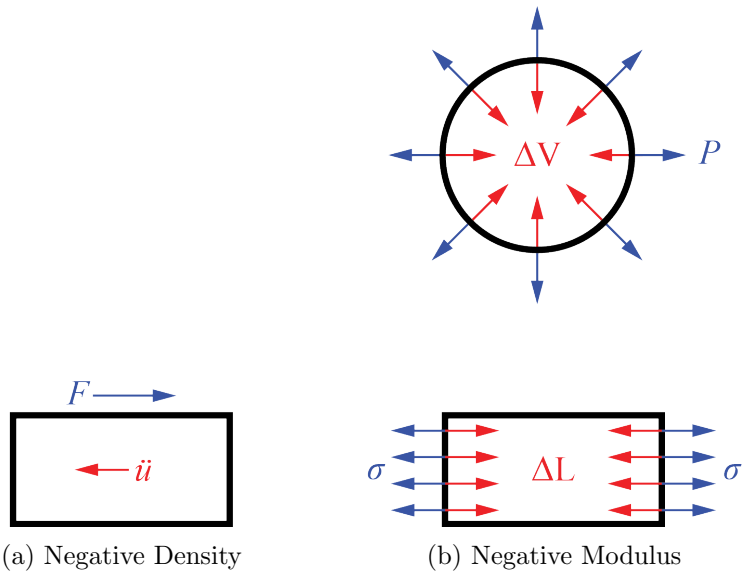

(a) Negative Density (b) Negative Modulus

Figure 1.5: Scenarios for which negative effective density and modulus emerge.

ate design of their internal structure, manifest unusual properties that exist beyond conventional materials and phononic crystals. From a dynamics perspective, the effective mass density and modulus become frequency-dependent and separately [24–27] or simultaneously [28–31] negative in the vicinity of the resonance frequency. Dipolar and monopolar responses from the subwavelength resonators are the underlying mechanisms of negative effective density and modulus, respectively. Negative density implies that the acceleration is out of phase with the pressure/stress gradient [32]. Negative modulus suggests that the deformation is out of phase with the pressure/stress (see Fig. 1.5). Metamaterials hold the same potential as phononic crystals; however, in extending the range of material properties, they promise more extraordinary applications. For conventional imaging systems, diffraction places a physical limitation on the achievable resolution such that features smaller than one-half the probing wavelength are indistinguishable. This condition is due to the evanescent nature of the waves emerging from the fine features, which decay before being detected. Ambati *et al* [33] showed that metamaterial resonances could be used to enhance the evanescent waves associated with the subwavelength features of an imaged object, thus providing an avenue for acoustic super-resolution from metamaterial lenses. Nevertheless material damping remains a

practical limitation. A "hyperlens" for simultaneous super-resolution and magnification has also been reported [34]. In this case, the effective density and modulus of the metamaterial are not only negative, but strongly anisotropic as well. This anisotropy is also a requisite of cylindrical [35, 36] and spherical [37] acoustic cloaks for effective sound shielding. In the absence of losses to create an "acoustic shadow", the cloak bends an impinging plane-wave pressure field around an object embedded at its center to remerge undistorted on the leeward side. The concept has also been extended to elastic waves [38–40]. Recently, mechanical metamaterials, which exploit substructure instabilities (such as buckling) and connectivity, have been introduced. Using an externally applied load, Wang *et al* [41] harnessed instability within substructural beams to manipulate the metamaterial band gaps, demonstrating instability as a means of adapting wave propagation characteristics for smart systems. Nadkarni *et al* [42] used a periodic system of bi-stable (i.e., possessing a snap-through instability) elements to construct a single material with three wave propagation regimes activated by the wave amplitude: linear (elastic wave); nonlinear (envelope soliton); and strongly nonlinear (kink soliton). Ordinarily, instabilities are avoided, however, these illustrate the expanded functionality and dynamic characteristics of structured materials with intentionally implanted instabilities.

1.5 Damping in Phononic Structures and Materials

Phononic materials [43–45] are the acoustic/elastic analogue of photonic materials [engineered to manipulate electromagnetic (EM) waves] which preceded by a few years [46, 47]. As a scientific offspring, much of the applied research in phononic materials parallels developments in the photonic materials literature. However, the richer physics offered by acoustic and elastic waves, including both longitudinal and transverse polarizations (only transverse for EM waves), and the greater number and range of material tuning parameters, including density and two independent moduli (only two parameters for EM waves), present a greater potential for phononic materials. At present, much of the phenomena of wave propagation in phononic materials, from dispersion to dynamic effective properties, is understood from the perspective of linear elasticity. This comprehension grants a level of predictability of phononic material performance which is appreciated in ensuing

applied research. Realizing the full potential of phononic materials, however, requires an account of energy dissipation from material damping. This will provide an elevated level of predictability. It will also show material damping as a potential design parameter for tuning phononic materials and opening phononic materials to new applications. The treatment of damping in phononic materials clarifies the wave propagation phenomenon at a fundamental level, and thus, represents a significant contribution to the field. What follows is a review of studies in the literature regarding dissipative wave propagation in phononic materials.

In one of the early studies to consider dissipative wave propagation in phononic materials, Mead [48] examined the effect of viscous and hysteretic damping on the wavenumber for waves propagating in a one-dimensional, periodically supported beam. Given any real-valued frequency, the associated wavenumber is complex; damping enforces the decay of the wave amplitude from one unit cell to the next. This result explains the localization of wave energy near the source of excitation in damped homogeneous and periodic structures (finite) [49,50]. In addition, because the complex wavenumbers exist throughout the frequency spectrum, band gaps become less distinct (an effect which becomes more pronounced at higher frequencies). This result was reproduced qualitatively by Tassily [14] in his study of damped phononic beams with material periodicity. Seemingly contradictory, Psarobas [51] reported the persistence of a complete band gap when damping was introduced to a three-dimensional system of closed-packed rubber spheres in air. However, since material damping was exclusive to the rubber spheres, the effects of energy loss was most apparent around the sphere resonant frequencies when the acoustic wave field is localized within the spheres. Corroboratively, Moiseyenko and Laude [52] concluded that flat bands associated with low group velocity acquire an enhanced damping and that losses have a greater influence on the propagating modes than on the evanescent. In addition, using an extended plane-wave expansion method, Ref. [52] produced the complete band diagram (propagating and evanescent modes) for a two-dimensional, damped phononic crystal. The interaction between material damping and sound/shock wave transmission was the focus of additional research [53–56]. Other studies considered the application of Bloch theorem to phononic materials [57] with damping and the efficient

characterization thereof [58]. The Schrödinger equation, for which Bloch theorem provides a solution, does not account for dissipation, yet wave propagation in materials is, in fact, dissipative. Farzbod and Leamy [57] presented a mathematical treatment for the unit cell analysis of damped phononic materials. Collet *et al* [58] developed a numerical formulation amenable to phononic materials with complex, frequency-dependent damping definitions. In each of the above cases, the frequency had a prescribed real value such that the temporal parameter $\lambda = \mathrm{i}\omega$ was purely imaginary. This situation represents a plurality of the wave propagation research incorporating damping and corresponds to a steady-state perspective where material motion is driven at a given frequency.

Alternatively, the transient perspective has the wave amplitude decrease in time and, with the frequency unprescribed, is referred to as free wave propagation. In considering the propagation of longitudinal waves in homogeneous rods, Cady [59] allowed the temporal parameter to become complex, $\lambda = \mathrm{i}(\omega_\mathrm{d} + \mathrm{i}\xi\omega) = -\xi\omega + \mathrm{i}\omega_\mathrm{d}$, such that ω_d is the damped propagation frequency and $-\xi\omega$ is the temporal attenuation constant. Regarding periodic media, for one-dimensional phononic materials, Mukherjee and Lee [60] appear to be the first to develop a dispersion diagram for each the frequency and temporal attenuation constant; however, the solution technique (the finite difference method) yielded only the κ_R-pane. Other studies also investigated the dispersion properties of damped phononic materials using complex frequencies (i.e., complex temporal parameter). Opening complete band gaps in phononic materials composed of solids within a fluid matrix is notoriously difficult due to the suppression of transverse waves in the fluid phase. However, recognizing the viscous penetration depth as an additional length scale for fluid-solid phononic materials, Sprik and Wegdam [61] were able to open complete band gaps in a phononic material composed of silica spheres in a liquid matrix of a glycerol/water-like mixture. Moreover, Zhang *et al* [62] found the viscosity of the liquid to assist in widening the band gap. Later, reminiscent of vibration in structures, Hussein [63] extracted a damping ratio band structure from $\mathrm{Re}[\lambda]$ and demonstrated intriguing phenomena such as branch overtaking and branch cut-off. This dissertation will primarily take the perspective of free wave propagation.

In addition to the dispersive properties of phononic materials, Sec. 1.4 described the utility of

the effective material properties that emerge out of the substructure dynamics; however, predicting these dynamic effective properties is not as straight-forward a procedure as in the static case. In the static case, the homogenization of composite involves the volume fractions of each constituent material [64–66] and yields the static effective density and moduli. However, for phononic materials (and composites in general), relative motion among the substructure yields dynamic effective properties that differ from there static counterparts, even in the long wavelength regime [21,67,68]. In addition, the correspondence principle, which determines the effective viscoelastic properties from the static solutions, is limited to the low-frequency regime to avoid inertial effects. Chapter 3 provides several references for which predicting the dynamic effective properties beyond the low-frequency regime is the principal objective. Only one of these considers the effects of damping [69]. From the perspective of wave propagation at a prescribed frequency, Nemat-Nasser and Srivastava [69] showed the effective density and elasticity to become complex in response to damping, although the real parts are close to the undamped values. Chapter 3 adds the perspective of free wave propagation and, for the first time, an effective damping constant.

1.6 Overview of Dissertation

As expressed in the chapter's opening paragraphs, the ability to tailor the dynamic properties of phononic structures opens them to many applications in engineering. More comprehensive than a structural analysis, a unit cell analysis encompasses the wave propagation characteristics of a particular material design in the form of the frequency band structure and is essential to the development of phononic-based devices. However, a review of the phononics literature shows relatively little regard for the implications of dissipative wave propagation due to material damping. In order to narrow the gap between theoretical prediction and empirical evidence, which supports design and optimization efforts, as well as to open phononic materials to new applications, dissipative dynamics must be considered. The aim of this dissertation is not only to address the nature of dissipative wave propagation in damped phononic materials, but also to exploit this quality for applications requiring materials with simultaneously enhanced dissipation and load-bearing capability. In prac-

tice, damping is the result of a number of material processes and choosing to model only the most dominant of mechanisms greatly simplifies analysis. For its mathematical convenience, the viscous damping model is popular in many dynamics software packages and the results from modal testing are often fitted to this model. In this dissertation, where damping is treated in a general sense and not specific to any material, the viscous damping model is used primarily (Ch. 6 considers a viscoelastic damping model). The organization of the dissertation and the contributions to the subject are as follows:

- Many composites in operation are composed of layers and, with the requisite periodic arrangement, may form a phononic material. Chapter 2, examines the damped band structures generated under assumed real and complex frequencies for layered phononic materials. In the case of real frequencies, damping closes the band gap such that the wave energy is strongly in space localized within the material. For complex frequencies, the amplitude of propagating waves diminishes in time only. In each case, a connection between the dynamics of the infinite material and the finite structure is drawn.

- In the case of phononic materials, the effective mass density and elasticity become frequency-dependent and, due to relative motion of the microstructure, may achieve negative values. Chapter 3 shows the frequency-dependent effective properties, like the band structure, are sensitive to dissipative influences and whether the propagating wave was free or prescribed. These dynamic effective properties are central to many novel acoustic devices including the superlenses and cloaks referenced earlier. In addition, to account for the material damping, Chapter 3 introduces the first expression of an effective damping constant.

- Chapter 4 introduces dissipative wave propagation in the context of both lumped parameter and discretized continuous phononic materials. With a viscous damping model, we extend the structural dynamics techniques of modal analysis and the state-space transformation to the wave propagation problem. These techniques and our choice of complex frequencies in the Bloch formulation uniquely allows for the determination of damped frequency *and*

damping ratio band structures. We also describe the phenomena of *branch-overtaking* and *branch cut-off*.

- Chapter 5 introduces the concept of *metadamping* to describe the phenomenon of damping emergence from locally resonant sonic materials (LSRMs). Specifically, when compared to a statically equivalent phononic crystal (i.e., one of equal mass and sound speed) with identically prescribed damping, a LRSM may exhibit a greater dissipative capacity. To combat potentially damaging dynamic loads, it is desirable for an engineering material to possess a high dissipative capacity while maintaining its load-bearing capability (stiffness). However, for classic materials, an advantage in one of these traits comes at the expense of the other. The phenomenon of metadamping answers the challenge of simultaneously high stiffness and high damping within a material.

- In Chapter 6, using convolution integrals over exponentially decreasing kernel functions, we extend the damping model from a viscous to a linear viscoelastic type. The viscoelastic model describes a greater number of materials than the viscous. By adopting a special form for the kernel functions and associating them with the damping matrix, a legitimate comparison between the two models remains possible. In addition, a single parameter of the kernel functions may be adjusted to smoothly transition the damping type from viscous to viscoelastic to undamped. The band structures reflect these transitions and allow us to establish a viscous-to-viscoelastic transition.

- Chapter 7 offers some closing remarks on the subject and proposes future research directions.

Chapter 2

Exact dispersion relation for a damped periodic rod considering free and forced motion[1]

2.1 Abstract

The effects of damping in phononic materials is investigated in the context of free and prescribed wave propagation. Damping is an inherent material property that may significantly affect the dynamics of system. Moreover, the interpretation of dynamical properties of damped phononic materials is subject to the type of wave propagation considered. Free wave propagation permits both spatial and temporal decay and relates properties intrinsic to the material. Prescribed wave propagation allows only spatial attenuation and relates properties extrinsic to the material. We adapted the transfer matrix method for one-dimensional, layered phononic materials to incorporate a viscosity term that accounts for the material damping in each layer. Thus modified and applied to the generation of band diagrams and mode shapes, we identify and explain key differences between the two propagation models using a representative damped phononic crystal. We also demonstrate the level correspondence between the material and its structural counterpart.

2.2 Introduction

Since their resurgence more than twenty years ago [43, 45], phononic materials have been the subject of intense research interest in the fields of materials science and engineering. The inherent dynamical properties of these materials, which may be tailored by design, impact numerous

[1] This chapter is adapted from a manuscript being prepared for journal submission.

applications ranging from vibration control [70, 71] and waveguides [15] through sub-wavelength sound focusing [22, 72] and cloaking [35, 73]. Bloch's theorem [3] describes waves in phononic materials as the product of a periodic function $\phi(\mathbf{r})$, a plane-wave envelope $e^{i\kappa\cdot\mathbf{x}}$, and a temporal function $e^{\lambda t}$. In the absence of energy dissipation stemming from material damping, $\lambda = i\omega$ and Bloch analysis generates the dispersion relations which tie the wave frequency ω to the wavevector κ. From the dispersion relations, many dynamical properties may be determined

However, material damping is a physical reality that, once experimentally characterized, must be incorporated into the equations of motion for an accurate depiction of the dynamical properties. Moreover, the frame within which Bloch analysis is performed is dependent upon the temporal parameter λ. In the presence of damping, wave propagation through phononic materials may be prescribed such that $\lambda = i\omega$ is maintained and damping effects are expressed solely through the wavevector. Alternatively, $\lambda = -\xi\omega \pm i\omega_d$ may assume any value in the left complex plane in response to the damping intensity such that a wave is free to propagate with a modified frequency $\omega_d = \text{Im}[\lambda]$ and a rate of amplitude decay specified by Abs[Re[λ]]. In the former context, dynamic properties are acquired; in the latter, they are interpreted as intrinsic.

There are several articles in the literature investigating the effects of material damping in phononic materials under the circumstance of prescribed motion. Mead [48] applies a complex stiffness to a periodically supported beam to study the impact of damping on the value of wavenumbers in the complex plane. Langley [50] and Tassilly [14] also consider periodically supported beams in their studies on the vibration localization effects of damping and bending waves, respectively. For Langley, damping is formulated as a complex inertial term, while Tassilly employs a separate viscosity parameter. More complex damping models – ones accounting for the time history of motion – are also considered. Merheb *et al* [54] uses the finite difference time domain method to examine the audible transmission properties of periodic rubber-air composites where the rheological behavior of the rubber follows the Maxwell-Weichert model of viscoelasticity. Zhao and Wei [74] use the plane-wave expansion method to evaluate band gaps in a one-dimensional phononic material with various standard model viscoelastic constituents. Additional studies [51, 52, 57, 75, 76] of one- and

two-dimensional phononic materials with viscous/viscoelastic damping may be located.

There are comparatively fewer articles in the literature regarding free wave propagation in damped phononic materials. Mukherjee and Lee [60] use finite difference methods to obtain the dispersion curves and mode shapes of laminated media with standard linear solid constituents. They study both prescribed waves with complex wavenumbers and free waves (featuring complex λ) with real wavenumbers. Zhang *et al* [62] and Sprik and Wegdam [61] achieve similar results for two- and three-dimensional composites of solids immersed in a fluid with complex Lamé constants. Hussein [63] and Hussein and Frazier [77] derive the dispersion relations for viscously damped phononic materials. Viscoelasticity is also considered [78].

The objective of this chapter is to compare prescribed and free wave propagation in damped phononic materials. To this end, the damping model and material design are common between the two propagation modes. The chapter is divided into four sections including the present introductory remarks. Beginning with the free and prescribed dynamics of a damped, homogeneous material, section 2.3 develops the theory for one-dimensional wave propagation in phononic crystals with viscous damping. Matrix methods for elastodynamics form the mathematical foundation of this section and the appendices. Section 2.4 contrasts the two propagation varieties using the dispersion curves and mode shapes of a typical phononic crystal. Here, we also show the correlation between the infinite medium and the finite structure: free wave propagation with natural frequencies, and prescribed wave propagation with frequency response. Finally, section 2.5 restates the objective of the paper and summarizes the results.

2.3 Damped Waves in 1D Phononic Materials

In this section, our interest is the dynamics of an infinite periodic material. Accordingly, we seek the dispersion relations describing the wave propagation characteristics of a periodic medium. To achieve this goal, we adopt the transfer matrix method [79, 80] and adapt it to incorporate dissipative and prescribed motion. By formulating an eigenvalue problem, the method not only yields a set of eigenvalues containing the dispersion relations, but also supplies a set of eigenvectors

from which to construct the corresponding mode shapes. However, before the details of the method are presented, we examine the dynamic characteristics of a homogeneous medium in the context of both free and frequency-prescribed motion.

2.3.1 Waves in Homogeneous Materials

We begin our dynamic analysis of a homogeneous material, naturally, with the statement of the equation of motion in one dimension

$$\sigma_x + f = \rho u_{tt}, \tag{2.1}$$

where $\sigma = \sigma(x,t)$, $f = f(x,t)$, ρ, and $u = u(x,t)$ denote the stress, external force, material density, and displacement, respectively. As indicated, the value of each of these quantities, with the exception of the material density, is dependent upon the position, x, within the medium and time, t. Differentiation with respect to position and/or time is denoted by the appropriate subscript following a quantity. For example, $(\cdot)_x$ indicates differentiation with respect to position while $(\cdot)_{tt}$ signifies double differentiation with respect to time.

Due to the diversity and complexity of dissipative mechanisms, the development of a universal damping model stands as a major challenge. A rather simple model proposed by Rayleigh [81] and observed in this article is the *viscous damping* model in which the instantaneous generalized velocity, u_t, is the only relevant state variable in the determination of the damping force. Consequently, the stress is not only a function of the strain, u_x, but the strain rate, u_{xt}, as well. The constitutive relationship then becomes

$$\sigma = Eu_x + \eta u_{xt} \tag{2.2}$$

where E is the material Young's modulus and η is the viscosity. In the absence of body forces, substitution of Eq. (2.2) into Eq. (2.1) yields the general equation for wave propagation in a viscously damped homogeneous 1D medium,

$$Eu_{xx} + \eta u_{xxt} = \rho u_{tt}. \tag{2.3}$$

We may use Eq. (2.3) to study the propagation of waves in homogeneous, linearly elastic materials. In particular, if we have a material of infinite extent (i.e., having no external boundaries off which waves may reflect), then we may apply a plane wave solution of the form

$$u(x,t) = A\mathrm{e}^{\mathrm{i}\kappa x} g(t), \tag{2.4}$$

where $\mathrm{i} = \sqrt{-1}$, A is the complex wave amplitude, κ is the wavenumber, and $g(t)$ is an exponential function of time. For prescribed propagation, $g(t) = \mathrm{e}^{-\mathrm{i}\omega t}$ where ω is the oscillation frequency. Critically, for free wave motion, $g(t) = \mathrm{e}^{\lambda t}$ where λ, generally complex, encompasses an oscillation frequency *and* rate of decay. When the motion is prescribed, establishing a dispersion relation is comparatively straightforward. Substituting Eq. (2.4) into Eq. (2.3) produces a quadratic equation in κ whose two solutions [Eq. (2.5)], respectively, represent forward and backward traveling waves.

$$\kappa^2(E - \mathrm{i}\omega\eta) = \omega^2\rho \tag{2.5}$$

For free wave propagation, establishing a dispersion relation requires some insight and an intermediate step. Following the substitution of Eq. (2.4) into Eq. (2.3), with $c = \sqrt{E/\rho}$, we first solve the resulting quadratic equation [Eq. (2.6)] for λ [Eq. (2.7)] rather than κ

$$-\kappa^2(E + \lambda\eta) = \lambda^2\rho \tag{2.6}$$

$$\lambda = -\left(\frac{\eta\kappa}{2\rho c}\right)(\kappa c) \pm \mathrm{i}\kappa c\sqrt{1 - \left(\frac{\eta\kappa}{2\rho c}\right)^2}, \tag{2.7}$$

which reflects the form suggested by Refs. [59, 63, 77]

$$\begin{aligned} \lambda &= -\xi\omega \pm \mathrm{i}\omega\sqrt{1-\xi^2} \\ &= -\xi\omega \pm \mathrm{i}\omega_{\mathrm{d}}, \end{aligned} \tag{2.8}$$

where ω, ω_{d}, and ξ are the undamped and damped wave frequencies, and associated damping ratio, respectively. By equating the squares of the imaginary terms in Eqs. (2.7) and (2.8), we develop a quadratic equation in κ^2

$$\kappa^4\left(\frac{\eta}{2\rho}\right)^2 - \kappa^2 c^2 + \omega_{\mathrm{d}}^2 = 0. \tag{2.9}$$

Although there are four κ solutions for Eq. (2.9), only the two smallest in magnitude are physical.

2.3.2 Waves in Phononic Materials – Dispersion

For a layered periodic medium (Fig. 2.1) composed of two or more material layers, the transfer matrix method enforces the continuity conditions that exist between layers to relate layer boundary states (displacement and stress) from one layer to the next. If the displacement and stress states at the boundary of one layer are known, then the corresponding states at the opposite boundary (shared by the current layer and the adjacent layer) can be derived from a simple matrix operation. Thus transferring boundary states across each layer of the unit cell produces a system matrix that relates the states at opposite ends of the unit cell. In conjunction with Bloch's theorem, this system matrix is then utilized to generate an eigenvalue problem. The mathematical derivation of this method is provided below.

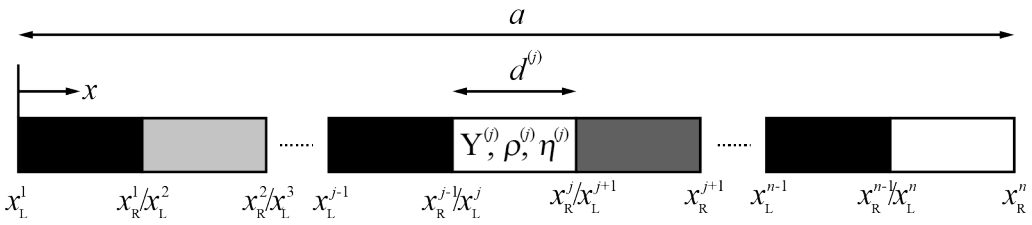

Figure 2.1: Continuous model of a two-phased 1D phononic crystal with lattice spacing a. The unit cell is enclosed in a red, dashed box.

For an arbitrary homogeneous layer j in the unit cell, the associated material properties are denoted as $\rho^{(j)}$, $E^{(j)}$, and $\eta^{(j)}$. The layer is bordered by layer $j-1$ on the left and layer $j+1$ on the right. Given the thickness of any layer j of the unit cell is $d^{(j)}$, the lattice spacing is $a = \Sigma_{j=1}^{n} d^{(j)}$ for a unit cell with n layers. Following this notation and accounting for forward and backward traveling waves, Eq. (2.4) becomes

$$u(x,t) = [A_{+}^{(j)} \mathrm{e}^{\mathrm{i}\kappa^{(j)}x} + A_{-}^{(j)} \mathrm{e}^{-\mathrm{i}\kappa^{(j)}x}]g(t), \tag{2.10}$$

where $\kappa^{(j)}$ is the layer-specific wavenumber. We can write the spatial components of Eqs. (2.2)

and (3.11) in matrix form as

$$\begin{bmatrix} u(x) \\ \sigma(x) \end{bmatrix} = \begin{bmatrix} 1 & 1 \\ \mathrm{i}Z^{(j)} & -\mathrm{i}Z^{(j)} \end{bmatrix} \begin{bmatrix} \mathrm{e}^{\mathrm{i}\kappa^{(j)}x} & 0 \\ 0 & \mathrm{e}^{-\mathrm{i}\kappa^{(j)}x} \end{bmatrix} \begin{bmatrix} A_+^{(j)} \\ A_-^{(j)} \end{bmatrix} = \mathbf{B}_j\mathbf{C}_j(x)\mathbf{a}_j. \tag{2.11}$$

where $Z^{(j)} = \kappa^{(j)}(E^{(j)} - \mathrm{i}\omega\eta^{(j)})$ if the motion is prescribed, otherwise $Z^{(j)} = \kappa^{(j)}(E^{(j)} + \lambda\eta^{(j)})$.

We now seek to relate the boundary states at the left boundary, $x = x_{\mathrm{L}}^{(j)}$, of an arbitrary layer to those at the right boundary, $x = x_{\mathrm{R}}^{(j)}$. To accomplish this, we define $x_{\mathrm{R}}^{(j)} = x_{\mathrm{L}}^{(j)} + d^{(j)}$ and insert this into Eq. (2.11) as follows:

$$\begin{bmatrix} u(x_{\mathrm{R}}^{(j)}) \\ \sigma(x_{\mathrm{R}}^{(j)}) \end{bmatrix} = \mathbf{B}_j\mathbf{C}_j(d^{(j)})\mathbf{C}_j(x_{\mathrm{L}}^{(j)})\mathbf{a}_j. \tag{2.12}$$

By setting $x = x_{\mathrm{L}}^{(j)}$ in Eq. (2.11), we rewrite Eq. (3.13) as

$$\begin{bmatrix} u(x_{\mathrm{R}}^{(j)}) \\ \sigma(x_{\mathrm{R}}^{(j)}) \end{bmatrix} = \mathbf{B}_j\mathbf{C}_j(d^{(j)})\mathbf{B}_j^{-1} \begin{bmatrix} u(x_{\mathrm{L}}^{(j)}) \\ \sigma(x_{\mathrm{L}}^{(j)}) \end{bmatrix} = \mathbf{T}_j \begin{bmatrix} u(x_{\mathrm{L}}^{(j)}) \\ \sigma(x_{\mathrm{L}}^{(j)}) \end{bmatrix}, \tag{2.13}$$

where $\mathbf{T}_j$, the *transfer matrix* for layer j, has the expanded form

$$\mathbf{T}_j = \begin{bmatrix} \cos(\kappa^{(j)}d^{(j)}) & (1/Z^{(j)})\sin(\kappa^{(j)}d^{(j)}) \\ -Z^{(j)}\sin(\kappa^{(j)}d^{(j)}) & \cos(\kappa^{(j)}d^{(j)}) \end{bmatrix}. \tag{2.14}$$

Equation (2.13) relates the displacement and stress at $x_{\mathrm{L}}^{(j)}$ to those at $x_{\mathrm{R}}^{(j)}$ of the same layer. However, since the construction of the transfer matrix is valid for any layer and $x_{\mathrm{R}}^{(j)} \equiv x_{\mathrm{L}}^{(j+1)}$, the result in Eq. (2.13) can be extended recursively across several layers. Thus,

$$\begin{aligned} &\mathbf{y}(x_{\mathrm{R}}^1) = \mathbf{T}_1\mathbf{y}(x_{\mathrm{L}}^1) = \mathbf{y}(x_{\mathrm{L}}^2), \\ &\mathbf{y}(x_{\mathrm{R}}^2) = \mathbf{T}_2\mathbf{y}(x_{\mathrm{L}}^2) = \mathbf{T}_2\mathbf{T}_1\mathbf{y}(x_{\mathrm{L}}^1) = \mathbf{y}(x_{\mathrm{L}}^3), \\ &\mathbf{y}(x_{\mathrm{R}}^3) = \mathbf{T}_3\mathbf{y}(x_{\mathrm{L}}^3) = \mathbf{T}_3\mathbf{T}_2\mathbf{T}_1\mathbf{y}(x_{\mathrm{L}}^1) = \mathbf{y}(x_{\mathrm{L}}^4), \\ &\vdots \\ &\mathbf{y}(x_{\mathrm{R}}^n) = \mathbf{T}_n\mathbf{T}_{n-1}\cdots\mathbf{T}_1\mathbf{y}(x_{\mathrm{L}}^1) = \mathbf{T}\mathbf{y}(x_{\mathrm{L}}^1). \end{aligned} \tag{2.15}$$

In the interest of clarity, we have defined $y(x) = [u(x)\ \ \sigma(x)]^{\mathrm{T}}$ to be the state vector at x. Ultimately, the displacement and stress at the left end of the first layer ($x = x_{\mathrm{L}}^1$) in a unit cell are related to

those at the right boundary of the nth layer ($x = x_{\mathrm{R}}^n$) by the *cumulative transfer matrix*, $\mathbf{T}$. More direct, Bloch's theorem asserts that the state at a given point in a unit cell differs from that of the corresponding point in an adjacent unit cell by only a phase multiplier of $\mathrm{e}^{\mathrm{i}\kappa a}$ (κ is the global wavenumber applying to the periodic medium). This relation is given by $h(x+a) = h(x)\mathrm{e}^{\mathrm{i}\kappa a}$, which, for the problem at hand, entails

$$\mathbf{y}(x_{\mathrm{R}}^n) = \mathrm{e}^{\mathrm{i}\kappa a}\mathbf{y}(x_{\mathrm{L}}^1). \tag{2.16}$$

Equating Eqs. (2.15) and (2.16) yields the eigenvalue problem

$$[\mathbf{T} - \mathbf{I}\gamma]\mathbf{y}(x_{\mathrm{L}}^1) = \mathbf{0}, \tag{2.17}$$

where $\gamma = \mathrm{e}^{\mathrm{i}\kappa a}$. The solution of Eq. (2.17), which appears in complex conjugate pairs, provides the dispersion relations for the 1D phononic crystal. Real-valued wavenumbers, calculated from γ using Eq. (2.18a), support the propagating modes, whereas imaginary wavenumbers, extracted from γ using Eq. (2.18b), represent evanescent modes which decay in space. Together, $\kappa = \kappa_{\mathrm{R}} + \mathrm{i}\kappa_{\mathrm{I}}$.

$$\kappa_{\mathrm{R}} = \frac{1}{a}\mathrm{Re}[-\mathrm{iln}\gamma] \tag{2.18a}$$

$$\kappa_{\mathrm{I}} = \frac{1}{a}\mathrm{Im}[-\mathrm{iln}\gamma] \tag{2.18b}$$

2.4 Results

The technique presented in section 2.3 is specific to one-dimensional wave propagation in layered phononic crystals although a similar approach can be applied to layered, periodic acoustic metamaterials. Within this scope, the design of the unit cell is arbitrary. For purposes of demonstration we consider a bi-material ($n = 2$) unit cell in with $d^{(1)} = d^{(2)}$ and the material parameters listed in Table 2.1. To give a good representation of the dissipative effects, we vary the viscosity $\eta^{(j)} = qE^{(j)}$ using the scaling parameter q. Through the band diagrams and mode shapes of the infinite medium, and the natural frequencies and spatial attenuation effects of the finite structure, we expose the properties of dissipative free ($\mathrm{e}^{\lambda t}$) and prescribed ($\mathrm{e}^{-\mathrm{i}\omega t}$) motion.

Table 2.1: Phononic crystal properties

ABS polymer	$\rho^{(1)} = 1040\text{kg/m}^3$	$E^{(1)} = 2.4\text{GPa}$
Aluminum	$\rho^{(2)} = 2700\text{kg/m}^3$	$E^{(2)} = 68.9\text{GPa}$

2.4.1 Infinite Material

In Fig. 2.2, we show the frequency (non-dimensional) and damping ratio band structures for our bi-material model. Each plot is divided into positive and negative wavenumber (non-dimensional) domains representing the propagating and evanescent modes, respectively. In actuality, the evanescent wavenumbers are not negative; rather, they are indicated as such to emphasize their attenuating nature. As anticipated, and evident in Figs. 2.2a and 2.2c, material damping alters the appearance of the frequency band structure; however, the response of the band structure depends on whether the propagation is free or prescribed.

We focus, for the moment, on the free propagation scenario (Fig. 2.2a). One may imagine this scenario as the result of an initial displacement at the end of a semi-infinite medium. The discrepancy between the undamped and damped band structures increases with frequency, illustrating the impact of the strain rate in Eq. (2.2). In this scenario, the higher frequency bands descend more rapidly than those below, leading to the simultaneous reduction of band gap frequency ranges and shift in band gap central frequencies. A possible eventuality is band gap annihilation as damping causes a higher mode to overtake a lower one [63, 77], however, the current $\kappa(\lambda)$ formulation does not support this action. In all damping conditions, propagating and evanescent modes occupy distinct frequency ranges – a consequence of real-valued layer wavenumbers.

Coincident with its interpretation in structural dynamics, in the context of wave propagation, the damping ratio diagram (Fig. 2.2c) is a measure of the material opposition to oscillation (through energy loss). The reduction in frequency illustrated in Fig. 2.2a is one manifestation of this material resistance. A second is exhibited in Fig. 2.3a where a set of mode shapes corresponding to an undamped and damped condition at $\omega_{\text{d}} a/c^{(1)} = 1$ are compared. A study of each frame reveals a

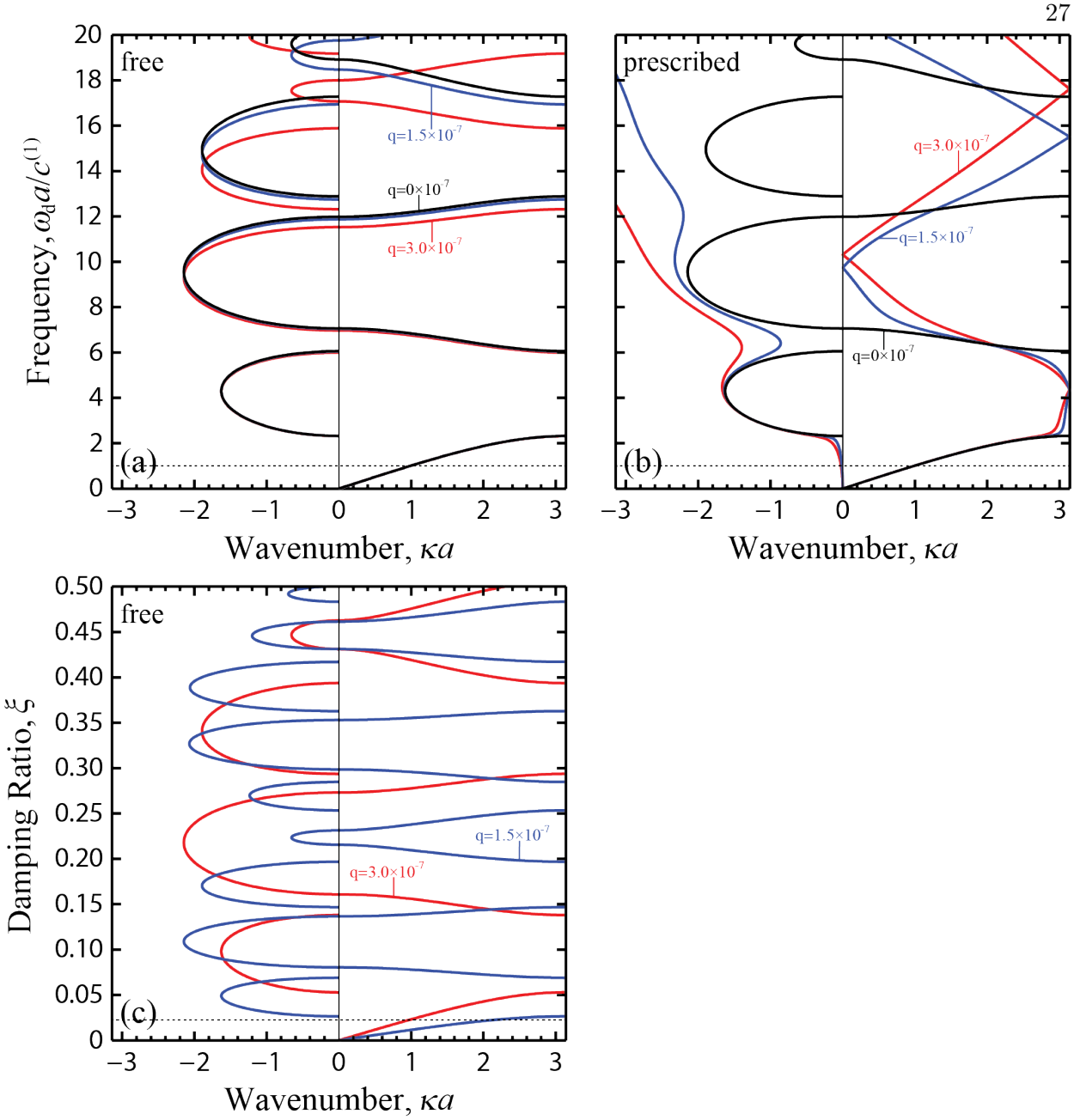

Figure 2.2: The frequency band structure for free (a) and prescribed (b) wave propagation. In addition to the undamped case, indicated by (—) $q = 0$, two damping intensities, (—) $q = 1.5\times10^{-7}$ and (—) $q = 3.0 \times 10^{-7}$, are displayed for comparison. The damping ratio band structure (c) is unique to dissipative free wave propagation. The horizontal dotted lines at $\omega_d a/c^{(1)} = \omega a/c^{(1)} = 1$ and $\xi = 0.024$ identify the modes plotted in Fig.2.3.

clear diminishing of the wave amplitude over time; independent of spatial extent. However, within a band gap, amplitude attenuation occurs over both time and space (not shown), the former the

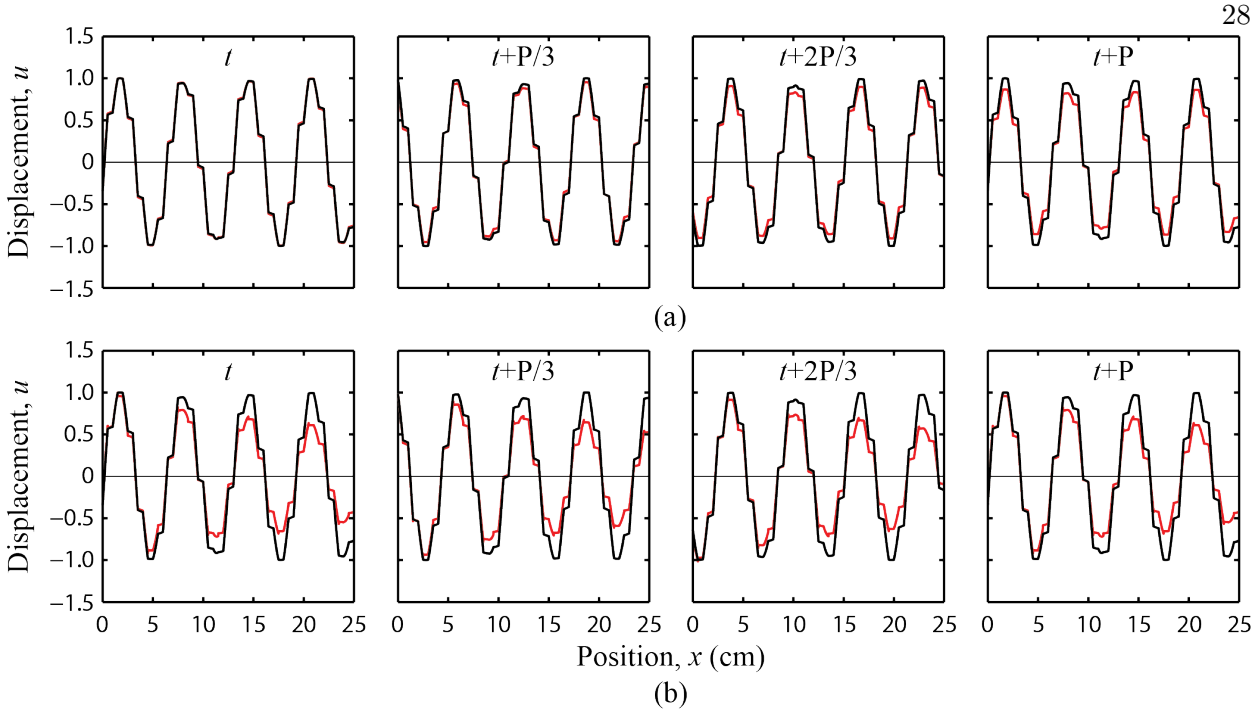

Figure 2.3: Mode shapes for bi-material phononic crystal corresponding to (a) $\omega_{\mathrm{d}}a/c^{(1)} = 1$ and $\xi = 0.024$, and (b) $\omega a/c^{(1)} = 1$ in Fig. 2.2 for an undamped (—) $q = 0$ and damped (—) $q = 3.0 \times 10^{-7}$ case. Snapshots are depicted for times between some initial time and the duration of one period, P, inclusive.

result of material damping and the later the outcome of adverse wave interference.

Now, we turn our attention to the prescribed propagation scenario (Fig. 2.2b). One may imagine the prescribed propagation scenario as the result of sustained harmonic forcing at the end of a semi-infinite medium. In the absence of damping, as verified in Figs. 2.2a and 2.2b, the two statements on the origins of free and prescribed propagation are equivalent (i.e., $\lambda = \mathrm{i}\omega$). In the presence of damping, we distinguish prescribed propagation from its free counterpart in three ways. In one, because the layer wavenumbers are complex, the destructive interference that generates a band gap is less than optimal [82]. Thus, as we observe in Fig. 2.2b, waves in the damped phononic crystal simultaneously propagate and decay in space, challenging the theoretical notion of a band gap where propagation is prohibited. In a second aspect, the inability of prescribed propagation to support temporal attenuation precludes the generation of a damping ratio band diagram. In Fig. 2.3b, the damped wave amplitude corresponding to $\omega a/c^{(1)} = 1$ attenuates over the plotted spatial

extent, but is unaffected over the passage of time. With the application of material damping, a third distinction between the two wave propagation models presents itself as the ascent of frequency bands in Fig. 2.2b while bands in Fig. 2.2a are compelled downward.

2.4.2 Infinite-Finite Correspondence

The interpretations of free and prescribed wave propagation offered in the previous section allow us to establish a link between the performance of the phononic material (infinite in extent) and the phononic structure (finite in extent). As the result of some initial disturbance, free wave propagation represents the innate dynamic characteristics of a material in analogy to the natural frequencies of a structure. As the product of enforced motion, prescribed wave propagation represents the stimulated response of a material, paralleling the frequency response of a structure. In Figs. 2.4a and 2.4b, we illustrate the strength of the infinite-finite correspondence.

Figure 2.4a contains the frequency dispersion curves for our phononic medium assuming free propagation. In addition, superimposed are the natural frequencies and wavenumbers of a corresponding phononic structure of ten cells. There is superb agreement between the two systems. Irrespective of damping condition, the mode shape amplitude of the phononic structure remain constant over the structural extent. Unique to the free wave assumption, propagating modes do not simultaneously attenuate with propagation distance. Due to this similarity concerning the wavenumber and the common temporal freedom $e^{\lambda t}$, the infinite-finite correspondence is confined to the right panel of Fig. 2.4a. A similar agreement could be illustrated using the damping ratios, respectively, of the infinite and finite systems.

Figure 2.4b shows the prescribed frequency dispersion curves of our phononic material. Superimposed is the reconstructed imaginary component of the wavenumber extracted from the frequency response of the same phononic structure described above. Because we compare the magnitude of a boundary state at two locations within the structure, the frequency response can inform us of the attenuation (if any) that occurs with distance. Resonance-induced amplification of the boundary states, especially in the absence of damping, causes some of the extracted κ_{I} to appear misleadingly

in the right panel. Nevertheless, the good agreement between the two systems with and without damping demonstrates the infinite-finite correspondence where motion is described by $e^{-i\omega t}$.

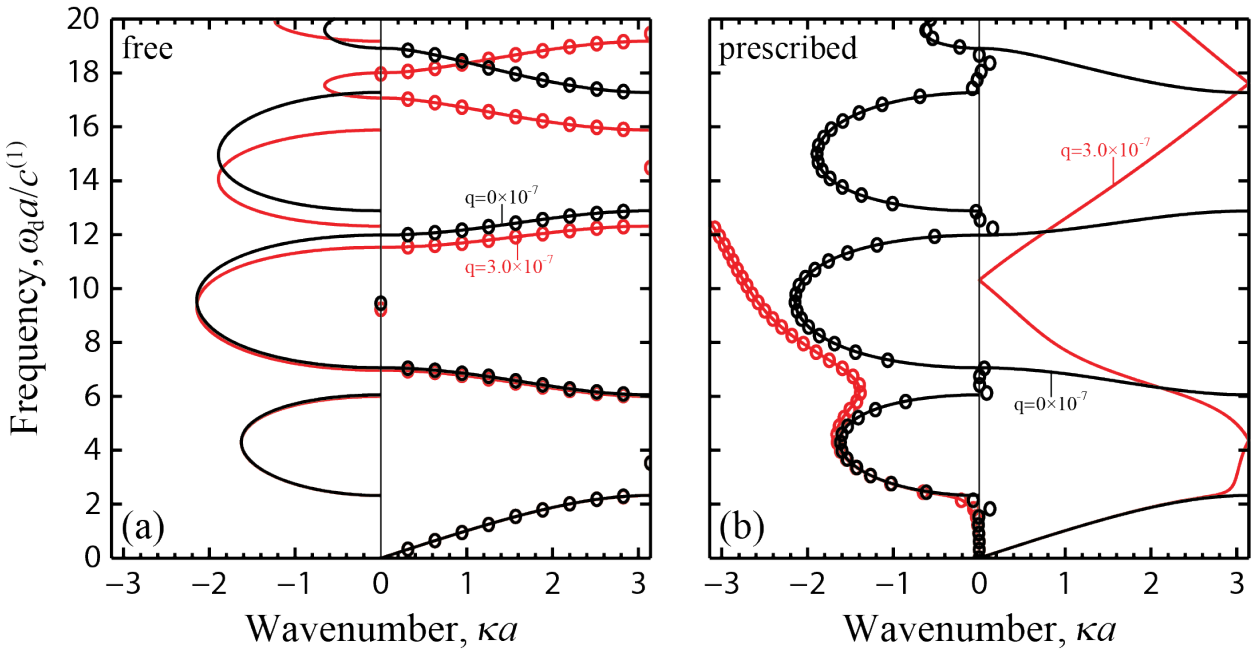

Figure 2.4: Correlation between the phononic material (curves) and a phononic structure (open circles) of ten unit cells. The undamped $q = 0$ (black) and damped $q = 3.0 \times 10^{-7}$ (red) cases are illustrated. (a) Free propagation frequency bands relate to the natural frequency distribution and discretized wavenumbers of the phononic structure. (b) Prescribed propagation frequency bands relate to the attenuation of boundary states within the phononic structure

2.5 Conclusions

The effects of damping in phononic materials is investigated in the context of free and prescribed wave propagation. Free wave propagation, adhering to $e^{\lambda t}$ and permitting both spatial and temporal decay, may be conceptualized as the result of an initial displacement/velocity or impulse applied to the end of a semi-infinite medium. Prescribed wave propagation, governed by $e^{i\omega t}$ and allowing only spatial attenuation, may be envisioned as the response of a semi-infinite medium to an imposed harmonic end displacement or harmonic forcing.

We adapted the transfer matrix method for one-dimensional, layered phononic materials to incorporate a viscosity term that accounts for the material damping in each layer. Thus modified

and applied to the generation of band diagrams and mode shapes, we identify and explain key differences between the two propagation models using a representative damped phononic crystal. (1) Free propagation supports waves that either propagate through space or exponentially decay while simultaneous propagation and decay is possible for prescribed propagation. (2) Free propagation, permitting temporal decay, is described by a combination frequency and damping ratio band diagram while prescribed propagation may only be represented by the former. (3) Damping reduces the frequencies of freely propagating waves and increases the frequencies of prescribed waves.

Whether the analyst adheres to the free or the prescribed propagation model is dependent upon the research objective. For each propagation model, we have demonstrated the level correspondence between the material description and structural counterpart. Free wave propagation describes the intrinsic dynamics of phononic materials, a characteristic that parallels the natural frequencies of structures subject to impulsive loading. Prescribed wave propagation describes the response of a material to enforced harmonic motion similar to a harmonically excited structure.

Chapter 3

Dynamic effective properties of damped periodic materials under free and forced wave motion[2]

3.1 Abstract

Bloch wave propagation in elastic materials may be represented by either of two temporal exponential functions: $e^{-i\omega t}$ and $e^{\lambda t}$. The former describes waves that propagate at a prescribed frequency analogous to those stimulated by harmonic forcing at the end of a semi-infinite medium. The latter, with λ generally in the left complex plane, characterizes free waves that propagate at a frequency innate to the supporting material and decay in time analogous to those generated by an impulse at one end of a lossy semi-infinite medium. For damped periodic materials, energy dissipation affects prescribed and free waves uniquely, resulting in two distinct sets of dispersion diagrams. Predictably, as energy dissipation influences the frequency band structure, its effects extend to the dynamic effective properties (density and Young's modulus) of the homogenized medium. In this article, we explore the role of energy dissipation and wave propagation variety in the formation of the band structure and the dynamic effective properties for one-dimensional phononic crystals. To the best of our knowledge, ours is the first to manifest a dynamic effective damping constant. Together with the effective density and effective Young's modulus, the effective damping constant completes the set of parameters describing a homogenized lossy composite.

[2] This chapter is adapted from a manuscript being prepared for journal submission.

3.2 Introduction

Often, the aim of composite design is the realization of effective properties unavailable from the constituent phases themselves, or denied by nature entirely. In the static case, taking into account the constituent material filling ratios, the determination of effective mechanical properties (i.e., effective density and effective compliance) can be quite straightforward. In the dynamic case, relative motion among the constituent material phases complicates the calculation. While adherence to Newton's second law of motion is absolute at the length scale of the microstructure, relative motion beyond the resolution of a traveling wave, under certain conditions, may give the illusion that the classical equation of motion fails. The apparent violation at the macro-scale can be rectified by the substitution of a dynamic effective density and compliance for the static versions. Thus, for the dynamic case, especially when a high degree of mechanical mismatch exists between the constituent phases, some method of dynamic homogenization is necessary.

By definition, the effective medium arising from the static homogenization of a composite is non-dispersive as the assumption of wave field homogeneity is a fundamental assumption. An averaging scheme based on the volume fraction of the constituent microstructure gives the static effective parameters. Conversely, by acknowledging the varying sound speeds of the microstructure and interface scattering, the effective medium resulting from dynamic homogenization maintains the dispersive fingerprint of the original composite microstructure. An ensemble averaging scheme accounting for the state of the microstructure under dynamic conditions returns the dynamic effective parameters. At this point, we offer a brief, non-exhaustive history of homogenization.

Premier attempts at dynamic homogenization considered the long-wavelength, quasi-static limit in which it is revealed that the effective parameters are nonlocal [83]. With the aid of energy methods, [84] and [85] sought to place bounds on the elastic properties of randomly inhomogeneous composites. Earlier, Ref. [67] asserted that the dynamic effective density could differ from the static version even in the long-wavelength regime. However, due to a lack of experimental reinforcement among other limitations, further theoretical and experimental support was needed, for example,

as given by Refs. [68] and [21], respectively. In general, the dynamic effective properties of a homogenized medium are nonlocal in space and time. For the general dynamic case, Ref. [86] rigorously demonstrated a revised constitutive model in which stress is not only coupled to strain but also the material velocity, and the momentum density is not only related to the material velocity but the strain as well. The elegance of the Willis constitutive model, however, does not explicitly lend itself to the determination of the effective material parameters at finite frequencies. In one dimension, Ref. [87] addressed this by employing a Magnus series expansion of a Floquet wavenumber matrix. Using the plane wave expansion method, Ref. [88] extended the analytic determination of effective material properties to three dimensions. In addition, several numerical techniques were developed for one-dimensional [89, 90] and three-dimensional periodic composites [91]. Other techniques expedite classical band structure calculations [92, 93].

In recent years, periodic elastic composites have garnered the attention of the scientific and engineering community. Whether due to Bragg scattering [45] or local resonances [8], the dispersive nature of periodic materials can be exploited as a passive form of vibration control. Certain extraordinary applications such as sub-wavelength acoustic imaging [72], acoustic cloaking [94], and flow control [95] are also the subject of many ambitious investigations. The effective properties acquired by periodic materials are key to the development of many of these applications. Composites with certain internal components have been shown to acquire negative or anisotropic effective properties [96, 97]. Reference [90] demonstrated simultaneously negative dynamic effective density and compliance due to local resonance. Recently, an elastic composite with multiple resonating microstructures exhibited fluid-like behavior within a specific range where only compression wave propagation was permitted [27].

In the context of Bloch's theorem, the temporal parameter describing damped wave behavior in time may, in general, take one of two forms: imaginary [14, 48] or complex [60, 63, 77]. In the former circumstance, wave motion is prescribed at a given frequency. One may imagine this scenario as the result of sustained harmonic forcing at the end of a semi-infinite medium. In the latter event, free wave propagation occurs. One may imagine this scenario as the result of an initial

impulse at the end of a semi-infinite medium. Absent energy dissipation, the propagating wave is identical both conditions. In one situation, energy dissipates over propagation distance. In the other condition, energy dissipates over time. Naturally, the effective properties respond to damping and the distinction between the two forms of wave motion. Motivated by the unique behavior of prescribed and free wave propagation in dissipative environments, and the consequences for the calculated the effective properties, this chapter seeks to illustrate the effects of material damping on the frequency band structure and effective properties of periodic materials.

3.3 Theory

In this section, the necessary mathematical procedures are developed to calculate the dynamic effective properties of a one-dimensional, layered periodic material (a phononic crystal) with material damping. The strategy rests on the spatial averaging of the periodic field quantities; however, as the determination of the field variables is a secondary consideration, the presentation of the homogenization procedure is followed by a brief review of the transfer matrix method used in the field variable calculation.

3.3.1 Homogenization for a 1D Phononic Crystal with Damping

Before addressing the homogenization method, we briefly discuss the distinguishing characteristics of prescribed and free wave propagation. These can be revealed by examining the one-dimensional equations of motion for a damped, homogeneous material.

$$Eu_{xx} + \eta u_{xxt} = \rho u_{tt} \tag{3.1}$$

In this case, the density ρ, Young's modulus E, and viscous dissipation parameter η, as well as the field quantities are all nonlocal. In the extended medium, a plane wave solution describes the propagating wave.

$$u(x,t) = U\mathrm{e}^{\mathrm{i}\kappa x+\lambda t} \tag{3.2}$$

Naturally, the variables x and t represent position and time, respectively. In the exponent, the wave envelope is characterized by the wavenumber κ, which defines the wave spatial frequency, and the parameter λ, which describes different time-dependent wave attributes for prescribed and free propagation.

For prescribed propagation, λ has a defined, strictly imaginary value representing the wave oscillation frequency. When the motion is prescribed, $\lambda = -\mathrm{i}\omega$ and a particular secular equation emerges from equations (3.1) and (3.2):

$$-\kappa^2(E - \mathrm{i}\omega\eta) + \omega^2\rho = 0. \tag{3.3}$$

The mandate of prescribed motion that the frequency ω be a real value obligates the wavenumber to reconcile the conservative and dissipative forces by adopting a complex value for all $\omega > 0$. Thus, energy is dissipated over propagation distance.

Different wave characteristics emerge from (3.1) and (3.2) in the free propagation condition for which λ is not predefined:

$$\kappa^2(E + \lambda\eta) + \lambda^2\rho = 0. \tag{3.4}$$

From (3.4) and the work of Ref. [59], we expect λ to be constructed as follows:

$$\begin{aligned} \lambda &= -\left(\frac{\kappa\eta}{2\rho c}\right)(\kappa c) \pm \mathrm{i}\kappa c\sqrt{1 - \left(\frac{\kappa\eta}{2\rho c}\right)^2} \\ &= -\xi\omega \pm \mathrm{i}\omega\sqrt{1 - \xi^2} \\ &= -\xi\omega \pm \mathrm{i}\omega_\mathrm{d}, \end{aligned} \tag{3.5}$$

where $c = \sqrt{E/\rho}$ is the speed of sound in the medium, and ω, ω_d, and ξ, respectively, are the undamped and damped wave frequencies, and associated damping ratio. With λ free to acquire any value in the left complex plane, a damped wave dissipates energy over time. Only in the absence of damping are the prescribed and free propagation models necessarily equivalent and $\lambda = \mathrm{i}\omega$.

Turning to heterogeneous, periodic materials, in the context of Bloch wave propagation, the

relevant one-dimensional field variables are modified by a time-dependent plane wave envelope:

$$u(x,t) = U(x)\mathrm{e}^{\mathrm{i}\kappa x+\lambda t}, \tag{3.6a}$$

$$\epsilon(x,t) = u_x = \mathcal{E}(x)\mathrm{e}^{\mathrm{i}\kappa x+\lambda t}, \tag{3.6b}$$

$$s(x,t) = u_{xt} = \lambda\mathcal{E}(x)\mathrm{e}^{\mathrm{i}\kappa x+\lambda t}, \tag{3.6c}$$

$$\sigma(x,t) = [E(x)+\lambda\eta(x)]\mathcal{E}(x)\mathrm{e}^{\mathrm{i}\kappa x+\lambda t} = [\Sigma_{\mathrm{c}}(x)+\Sigma_{\mathrm{nc}}(x)]\mathrm{e}^{\mathrm{i}\kappa x+\lambda t}, \tag{3.6d}$$

where equations (3.6) are, respectively, the displacement, strain, strain-rate, and stress. Notice, the stress is composed of both conservative and nonconservative components, proportional to both the strain and the strain-rate, respectively. Adhering to Bloch's theorem, the field quantities $U(x)$, $\mathcal{E}(x)$, $\Sigma_{\mathrm{c}}(x)$, and $\Sigma_{\mathrm{nc}}(x)$ have the periodicity of the phononic crystal unit cell.

The homogenization scheme presented here is adapted from that of Ref. [89] to incorporate a viscous dissipation parameter. For a periodically layered material, we define the reference position $x = 0$ to be the left boundary of the phononic crystal unit cell. To arrive at the homogenized medium, each of the periodic field variables is averaged over the span of the unit cell to render them nonlocal

$$\bar{A} = \frac{1}{a}\int_0^a A(x)\mathrm{d}x, \tag{3.7}$$

where a is the lattice constant and $A(x)$ is an arbitrary field quantity. It is worth noting that, in the absence of spatial attenuation (due to damping or wave interference), real-valued effective parameters emerge if the average is calculated over a symmetric unit cell. Coupling among the field variables yields complex effective parameters if the unit cell is not symmetric [89]. With the homogenized field quantities, we may identify separate relations for prescribed and free wave propagation leading to the formulation of effective material parameters.

For the homogenized medium, the following mean constitutive relation and characteristic equation hold for every (κ,λ) pair of the original dispersion relation

$$\bar{\Sigma} = \bar{\Sigma}_{\mathrm{c}} + \bar{\Sigma}_{\mathrm{nc}} = (E_{\mathrm{eff}} + \lambda\eta_{\mathrm{eff}})\bar{\mathcal{E}}, \tag{3.8}$$

$$\kappa^2(E_{\mathrm{eff}} + \lambda\eta_{\mathrm{eff}}) + \lambda^2\rho_{\mathrm{eff}} = 0, \tag{3.9}$$

with λ representative of either prescribed or free wave propagation. Together, equations (3.8) and (3.9) allow the formulation of the effective properties in terms of the homogenized strain and stress components.

$$\rho_{\text{eff}} = -\frac{\kappa^2 \bar{\Sigma}}{\lambda^2 \bar{\mathcal{E}}} \tag{3.10a}$$

$$\eta_{\text{eff}} = \frac{\bar{\Sigma}_{\text{nc}}}{\lambda \bar{\mathcal{E}}} \tag{3.10b}$$

$$E_{\text{eff}} = \frac{\bar{\Sigma}_{\text{c}}}{\bar{\mathcal{E}}} \tag{3.10c}$$

3.3.2 Transfer Matrix Implementation

For a layered periodic medium (Fig. 3.1) composed of two or more material layers, the transfer matrix method enforces the continuity conditions that exist between layers to relate layer boundary states (displacement and stress) from one layer to the next. If the displacement and stress states at the boundary of one layer are known, then the corresponding states at the opposite boundary (shared by the current layer and the adjacent layer) can be derived from a simple matrix operation. Thus transferring boundary states across each layer of the unit cell produces a system matrix that relates the states at opposite ends of the unit cell. In conjunction with Bloch's theorem, this system matrix is then utilized to generate an eigenvalue problem. The mathematical derivation of this method is provided below.

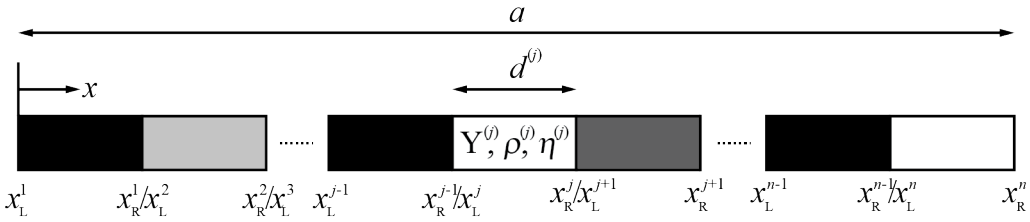

Figure 3.1: Continuous model of a multi-phased 1D phononic crystal with lattice spacing a.

For an arbitrary homogeneous layer j in the unit cell, the associated material properties are denoted as $\rho^{(j)}$, $E^{(j)}$, and $\eta^{(j)}$. The layer is bordered by layer $j-1$ on the left and layer $j+1$ on the right. Given the thickness of any layer j of the unit cell is $d^{(j)}$, the lattice spacing is $a = \sum_{j=1}^{n} d^{(j)}$

for a unit cell with n layers. Following this notation and accounting for forward and backward traveling waves, equation (3.2) becomes

$$u(x,t) = \left[U_+^{(j)} \mathrm{e}^{\mathrm{i}\kappa^{(j)}x} + U_-^{(j)} \mathrm{e}^{-\mathrm{i}\kappa^{(j)}x}\right] \mathrm{e}^{\lambda t}, \tag{3.11}$$

where $\kappa^{(j)}$ is the layer-specific wavenumber determined by solving either equation (3.3) or, according to equation (3.4), $[\kappa^{(j)}]^4(\eta^{(j)}/2\rho^{(j)})^2 - [\kappa^{(j)}c^{(j)}]^2 + \omega_\mathrm{d}^2 = 0$ (the smallest magnitude solutions are physical). We can write the spatial components of displacement and stress in matrix form as

$$\begin{bmatrix} u(x) \\ \sigma(x) \end{bmatrix} = \begin{bmatrix} 1 & 1 \\ \mathrm{i}Z^{(j)} & -\mathrm{i}Z^{(j)} \end{bmatrix} \begin{bmatrix} \mathrm{e}^{\mathrm{i}\kappa^{(j)}x} & 0 \\ 0 & \mathrm{e}^{-\mathrm{i}\kappa^{(j)}x} \end{bmatrix} \begin{bmatrix} U_+^{(j)} \\ U_-^{(j)} \end{bmatrix} = \mathbf{B}_j \mathbf{C}_j(x) \mathbf{u}_j. \tag{3.12}$$

where $Z^{(j)} = \kappa^{(j)}(E^{(j)} - \mathrm{i}\omega\eta^{(j)})$ if the motion is prescribed, otherwise $Z^{(j)} = \kappa^{(j)}(E^{(j)} + \lambda\eta^{(j)})$.

We now seek to relate the boundary states at the left boundary, $x = x_\mathrm{L}^{(j)}$, of an arbitrary layer to those at the right boundary, $x = x_\mathrm{R}^{(j)}$. To accomplish this, we define $x_\mathrm{R}^{(j)} = x_\mathrm{L}^{(j)} + d^{(j)}$ and insert this into Eq. (3.12) as follows:

$$\begin{bmatrix} u(x_\mathrm{R}^{(j)}) \\ \sigma(x_\mathrm{R}^{(j)}) \end{bmatrix} = \mathbf{B}_j \mathbf{C}_j(d^{(j)}) \mathbf{C}_j(x_\mathrm{L}^{(j)}) \mathbf{u}_j. \tag{3.13}$$

By setting $x = x_\mathrm{L}^{(j)}$ in Eq. (3.12), we rewrite Eq. (3.13) as

$$\begin{bmatrix} u(x_\mathrm{R}^{(j)}) \\ \sigma(x_\mathrm{R}^{(j)}) \end{bmatrix} = \mathbf{B}_j \mathbf{C}_j(d^{(j)}) \mathbf{B}_j^{-1} \begin{bmatrix} u(x_\mathrm{L}^{(j)}) \\ \sigma(x_\mathrm{L}^{(j)}) \end{bmatrix} = \mathbf{T}_j \begin{bmatrix} u(x_\mathrm{L}^{(j)}) \\ \sigma(x_\mathrm{L}^{(j)}) \end{bmatrix}, \tag{3.14}$$

where $\mathbf{T}_j$, the *transfer matrix* for layer j, has the expanded form

$$\mathbf{T}_j = \begin{bmatrix} \cos(\kappa^{(j)}d^{(j)}) & (1/Z^{(j)})\sin(\kappa^{(j)}d^{(j)}) \\ -Z^{(j)}\sin(\kappa^{(j)}d^{(j)}) & \cos(\kappa^{(j)}d^{(j)}) \end{bmatrix}. \tag{3.15}$$

Equation (3.14) relates the displacement and stress at $x_\mathrm{L}^{(j)}$ to those at $x_\mathrm{R}^{(j)}$ of the same layer. However, since the construction of the transfer matrix is valid for any layer and $x_\mathrm{R}^{(j)} \equiv x_\mathrm{L}^{(j+1)}$, the

result in Eq. (3.14) can be extended recursively across several layers. Thus,

$$\begin{aligned}
&\mathbf{y}(x_{\mathrm{R}}^1) = \mathbf{T}_1\mathbf{y}(x_{\mathrm{L}}^1) = \mathbf{y}(x_{\mathrm{L}}^2),\\
&\mathbf{y}(x_{\mathrm{R}}^2) = \mathbf{T}_2\mathbf{y}(x_{\mathrm{L}}^2) = \mathbf{T}_2\mathbf{T}_1\mathbf{y}(x_{\mathrm{L}}^1) = \mathbf{y}(x_{\mathrm{L}}^3),\\
&\mathbf{y}(x_{\mathrm{R}}^3) = \mathbf{T}_3\mathbf{y}(x_{\mathrm{L}}^3) = \mathbf{T}_3\mathbf{T}_2\mathbf{T}_1\mathbf{y}(x_{\mathrm{L}}^1) = \mathbf{y}(x_{\mathrm{L}}^4),\\
&\vdots\\
&\mathbf{y}(x_{\mathrm{R}}^n) = \mathbf{T}_n\mathbf{T}_{n-1}\cdots\mathbf{T}_1\mathbf{y}(x_{\mathrm{L}}^1) = \mathbf{T}\mathbf{y}(x_{\mathrm{L}}^1).
\end{aligned} \tag{3.16}$$

In the interest of clarity, we have defined $y(x) = [u(x)\ \ \sigma(x)]^{\mathrm{T}}$ to be the state vector at x. Ultimately, the displacement and stress at the left end of the first layer ($x = x_{\mathrm{L}}^1$) in a unit cell are related to those at the right boundary of the nth layer ($x = x_{\mathrm{R}}^n$) by the *cumulative transfer matrix*, $\mathbf{T}$. More direct, Bloch's theorem asserts that the state at a given point in a unit cell differs from that of the corresponding point in an adjacent unit cell by only a phase multiplier of $\mathrm{e}^{\mathrm{i}\kappa a}$ (κ is the global wavenumber applying to the periodic medium). This relation is given by $h(x + a) = h(x)\mathrm{e}^{\mathrm{i}\kappa a}$, which, for the problem at hand, entails

$$\mathbf{y}(x_{\mathrm{R}}^n) = \mathrm{e}^{\mathrm{i}\kappa a}\mathbf{y}(x_{\mathrm{L}}^1). \tag{3.17}$$

Equating Eqs. (3.16) and (3.17) yields the eigenvalue problem

$$[\mathbf{T} - \mathbf{I}\gamma]\mathbf{y}(x_{\mathrm{L}}^1) = \mathbf{0}, \tag{3.18}$$

where $\gamma = \mathrm{e}^{\mathrm{i}\kappa a}$. The solution of Eq. (3.18), which appears in complex conjugate pairs, provides the dispersion relations for the 1D phononic crystal. Real-valued wavenumbers, calculated from γ using Eq. (3.19a), support the propagating modes, whereas imaginary wavenumbers, extracted from γ using Eq. (3.19b), represent evanescent modes which decay in space. Together, $\kappa = \kappa_{\mathrm{R}} + \mathrm{i}\kappa_{\mathrm{I}}$.

$$\kappa_{\mathrm{R}} = \frac{1}{a}\mathrm{Re}[-\mathrm{iln}\gamma] \tag{3.19a}$$

$$\kappa_{\mathrm{I}} = \frac{1}{a}\mathrm{Im}[-\mathrm{iln}\gamma] \tag{3.19b}$$

In addition to the eigenvalue, γ, Eq. (3.18) yields the eigenvector (state vector), $\mathbf{y}(x_{\mathrm{L}}^1)$, containing the displacement and stress at the left boundary of the unit cell. With this result, we

present the following procedure for calculating the displacement and stress mode shapes in a 1D phononic material.

To have a fixed frame of reference, we designate the position of the left boundary of the unit cell at $x = x_{\mathrm{L}}^1 = 0$. Given that $\mathbf{C}_j(0) = \mathbf{I}$, according to Eq. (3.12), the eigenvector computed from Eq. (3.18) can expressed as:

$$\mathbf{y}(x_{\mathrm{L}}^1) = \mathbf{B}_1 \mathbf{u}_1. \tag{3.20}$$

Thus, the amplitude vector for the left end of the unit cell is easily determined:

$$\mathbf{u}_1 = \mathbf{B}_1^{-1} \mathbf{y}(x_{\mathrm{L}}^1). \tag{3.21}$$

Utilizing the transfer matrix, $\mathbf{T}_1$, we are able to relate $\mathbf{y}(x_{\mathrm{L}}^2)$ to $\mathbf{y}(x_{\mathrm{L}}^1)$ as

$$\mathbf{y}(x_{\mathrm{L}}^2) = \mathbf{T}_1 \mathbf{y}(x_{\mathrm{L}}^1) = \mathbf{B}_2 \mathbf{C}_2(x_{\mathrm{L}}^2) \mathbf{u}_2 \tag{3.22}$$

from which we obtain the amplitude vector for the left end of the second layer of a unit cell in terms of the computed eigenvector

$$\mathbf{u}_2 = \left[\mathbf{B}_2 \mathbf{C}_2(x_{\mathrm{L}}^2)\right]^{-1} \mathbf{T}_1 \mathbf{y}(x_{\mathrm{L}}^1). \tag{3.23}$$

With the aid of Eq. (3.16), this process may be extended to any layer j of a unit cell of n layers,

$$\mathbf{u}_j = \left[\mathbf{B}_j \mathbf{C}_j(x_{\mathrm{L}}^{(j)})\right]^{-1} \mathbf{T}_{j-1} \cdots \mathbf{T}_0 \mathbf{y}(x_{\mathrm{L}}^1) \tag{3.24}$$

where $\mathbf{T}_0 := \mathbf{I}$.

Once all $\mathbf{u}_j$ have been determined, the portion of the displacement and stress mode shapes within each layer in the first unit cell can be computed from Eq. (3.12). Specifically,

$$u(x) = U_+^{(j)} \mathrm{e}^{\mathrm{i}\kappa x} + U_-^{(j)} \mathrm{e}^{-\mathrm{i}\kappa x}, \tag{3.25a}$$

$$\sigma_{\mathrm{c}}(x) = \mathrm{i}\kappa^{(j)} E^{(j)} \left(U_+^{(j)} \mathrm{e}^{\mathrm{i}\kappa x} - U_-^{(j)} \mathrm{e}^{-\mathrm{i}\kappa x}\right), \tag{3.25b}$$

$$\sigma_{\mathrm{nc}}(x) = \omega \kappa^{(j)} \eta^{(j)} \left(U_+^{(j)} \mathrm{e}^{\mathrm{i}\kappa x} - U_-^{(j)} \mathrm{e}^{-\mathrm{i}\kappa x}\right), \tag{3.25c}$$

where, as anticipated, $\sigma(x) = \sigma_{\mathrm{c}}(x) + \sigma_{\mathrm{nc}}(x)$.

Table 3.1: Phononic crystal properties

Material 1	$\rho^{(1)} = 1000\text{kg/m}^3$	$E^{(1)} = 2\text{GPa}$
Material 2	$\rho^{(2)} = 3000\text{kg/m}^3$	$E^{(2)} = 200\text{GPa}$

3.4 Results and Discussion

The aim of this chapter, regarding to the dynamics of periodic media, is twofold: (1) to introduce the effective viscosity and to show the transformation of the effective properties in response to dissipative wave propagation, and (2) to illustrate the effects of material damping on the phononic band structure. Each of these objectives are pursued in the context of free and prescribed wave propagation. In essence, the homogenization procedure can be extended to two and three dimensions, however, in keeping with its one-dimensional presentation in this chapter, the results presented are for a one-dimensional phononic crystal. For simplicity, the phononic crystal is composed of two materials (Table 3.1) arranged such that the unit cell is symmetric – specifically $d^{(1)} = d^{(3)} = 2.5\text{mm}$ and $d^{(2)} = 5\text{mm}$. In the numerical case studies to follow, the density and Young's modulus of each constituent material remains constant while the viscosity is manipulated to show the evolution of the band structure and effective properties over a range of damping intensities. Although the viscosity of each constituent material may assume any positive value, we adopt the definition $\eta^{(j)} = qE^{(j)}$ [81], where q is a scaling parameter.

Figure 3.2 shows the dispersion curves corresponding to our bi-material phononic crystal and illustrates the effects of dissipation over a range of damping intensities. Each plot in Fig. 3.2 is divided into positive and negative wavenumber domains (non-dimensional) representing the propagating and evanescent modes, respectively. In actuality, the evanescent wavenumbers are not negative; rather, they are indicated as such to emphasize their attenuating nature. In addition the solid and dashed plotting styles that further distinguish real and imaginary components of the wavenumber, respectively, are a convention maintained in later figures.

First, we focus our attention on the free wave propagation scenario collectively depicted in

Figs 3.2a,c. By inspecting the frequency diagram in Fig. 3.2a, it is immediately evident that the influence dissipation increases with frequency, a consequence of the linear dependence of dissipative tractions on the strain-rate. The descent of the frequency band in response to material damping is supported by the corresponding damping ratio diagram in Fig. 3.2c. For the free propagation scenario, the damping ratio diagram measures the temporal attenuation of the wave in response to energy loss. Consistent with its structural dynamics interpretation, as the damping ratio approaches unity, temporal oscillations decrease to zero. Interestingly, as higher frequency bands descend more rapidly than those below, the frequency range of the band gap narrows and its central value shifts downward. Nevertheless, throughout the evolution of the band structure, the band gaps remain clearly identifiable provided $\kappa^{(j)} \in \mathbb{R}$ (i.e., $\omega_{\mathrm{d}}\eta^{(j)} \leq E^{(j)}$).

Now, we turn our attention to the prescribed propagation scenario illustrated by Figs. 3.2b. As stated earlier and verified in a comparison of Figs. 3.2a and 3.2b, in the absence of damping, free and prescribed wave propagation are identical. In the presence of damping, the two propagation types may be distinguished in several ways. Most apparent is the lack of a damping ratio diagram as a result of mandating $\lambda = -\mathrm{i}\omega$. In this case, energy dissipation occurs over the wave's propagation distance rather than over time. Thus band gaps, their identification less obvious, melt into propagating bands. The effect becomes more severe at higher frequencies as a near-linear dependency develops between the complex wavenumber and the real frequency.

Given their frequency dependence, the influence of dissipation extends beyond the frequency band structure to impact the effective parameters. For free and prescribed wave propagation, respectively, Figs. 3.3a,c,e and 3.3b,d,f display the effective dynamic material properties for our representative damped phononic crystal. By declaring the strain-rate, rather than the displacement or acceleration, to be the only relevant state variable in determination of dissipative tractions, dissipation causes the dynamic effective density and Young's modulus to be joined by a dynamic effective viscosity. Introducing damping through a complex Young's modulus, Ref. [90] found dissipation yielded imaginary components to the effective density and Young's modulus but no effective damping parameter. In Figs. 3.3a,c,e and 3.3b,d,f, complex components arise in regions of

spatial attenuation. These regions are the interference-induced band gaps in the free propagation scenario and the interference- and/or dissipation-induced attenuation for prescribed waves.

In the long-wavelength limit, a single wavelength encompasses many unit cells and loses its ability to resolve the inhomogeneity of the phononic crystal. Instead, the propagating wave observes the static effective properties (the filling-fraction weighted average of the unit cell constituent materials). In Fig. 3.2, this regime manifests itself in regions of the diagrams where there is near linear relationship between frequency and wavenumber. The results displayed in Fig. 3.3 provide a level of confidence in the homogenization procedure presented in section 3.3. In the long-wavelength limit, when the response of the phononic crystal is nearly static, each of the effective parameters in Fig. 3.3 approach the relevant unique effective static parameter irrespective of the dissipation. In addition, while the dynamic effective density and Young's modulus always return to the same effective static values in the long-wavelength limit regardless of damping, the dynamic effective viscosity returns to different static values as the level of damping changes. Moreover, due to our specific Rayleigh damping model, $\eta_{\text{eff}} = qE_{\text{eff}}$. Beyond the long-wavelength limit, the motion of the sub-wavelength constituents appreciably effect the wave dynamics, and a generalization of Newton's second law causes the dynamic effective properties to deviate from the static ones.

As a final testament to the damped dynamic homogenization procedure of section 3.3, we substitute λ and the appropriate effective parameters into equations (3.3) and (3.4), and then solve for κ to reconstruct the free (Fig. 3.4a and 3.4c) and prescribed (Fig. 3.4b) dispersion diagrams, validating the proposed scheme.

3.5 Conclusions

In this work, we demonstrated the consequences of prescribed and free dissipative wave propagation on the dynamic effective properties of a viscously damped periodic material. To this end, a modified form of the homogenization scheme in Ref. [89] was used to define the effective parameters in terms of the averaged field variables and the dispersion characteristics of our model phononic crystal. The calculated dynamic effective properties approach the appropriate static

values in the long-wavelength limit and are able to reconstruct the damped dispersion relations, providing solid verification of the results. This is the first time a frequency-dependent effective damping parameter has been determined. The incorporation of damping is a necessity as dissipation is an inherent and potentially functional property of actual materials. While this chapter employs a viscous damping model, we acknowledge that a nonviscous, hereditary dissipation model [54, 80] could yield qualitatively different results.

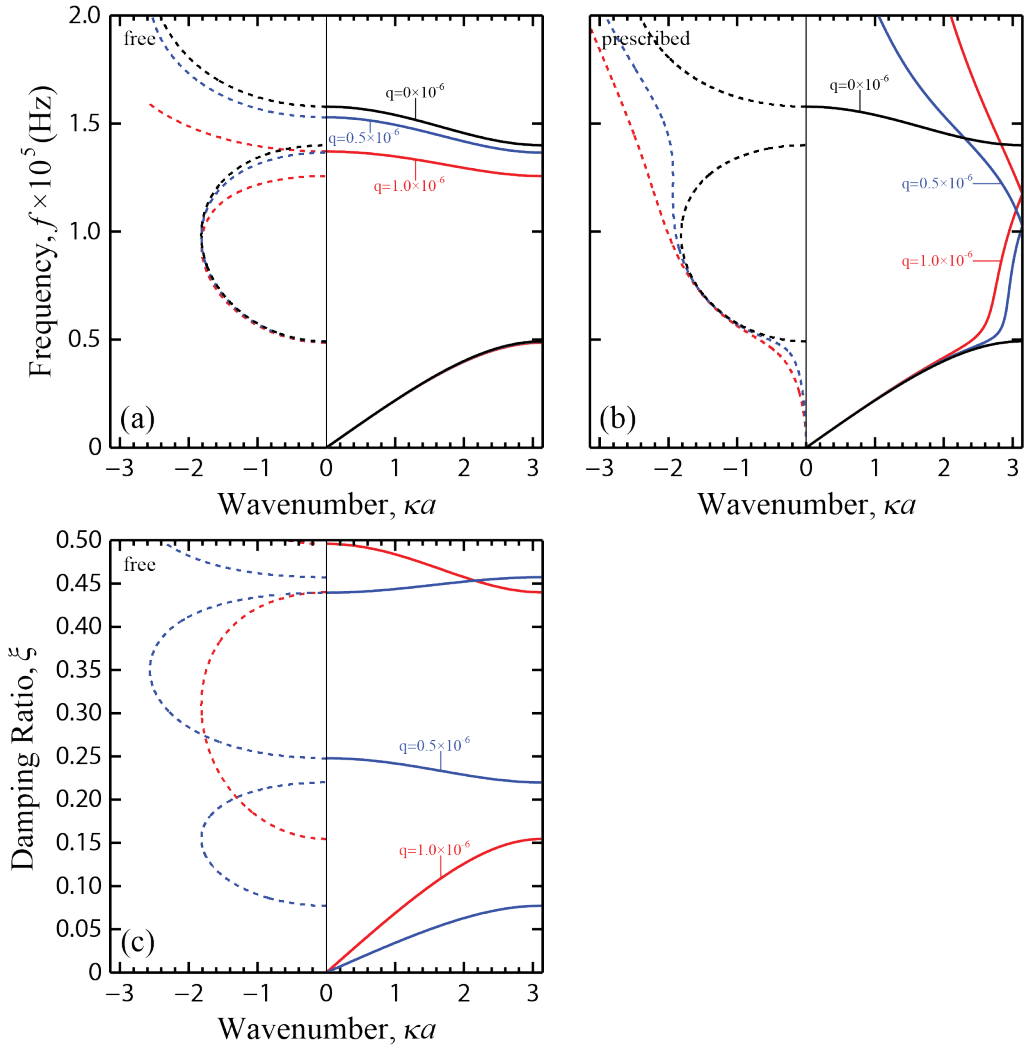

Figure 3.2: The frequency band structure for (a) free and (b) prescribed wave propagation under various damping conditions: undamped (—) $q = 0$, and damped (—) $q = 0.5 \times 10^{-6}$ and (—) $q = 1.0 \times 10^{-6}$. The damping ratio band structure (c) is unique to dissipative free wave propagation.

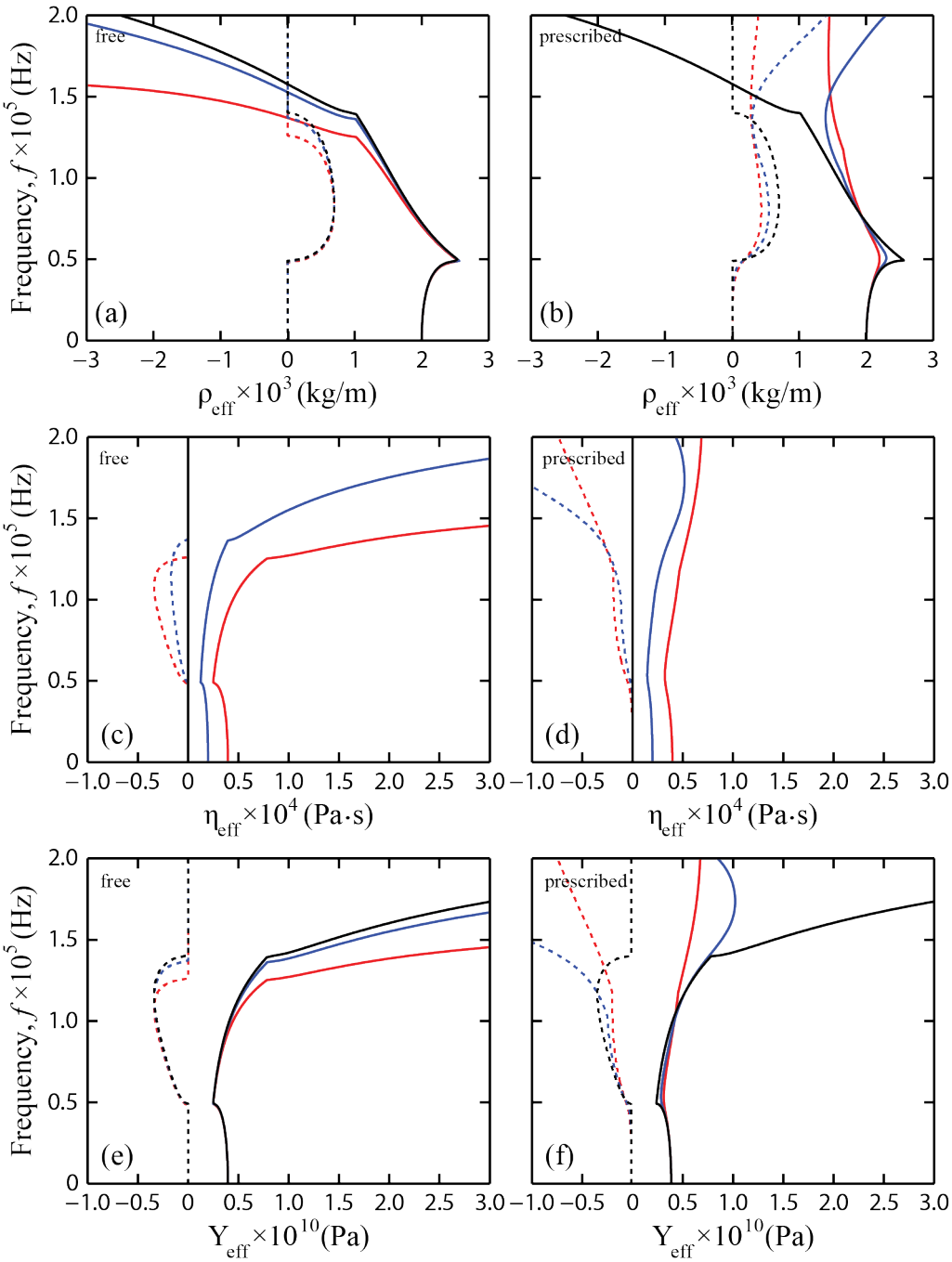

Figure 3.3: Dynamic effective material properties – density, viscosity, and Young's modulus – for a two-phased, one-dimensional phononic crystal experiencing free [(a), (c), and (e)] and prescribed [(b), (d), and (f)] wave propagation. Scaling parameters: (—) $q = 0$, (—) $q = 0.5 \times 10^{-6}$, and (—) $q = 1.0 \times 10^{-6}$.

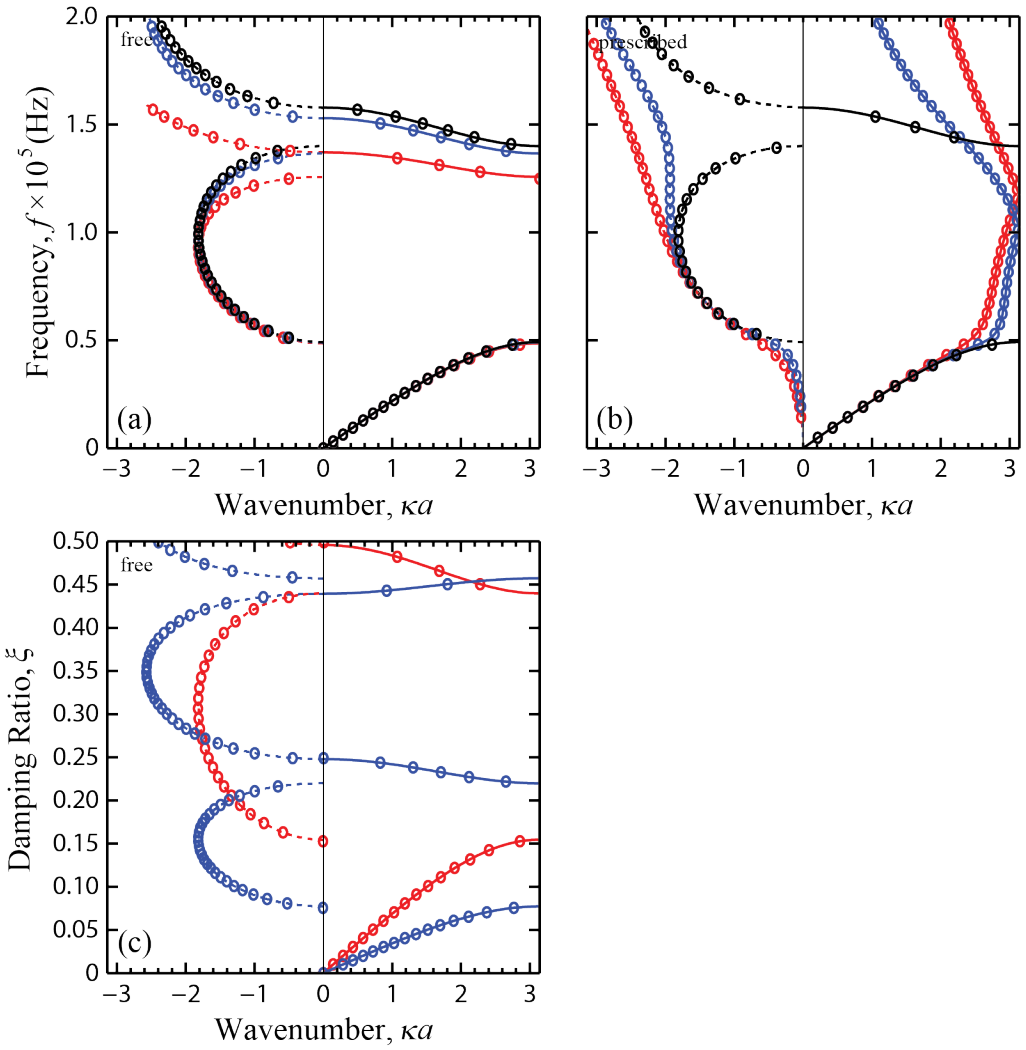

Figure 3.4: Comparing dispersion diagrams of a two-phased, one-dimensional phononic crystal (curves) and its homogeneous counterpart (open circles) with dynamic effective properties. Free [(a) and (b)] and prescribed (c) wave propagation are considered. Scaling parameters: (—) $q = 0$, (—) $q = 0.5 \times 10^{-6}$, and (—) $q = 1.0 \times 10^{-6}$.

Chapter 4

State-Space Formulation and Modal Analysis[3]

4.1 Abstract

In this chapter, we present theoretical formalisms for the study of wave dispersion in damped elastic periodic materials. We adopt the well-known structural dynamics techniques of modal analysis and state-space transformation and formulate them for the Bloch wave propagation problem. First, we consider a one-dimensional lumped parameter model of a phononic crystal whereby two masses connected by springs and viscous dashpot dampers compose the unit cell. We then extend our analysis to the study of a two-dimensional phononic crystal, modeled as a dissipative elastic continuum, and consisting of square inclusions periodically distributed within a host material. For our damping model, we consider both proportional damping and general damping. Our results demonstrate the effects of a range of damping levels on the frequency band structure for two distinct damping scenarios. In particular, we reveal two intriguing phenomena: branch overtaking and branch cut-off. The former may result in an abrupt drop in the relative band gap size, and the latter implies an opening of full or partial wavenumber (wave vector) band gaps. Following our frequency band structure analysis, we illustrate the concept of a damping ratio band structure.

4.2 Introduction

Phononic crystals are elastic materials whereby the microstructure geometry or constituent material phases are distributed periodically in space. With careful size scaling and choice of the

[3] This chapter is adapted from Hussein and Frazier, *Journal of Applied Physics* (2010).

constituent material phases and their spatial distribution within the periodic unit cell, phononic crystals can be designed to classically control the propagation of acoustic/elastic waves in a predetermined manner. In doing so, these modern materials have opened up a technological frontier in acoustic and elastic devices [17, 45, 98]. Bloch theory [3] provides the underlying mathematical framework for obtaining the fundamental wave propagation characteristics in phononic crystals. Through this theory, it is possible to obtain a relationship between frequency and wavenumber (wave vector) — this relationship is referred to as the frequency band structure. In many cases, one or more of the constituent materials are damped (i.e., dissipative), a good example is viscoelastic materials which are often used to form the matrix phase in phononic crystal composites. The presence of damping results in temporal and spatial attenuations of the elastic waves as they freely "progress" through the periodic media [48]. It is therefore necessary to establish rigorous theoretical formalisms for damped Bloch wave propagation, which is the objective of this chapter.

To follow is a brief survey of various studies in the literature that dealt with damping in infinite (and finite) periodic materials (and structures). In an early study focusing on one-dimensional (1D) discrete mass-spring-dashpot models, Mead [48] considered structural (velocity independent) damping as well as a hypothetical type of damping associated with what was referred to as "damped forced modes". Viscous damping was treated later on with various types of dissipative constitutive models. Mukherjee and Lee [60], for example, provided a dispersion relation using a complex elastic modulus to model viscoelasticity in a 1D laminated medium. Tassilly [14] on the other hand considered viscous damping which was mathematically incorporated in the governing equations as a *separate* term representing velocity-dependent damping forces. He analyzed 1D periodic beam structures suspended on an elastic foundation, which is a unique configuration that produces no acoustical branches in the frequency spectrum. In other studies, often the focus has been on finite structures or there was little consideration of the broad effects on the band structure characteristics (e.g., Refs. [51, 99, 100]). Some studies explicitly investigated the band structure using viscoelastic damping models, although limited to a fixed frequency [61, 62] or to low frequencies [75]. Wang *et al.* [76] analytically studied dispersion in 1D viscoelastic lattices with a model applicable to a wide

frequency range. Merheb *et al.* [54] also provided a study that was not limited to certain frequencies, using the finite difference time-domain method in addition to experiments. Yet both these studies did not provide a detailed analysis of the broad effects of damping on the dispersion band structure. In Ref. [54], the conclusions were focused on the spatial attenuation/decay effects. Recently, Lee *et al.* [101] proposed a method whereby effective medium theory is employed in conjunction with the transfer matrix method to analyze 1D damped periodically layered materials.

In Refs. [102] and [63], the concept of *Bloch modal analysis* has been introduced for the study of the dynamics of periodic media. The concept was first employed for the purpose of model reduction for band structure calculations [102], and was later utilized for the study of the effects of proportional (Rayleigh) damping on the band structure and phase and group velocity dispersion relations [63]. In this chapter, we further utilize Bloch modal analysis towards investigating the effects of both stiffness- and mass-proportional damping on the dispersion relation. Our primary objective, however, is to broaden our treatment of damped periodic media by developing a theoretical formalism, based on state-space transformation, for the study of systems with general damping. For both the proportional damping and general damping problems, we consider 1D and two-dimensional (2D) viscously damped phononic crystal models and explicitly show the effects of damping on the frequency versus wavenumber wave vector curves. In doing so, we highlight two intriguing phenomena — *branch overtaking* and *branch cut-off*. In branch overtaking the presence of damping causes the higher branches in the band structure to drop in frequency at rates that exceed the drop rates for lower branches, thus causing the overtake. Branch cut-off refers to a state whereby a dispersion branch does not cover the entire first Brillouin zone, thus creating a full or a partial band gap with respect to the wavenumber (wave vector) as opposed to the frequency. Finally we correlate our frequency band structure analysis with the corresponding representation of the damping ratio-wavenumber (wave vector) relations, i.e., *damping ratio band structure*.

In this work, we consider constant damping parameters in our treatment of viscous damping. However, since we assume harmonic motion in time, the viscous dissipation force, $\mathbf{f}_{\text{vd}}$ is frequency-dependent, i.e., $\mathbf{f}_{\text{vd}} = \hat{\mathbf{C}}\dot{\mathbf{u}} = \lambda(\omega)\hat{\mathbf{C}}\mathbf{u}$, where $\mathbf{u}$ denotes the displacement vector, $\hat{\mathbf{C}}$ denotes the

damping matrix, $\lambda(\omega)$ denotes a frequency-dependent coefficient, ω denotes frequency, and the dot symbolizes differentiation with respect to time. This is in contrast, for example, to what is known as structural damping which generates a frequency-independent force $\mathbf{f}_{\text{sd}} = \mathrm{i}\mu\hat{\mathbf{K}}\mathbf{u}$, where $\hat{\mathbf{K}}$ denotes the stiffness matrix, μ is a damping parameter, and $\mathrm{i} = \sqrt{-1}$. Reference to the frequency-dependence of damping is often made to the damping matrix itself as opposed to the damping forces. Incorporating frequency-dependence in the $\hat{\mathbf{C}}$ matrix, i.e., $\hat{\mathbf{C}} = \hat{\mathbf{C}}(\omega)$, is a subject for future research.

The layout of the chapter consists of two parts: Sec. 4.3 covers a discrete model and Sec. Sec. 4.4 covers a continuous model. In each section, we present the theory and subsequently provide numerical examples for both proportional and general damping.

4.3 Discrete Model

4.3.1 Theory

We begin our study of damped periodic materials by considering a simple 1D lumped parameter lattice model which we use to demonstrate the basic characteristics of dispersive behavior due to damping. Our system, which is by definition infinite in extent, is constructed by appending copies of the two-mass unit cell of Fig. 4.1 along the line of motion. The lattice spacing is denoted by a.

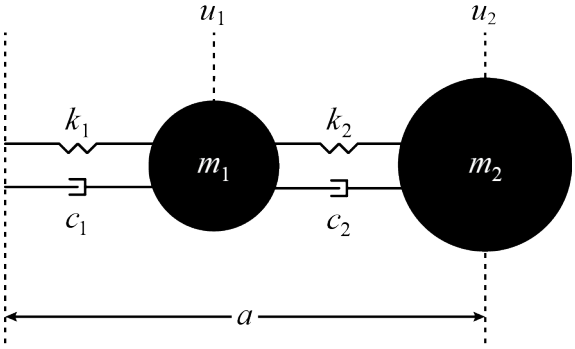

Figure 4.1: Discrete model of phononic crystal: two-mass unit cell.

The set of equations that describe the motion of the two masses, m_1 and m_2, in the unit cell

are

$$m_1\ddot{u}_1^j + (c_1+c_2)\dot{u}_1^j + (k_1+k_2)u_1^j - c_2\dot{u}_2^j - k_2u_2^j - c_1\dot{u}_2^{j-1} - k_1u_2^{j-1} = 0, \tag{4.1}$$

$$m_2\ddot{u}_2^j + (c_1+c_2)\dot{u}_2^j + (k_1+k_2)u_2^j - c_2\dot{u}_1^j - k_2u_1^j - c_1\dot{u}_1^{j+1} - k_1u_1^{j+1} = 0, \tag{4.2}$$

where u_ℓ^j represents the displacement of mass ℓ in the jth unit cell.

We assume a plane wave solution

$$u_\ell^j(x,\kappa,t) = \tilde{u}_\ell \mathrm{e}^{\mathrm{i}\kappa x+\lambda t}, \tag{4.3}$$

for mass ℓ at the jth lattice point, where $\tilde{u}_\ell$, κ, x, and t denote the complex wave amplitude, wavenumber, position, and time, respectively. It should be noted that x is not continuous, reflecting the discreteness of the material model. Moreover, because the unit cell resides at each lattice point, the wave may only be sampled at those points, i.e., $x = \{-ja, \ldots, -a, 0, a, \ldots, ja\}$ (j is an integer). Due to the periodicity of the solution, the following statement holds for the displacement of mass ℓ at neighboring lattice points.

$$u_\ell^{j+n}(x+na,\kappa,t) = u_\ell^j(x,\kappa,t)\mathrm{e}^{\mathrm{i}n\kappa a}, \tag{4.4}$$

In Eq. (4.4), the integer $n = 0$ for the present unit cell, $n = 1$ for the subsequent unit cell, and $n = -1$ for the previous unit cell. Substituting Eq. (4.4) into Eqs. (4.1) and (4.2) yields two homogeneous equations for u_1 and u_2, respectively, i.e., in matrix form

$$\hat{\mathbf{M}}\ddot{\mathbf{u}} + \hat{\mathbf{C}}\dot{\mathbf{u}} + \hat{\mathbf{K}}\mathbf{u} = \mathbf{0}, \tag{4.5}$$

where $\hat{\mathbf{M}}$ denotes the mass matrix and $\mathbf{u} = [u_1 \;\; u_2]^{\mathrm{T}}$ [$(\cdot)^{\mathrm{T}}$ denotes the transpose operation]. The

$\hat{\mathbf{M}}$, $\hat{\mathbf{C}}$, and $\hat{\mathbf{K}}$ matrices are explicitly defined as follows:

$$\hat{\mathbf{M}} = \begin{bmatrix} m_1 & 0 \\ 0 & m_2 \end{bmatrix}, \tag{4.6a}$$

$$\hat{\mathbf{C}} = \begin{bmatrix} c_1 + c_2 & -(\mathrm{e}^{-\mathrm{i}\kappa a} c_1 + c_2) \\ -(\mathrm{e}^{\mathrm{i}\kappa a} c_1 + c_2) & c_1 + c_2 \end{bmatrix}, \tag{4.6b}$$

$$\hat{\mathbf{K}} = \begin{bmatrix} k_1 + k_2 & -(\mathrm{e}^{-\mathrm{i}\kappa a} k_1 + k_2) \\ -(\mathrm{e}^{\mathrm{i}\kappa a} k_1 + k_2) & k_1 + k_2 \end{bmatrix}. \tag{4.6c}$$

Applying the time derivatives, Eq. (4.5) becomes

$$(\lambda^2 \hat{\mathbf{M}} + \lambda \hat{\mathbf{C}} + \hat{\mathbf{K}})\mathbf{u} = \mathbf{0}, \tag{4.7}$$

For $\hat{\mathbf{C}} = \mathbf{0}$, the familiar eigenvalue problem emerges. With eigenvalue $\lambda^2 = -\omega^2$, the dispersion relation is easily obtained. In the case of the phononic crystal represented by the unit cell in Fig. 4.1, the undamped frequency-wavenumber relation is

$$\omega_s(\kappa) = \sqrt{\frac{(k_1 + k_2)(m_1 + m_2) \mp \sqrt{[(k_1 + k_2)(m_1 + m_2)]^2 - 8(1 - \cos\kappa a) k_1 k_2 m_1 m_2}}{2 m_1 m_2}}, \qquad s = 1, 2, \tag{4.8}$$

where s refers to the mode number, which in the context of a dispersion band structure is the branch number.

4.3.1.1 General damping

For the case of general damping (where the damping matrix $\hat{\mathbf{C}}$ is nonzero, Hermitian, but nonproportional to $\hat{\mathbf{M}}$ or $\hat{\mathbf{K}}$) it is not possible to set up a Bloch eigenvalue problem in the usual way because of the presence of the viscous damping term. We therefore resort to converting the second-order problem to a first-order problem through a state-space transformation [103, 104]

$$\hat{\mathbf{A}}\dot{\hat{\mathbf{y}}} + \hat{\mathbf{B}}\hat{\mathbf{y}} = \mathbf{0}. \tag{4.9}$$

where

$$\hat{\mathbf{A}} = \begin{bmatrix} \mathbf{0} & \hat{\mathbf{M}} \\ \hat{\mathbf{M}} & \hat{\mathbf{C}} \end{bmatrix}, \tag{4.10a}$$

$$\hat{\mathbf{B}} = \mathrm{diag}\begin{bmatrix} -\hat{\mathbf{M}} & \hat{\mathbf{K}} \end{bmatrix}, \tag{4.10b}$$

$$\hat{\mathbf{y}} = \begin{bmatrix} \dot{\mathbf{u}} & \mathbf{u} \end{bmatrix}^{\mathrm{T}}. \tag{4.10c}$$

For convenience, we define $r_{\mathrm{m}} = m_2/m_1$, $r_{\mathrm{c}} = c_2/c_1$, $r_{\mathrm{k}} = k_2/k_1$, and subsequently write the $\hat{\mathbf{M}}$, $\hat{\mathbf{C}}$, and $\hat{\mathbf{K}}$ matrices in terms of only m_2, c_2, and k_2 respectively,

$$\hat{\mathbf{M}} = m_2\hat{\mathbf{M}}_{\mathrm{o}} = m_2 \begin{bmatrix} 1/r_{\mathrm{m}} & 0 \\ 0 & 1 \end{bmatrix}, \tag{4.11a}$$

$$\hat{\mathbf{C}} = c_2\hat{\mathbf{C}}_{\mathrm{o}} = c_2 \begin{bmatrix} 1 + 1/r_{\mathrm{c}} & -(\mathrm{e}^{-\mathrm{i}\kappa a}/r_{\mathrm{c}} + 1) \\ -(\mathrm{e}^{\mathrm{i}\kappa a}/r_{\mathrm{c}} + 1) & 1 + 1/r_{\mathrm{c}} \end{bmatrix}, \tag{4.11b}$$

$$\hat{\mathbf{K}} = k_2\hat{\mathbf{K}}_{\mathrm{o}} = k_2 \begin{bmatrix} 1 + 1/r_{\mathrm{k}} & -(\mathrm{e}^{-\mathrm{i}\kappa a}/r_{\mathrm{k}} + 1) \\ -(\mathrm{e}^{\mathrm{i}\kappa a}/r_{\mathrm{k}} + 1) & 1 + 1/r_{\mathrm{k}} \end{bmatrix}. \tag{4.11c}$$

Utilizing this notation and dividing by m_2, the state-space matrices $\hat{\mathbf{A}}$ and $\hat{\mathbf{B}}$ become

$$\hat{\mathbf{A}} = \begin{bmatrix} \mathbf{0} & \hat{\mathbf{M}}_{\mathrm{o}} \\ \hat{\mathbf{M}}_{\mathrm{o}} & \beta\hat{\mathbf{C}}_{\mathrm{o}} \end{bmatrix}, \tag{4.12a}$$

$$\hat{\mathbf{B}} = \mathrm{diag}\begin{bmatrix} -\hat{\mathbf{M}}_{\mathrm{o}} & \omega_0^2\hat{\mathbf{K}}_{\mathrm{o}} \end{bmatrix}, \tag{4.12b}$$

where $\omega_0 = \sqrt{k_2/m_2}$ and $\beta = c_2/m_2$. We assume a solution for Eq. (4.10) of the form $\hat{\mathbf{y}} = \bar{\mathbf{y}}\mathrm{e}^{\gamma t}$. The damped frequency band structure can now be obtained by solving the associated eigenvalue problem. The eigenvalues, which appear in complex conjugate pairs, are solutions to the characteristic equation

$$\gamma^4 + a\gamma^3 + b\gamma^2 + c\gamma + d = 0, \tag{4.13}$$

with

$$a = \frac{(1+r_{\mathrm{c}})(1+r_{\mathrm{m}})\beta}{r_{\mathrm{c}}}, \tag{4.14a}$$

$$b = \frac{2(1-\cos\kappa a)r_{\mathrm{k}}r_{\mathrm{m}}\beta^2 + (1+r_{\mathrm{k}})(1+r_{\mathrm{m}})r_{\mathrm{c}}\omega_0^2}{r_{\mathrm{c}}r_{\mathrm{k}}}, \tag{4.14b}$$

$$c = \frac{2(1-\cos\kappa a)(r_{\mathrm{c}}+r_{\mathrm{k}})r_{\mathrm{m}}\beta\omega_0^2}{r_{\mathrm{c}}r_{\mathrm{k}}}, \tag{4.14c}$$

$$d = \frac{2r_{\mathrm{m}}\omega_0^4(1-\cos\kappa a)}{r_{\mathrm{k}}}. \tag{4.14d}$$

The form of the solution resembles that from structural dynamics, except, in the context of Bloch wave propagation, the terms are dependent upon the wavenumber (wave vector).

$$\gamma(\kappa) = -\xi_s(\kappa)\omega_s(\kappa) \pm \mathrm{i}\omega_{\mathrm{d},s}(\kappa), \quad s = 1, 2, \tag{4.15}$$

In Eq. (4.15), the real part is the negative of the product of the wavenumber-dependent damping ratio, $\xi_s(\kappa)$, and the resonant frequency, $\omega_s(\kappa)$; the imaginary part is the wavenumber-dependent frequency of damped wave propagation $\omega_{\mathrm{d},s}(\kappa)$ for mode s. Corresponding to each eigenvalue, the frequency of damped free wave propagation and the associated damping ratio are simply

$$\omega_{\mathrm{d},s}(\kappa) = \mathrm{Im}[\gamma_s(\kappa)], \quad s = 1, 2, \tag{4.16}$$

$$\xi_s(\kappa) = -\frac{\mathrm{Re}[\gamma_s(\kappa)]}{\mathrm{Abs}[\gamma_s(\kappa)]}, \quad s = 1, 2. \tag{4.17}$$

Since each member of a conjugate pair describes the same wave with only the direction of propagation in opposition, no information is lost in considering only the member with $\mathrm{Im}[\gamma_s(\kappa)] > 0$.

4.3.1.2 Proportional (Rayleigh) damping

The advantage of the state-space formulation is its applicability to a generalized viscous damping matrix; however, the size of the eigenvalue problem doubles. For the special case of Rayleigh damping (see Ref. [105] for a discussion on the limitations of this model), $\hat{\mathbf{C}}$ is linearly proportional to $\hat{\mathbf{M}}$ and/or $\hat{\mathbf{K}}$, i.e.,

$$\hat{\mathbf{C}} = p\hat{\mathbf{M}} + q\hat{\mathbf{K}} \tag{4.18}$$

where $p, q \geq 0$ are scaling parameters. Naturally, $p, q = 0$ corresponds to the undamped case. In circumstances of proportional damping, the size of the problem need not be doubled through a state-space transformation. Instead, we can now employ the concept of Bloch modal analysis [63] which allows us to linearly transform the model degrees of freedom $\mathbf{u}$ to a set of Bloch generalized degrees of freedom, $\mathbf{v}$, that is, $\mathbf{u} = \mathbf{\Phi v}$. Unlike in Ref. [102] in which the aim is model reduction, here the matrix $\mathbf{\Phi}$ is formed using a set of mass-normalized Bloch vectors obtained by solving the standard undamped eigenvalue problem at the current κ point.

Substituting Eq. (4.18) into Eq. (4.7) yields

$$[\lambda^2\hat{\mathbf{M}} + \lambda(p\hat{\mathbf{M}} + q\hat{\mathbf{K}}) + \hat{\mathbf{K}}]\mathbf{u} = \mathbf{0}. \tag{4.19}$$

Utilizing the orthogonality condition that the Bloch vectors exhibit with respect to $\hat{\mathbf{M}}$ and $\hat{\mathbf{K}}$, the expansion uncouples the equations in Eq. (4.19). This is done by substituting $\mathbf{u}(t) = \mathbf{\Phi v}(t)$ into Eq. (4.19) and pre-multiplying by $\mathbf{\Phi}^{\mathrm{H}}$ [$(\cdot)^{\mathrm{H}}$ denotes the Hermitian transpose operation]

$$\mathbf{\Phi}^{\mathrm{H}}[\lambda^2\hat{\mathbf{M}} + \lambda(p\hat{\mathbf{M}} + q\hat{\mathbf{K}}) + \hat{\mathbf{K}}]\mathbf{\Phi v} = \mathbf{0}. \tag{4.20}$$

Equation (4.20) simplifies to

$$[\lambda^2\mathbf{I} + \lambda(p\mathbf{I} + q\mathbf{\Lambda}) + \mathbf{\Lambda}]\mathbf{v} = \mathbf{0}, \tag{4.21}$$

where $\mathbf{\Lambda}$ is a diagonal matrix of eigenvalues. Equation (4.21) represents two uncoupled equations expressed in matrix form. Analogous to the treatment of single degree-of-freedom finite systems in structural dynamics, each of these equations can be written in terms of the damping ratio $\xi_s(\kappa)$ and the undamped frequency $\omega_s(\kappa)$,

$$[\lambda_s^2 + 2\xi_s(\kappa)\omega_s(\kappa)\lambda + \omega_s^2(\kappa)]v_s = 0, \quad s = 1, 2. \tag{4.22}$$

Comparing Eqs. (4.21) and (4.22) gives

$$2\xi_s(\kappa)\omega_s(\kappa) = p + q\omega_s^2(\kappa). \tag{4.23}$$

From Eq. (4.23), the damping ratio is derived explicitly

$$\xi_s(\kappa) = \frac{1}{2}\left[\frac{p}{\omega_s(\kappa)} + q\omega_s(\kappa)\right], \quad s = 1, 2. \tag{4.24}$$

Solving for the roots of Eq. (4.22), we get

$$\lambda_s(\kappa) = -\xi_s(\kappa)\omega_s(\kappa) \pm \omega_s(\kappa)\sqrt{\xi_s^2(\kappa) - 1}, \quad s = 1, 2, \tag{4.25}$$

which, for the underdamped case, $[\xi_s(\kappa) < 1]$ is by definition equal to

$$\lambda_s(\kappa) = -\xi_s(\kappa)\omega_s(\kappa) \pm \mathrm{i}\omega_{\mathrm{d},s}(\kappa), \quad s = 1, 2. \tag{4.26}$$

Hence, the wavenumber-dependent frequency of damped wave propagation is

$$\begin{aligned} \omega_{\mathrm{d},s}(\kappa) &= \omega_s(\kappa)\sqrt{1 - \xi_s^2(\kappa)} \\ &= \omega_s(\kappa)\sqrt{1 - \frac{1}{4}\left[\frac{p}{\omega_s(\kappa)} + q\omega_s(\kappa)\right]^2}, \quad s = 1, 2. \end{aligned} \tag{4.27}$$

For the undamped case $[\xi_s(\kappa) = 0]$, the frequency of the sth branch of the original undamped band structure [i.e., $\omega_s(\kappa)$] is recovered. For $\xi_s(\kappa) > 1$, the medium is overdamped and temporal oscillations do not exist. The medium is critically damped when $\xi_s(\kappa) = 1$. It is noteworthy that this theory is analogous to the well-established modal analysis (modal decomposition) theory for proportionally damped finite structures [103, 104].

4.3.2 Results

To examine our formulation, we select a specific set of material constants for our two-mass model as follows:

$$r_{\mathrm{m}} = 9 \quad r_{\mathrm{c}} = 1/2 \quad r_{\mathrm{k}} = 1 \quad \omega_0 = \sqrt{k_2/m_2} = 150\mathrm{rad/s}. \tag{4.28}$$

4.3.2.1 Effects of different types of damping

We consider three different damping cases – stiffness-proportional, mass-proportional, and general damping – and, for each case, present both the frequency band structure and the damping ratio band structure for various levels of damping intensity. In all the figures concerned with this two-mass system, the frequency of the acoustical branch, $\omega_{\mathrm{d},1}$, is represented by a solid curve, while the frequency of the optical branch, $\omega_{\mathrm{d},2}$, is represented by a dashed curve. In addition, the undamped curves are always colored blue and the damped curves are colored otherwise.

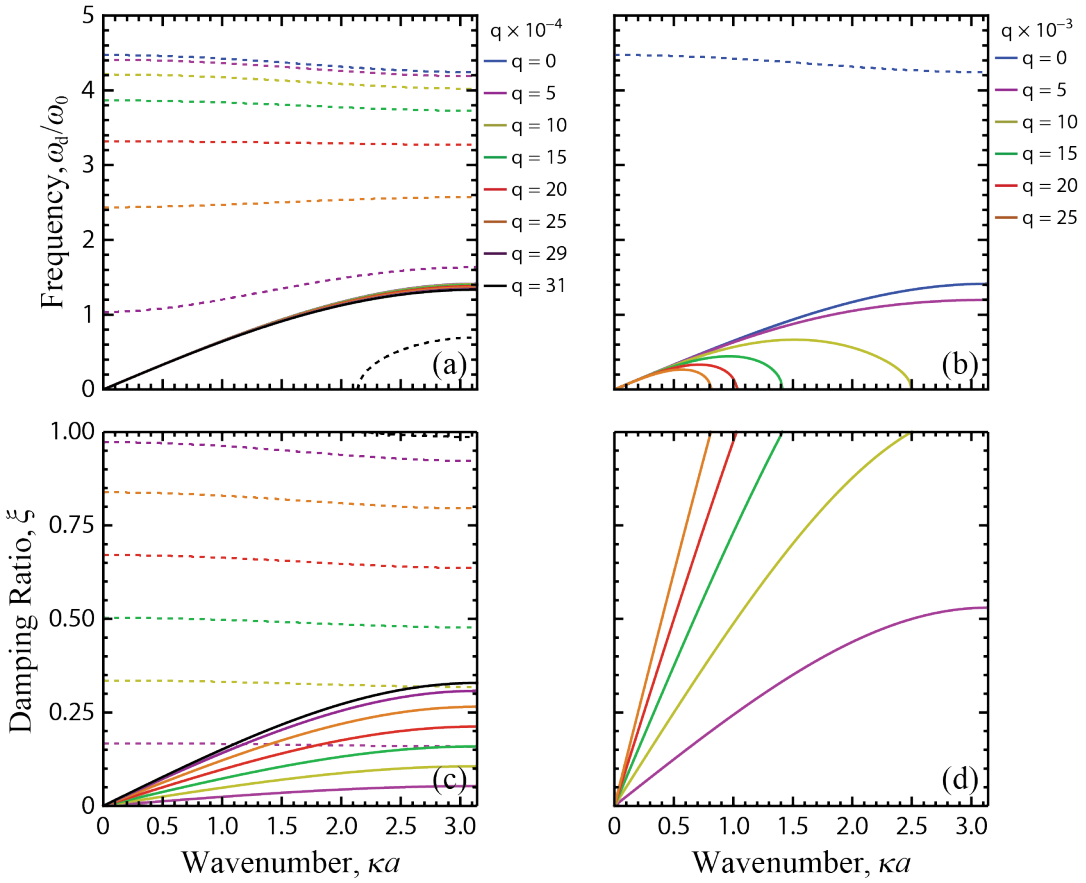

Figure 4.2: Stiffness-proportional damping dispersion curves and damping ratio band diagrams.

In Fig. 4.2, we show the results for the stiffness-proportional damping case (i.e., $p = 0$ and $q > 0$). It is apparent from Fig. 4.2a that the optical frequency branch is more affected by the damping than the acoustical frequency branch; indeed, as most apparent in Fig. 4.2c, the optical branch's corresponding value of damping ratio increases more rapidly than that of the acoustical branch. As the level of damping increases, the curve for $\omega_{d,2}/\omega_0$ flattens out and eventually transitions from being concave down to concave up before vanishing. The downward concavity of $\omega_{d,1}/\omega_0$ remains the same, but, as shown in Fig. 4.2b, the range of κa over which $\omega_{d,1}/\omega_0 > 0$ decreases as the damping intensifies.

The results for mass-proportional damping (i.e., $p > 0$ and $q = 0$) are shown in Fig. 4.3. Comparing Fig. 4.3a with Fig. 4.2a, it is clear that mass-proportional damping has the opposite effect on the acoustical and optical frequency branches than that induced by stiffness-proportional

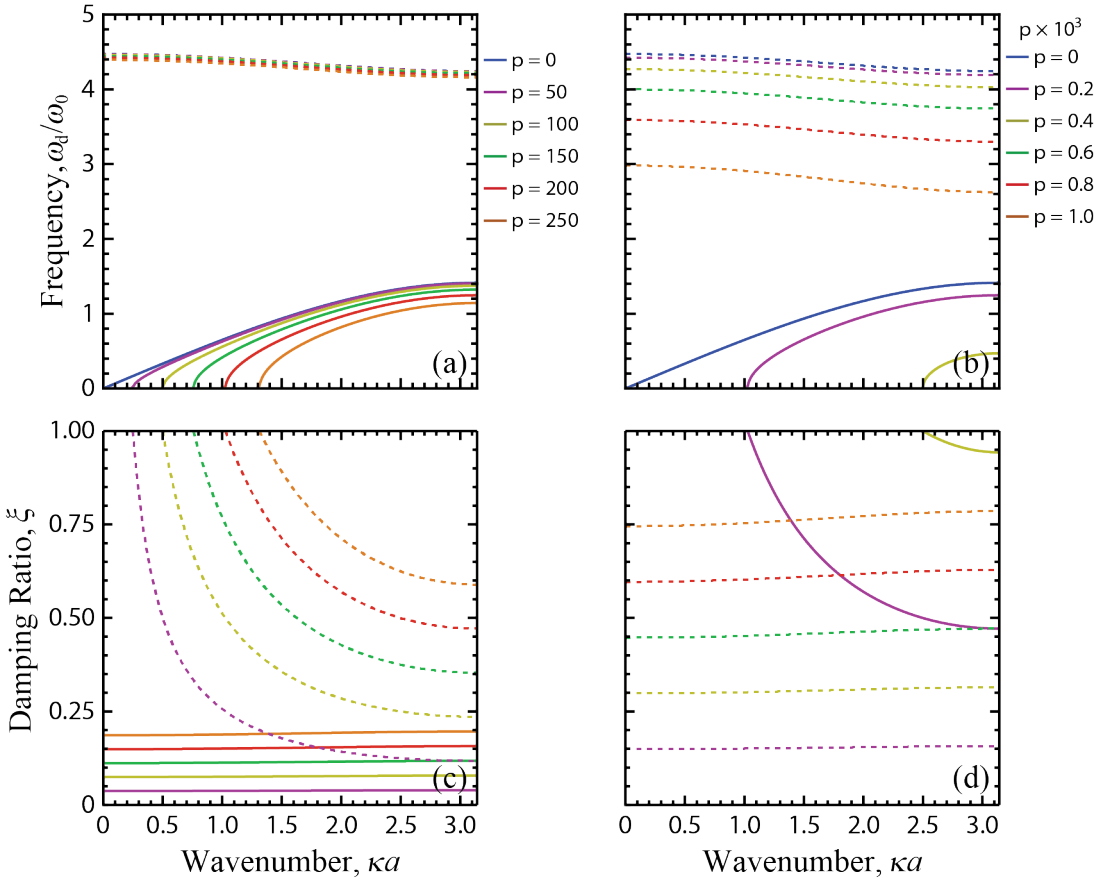

Figure 4.3: Mass-proportional damping dispersion curves and damping ratio band diagrams.

damping. The acoustical frequency branch is affected more by this type of damping and accordingly the corresponding damping ratio values increase more rapidly. Unlike in Fig. 4.2a, the concavity of both curves remains constant while, like in Fig. 4.2a, the range of κa over which propagation is possible ($\omega_{d,1}/\omega_0 > 0$) decreases. In this case, low-frequency waves possessing longer wavelengths ($\kappa a \to 0$) are the first to become overdamped.

Emerging from the state-space transformation approach, Fig. 4.4 presents the frequency band structure for a general damping model for various values of β/ω_0. A comparison of Figs. 4.2 and 4.4 reveals a similarity in the dispersive effects of stiffness-proportional damping and the present condition of general damping. These similarities in the dispersion band structure can be explained by the mathematical similarities between the $\hat{\mathbf{K}}$ matrix and the $\hat{\mathbf{C}}$ matrix due to the common placement of springs and viscous dampers in Fig. 4.1. $\hat{\mathbf{C}}$ and $q\hat{\mathbf{K}}$ are structurally similar being full

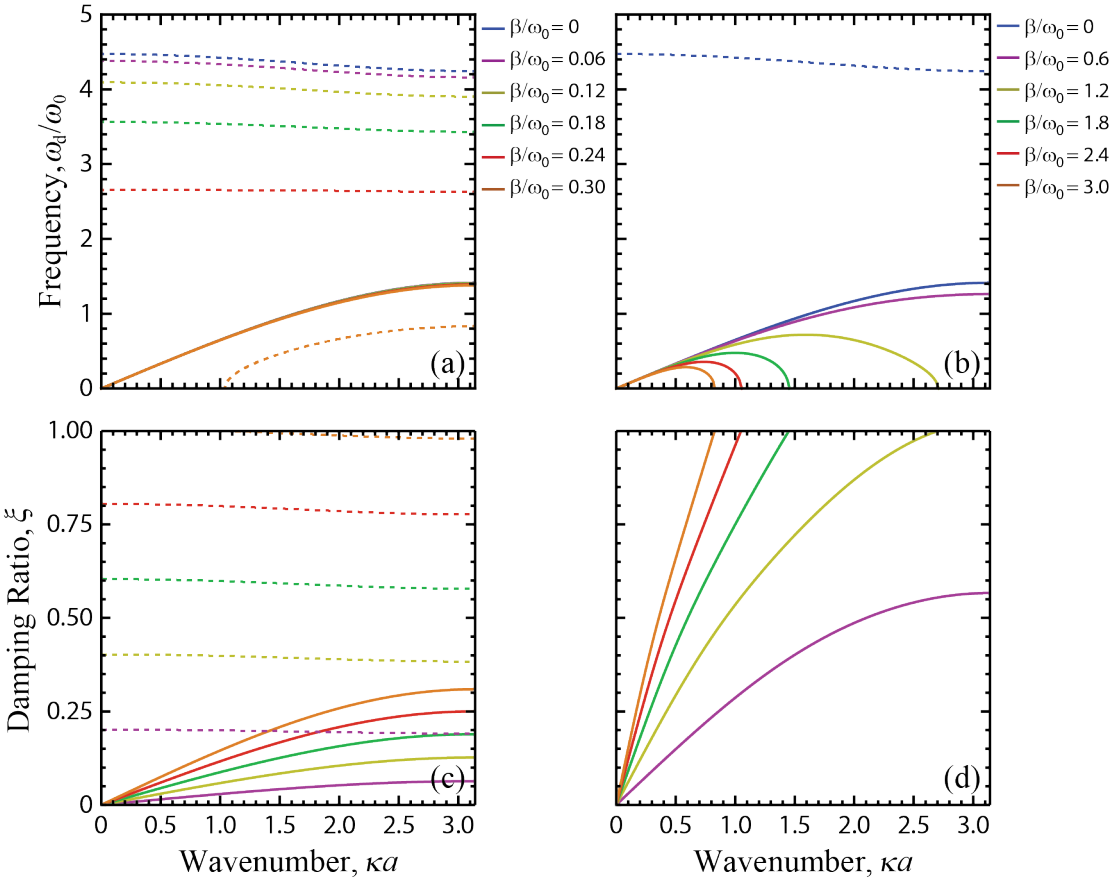

Figure 4.4: General damping dispersion curves.

matrices, while $\hat{\mathbf{C}}$ and the diagonal $p\hat{\mathbf{M}}$ are structurally dissimilar. As for stiffness-proportional damping, in Fig. 4.4, $\omega_{d,2}$ is more susceptible to the influences of damping than is $\omega_{d,1}$. The optical frequency branch flattens out before changing concavity (not shown in Fig. 4.4).

It is noteworthy that the band structure alterations described above induce both quantitative and qualitative changes to the group velocity dispersion curves. For example, it is possible for the group velocity of some branches to switch from positive to negative as a result of damping [63].

4.3.2.2 Branch overtaking and branch cut-off

In the results presented for the damped mass-spring periodic chain, we can observe two intriguing phenomena that emerge due to the presence of damping: *branch overtaking* and *branch cut-off*. Branch overtaking takes place when higher branches in the band structure drop in frequency

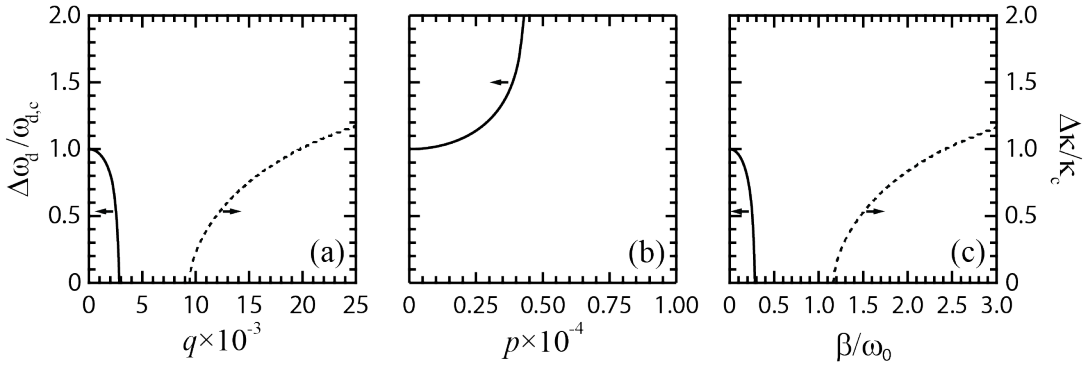

Figure 4.5: Frequency (solid lines) and wavenumber (dashed lines) band gaps as a function of damping level for the (a) stiffness-proportional, (b) mass-proportional, and (c) general damping cases considered.

at rates that exceed the drop rates for lower branches, thus causing the overtake. A branch cut-off refers to a state whereby a dispersion branch does not cover the entire first Brillouin zone, thus creating a partial band gap with respect to the wavenumber (or wave vector for a multi-dimensional problem) as opposed to the frequency.

In Figs. 4.2a and 4.4a, we observe cases of branch overtaking. In particular, we observe in each case that the location of the optical branch shifts down the frequency domain at a much faster rate than the acoustical branch as the intensity of damping is increased. For example, in Fig. 4.4a the optical branch is located below the acoustical branch when $\beta/\omega_0 = 0.3$. Damping and the higher drop rate of the optical branch causes the band gap to decrease in size at an increasing rate. This is quantitatively illustrated by tracking the relative size of the band gap with respect to its central frequency as a function of damping intensity, as illustrated in Fig. 4.5. Clearly the relative band gap size rate drops for the stiffness-proportional and general damping cases. For the mass-proportional damping situation, a greater rate of descent for the acoustical branch compared to the optical results in an increasing band gap and, therefore, no branch over-taking. In some cases (as reported in Ref. [63]), if the overtake takes place on an optical branch, a band gap can drop in size even more abruptly.

In Figs. 4.2b, 4.3a, and 4.4b, we observe another damping-induced phenomenon in the frequency band structure. We observe, that when the level of damping exceeds a certain value,

the acoustical branch gets cut off in the wavenumber domain, i.e., it does not span the entire first Brillouin zone. Moreover, since the optical branch eventually disappears in the cases of Figs. 4.2a and 4.4b (due to the presence of a high level of damping), we get a *wavenumber band gap*, i.e., a wavenumber range where waves are prohibited from propagation. This phenomenon is clearly analogous to the well-known concept of a frequency band gap. In the case presented in Fig. 4.3a, we observe a partial wavenumber band gap as the optical branch remains. In Fig. 4.5, we track the opening of the relative width of the wavenumber band gap for the three damping cases studied.

The damping-induced branch-overtaking and branch cut-off phenomena clearly present opportunities for design, building on already existing methodologies at the unit cell level [106, 107] and/or at the combination of the unit cell and structural levels [71].

4.4 Continuous Model

4.4.1 Theory

In this section, we consider a continuous phononic crystal governed by

$$\nabla \cdot \boldsymbol{\sigma} = \rho \ddot{\mathbf{u}}, \tag{4.29}$$

where $\boldsymbol{\sigma}$ is the stress tensor, ρ is the density, and $\mathbf{u} = \{u_x, u_y, u_z\}$ is now used to denote the displacement field. The constitutive behavior is treated phenomenologically assuming linear and isotropic elastic response and viscous damping,

$$\boldsymbol{\sigma} = \mathbf{C}_{\mathrm{K}} : \nabla^{\mathrm{S}}\mathbf{u} + \mathbf{C}_{\mathrm{C}} : \nabla^{\mathrm{S}}\dot{\mathbf{u}}, \tag{4.30}$$

where $\mathbf{C}_{\mathrm{K}}$ is the conventional elasticity tensor, $\mathbf{C}_{\mathrm{C}}$ is the viscous damping tensor, and ∇^{S} denotes the symmetric gradient operator, that is,

$$\nabla^{\mathrm{S}}\mathbf{u} = \frac{1}{2}[\nabla\mathbf{u} + (\nabla\mathbf{u})^{\mathrm{T}}]. \tag{4.31}$$

Substituting Eq. (4.30) into Eq. (4.29) yields

$$\nabla \cdot \mathbf{C}_{\mathrm{K}} : \nabla^{\mathrm{S}}\mathbf{u} + \nabla \cdot \mathbf{C}_{\mathrm{C}} : \nabla^{\mathrm{S}}\dot{\mathbf{u}} = \rho \ddot{\mathbf{u}}. \tag{4.32}$$

We will assume that the unit cell is composed of two or more material phases, and that the material-to-material interfaces are ideal. Equation (4.32) has a Bloch solution of the form

$$\mathbf{u}(\mathbf{x}, \boldsymbol{\kappa}, t) = \tilde{\mathbf{u}}(\mathbf{x}) \mathrm{e}^{\mathrm{i}\boldsymbol{\kappa}\cdot\mathbf{x}+\lambda t}, \tag{4.33}$$

where $\tilde{\mathbf{u}}(\mathbf{x})$ is the periodic displacement Bloch amplitude function with the periodicity of the medium, $\mathbf{x}$ is the position vector, and $\boldsymbol{\kappa}$ is the wave vector. Similar to discrete counterpart in Eq. (4.3), periodicity enforces the following identity

$$\mathbf{u}(\mathbf{x} + \mathbf{a}, \boldsymbol{\kappa}, t) = \mathbf{u}(\mathbf{x}, \boldsymbol{\kappa}, t) \mathrm{e}^{\mathrm{i}\boldsymbol{\kappa}\cdot\mathbf{a}}. \tag{4.34}$$

Using Eq. (4.33), the spatial component of the displacement gradient is

$$\nabla\mathbf{u} = (\nabla\tilde{\mathbf{u}} + \mathrm{i}\boldsymbol{\kappa} \otimes \tilde{\mathbf{u}}) \mathrm{e}^{\mathrm{i}\boldsymbol{\kappa}\cdot\mathbf{x}}, \tag{4.35}$$

where the symbol $\otimes$ denotes the outer product. Similarly, the velocity gradient is

$$\nabla\dot{\mathbf{u}} = (\nabla\dot{\tilde{\mathbf{u}}} + \mathrm{i}\boldsymbol{\kappa} \otimes \dot{\tilde{\mathbf{u}}}) \mathrm{e}^{\mathrm{i}\boldsymbol{\kappa}\cdot\mathbf{x}}. \tag{4.36}$$

Substitution of Eqs. (4.31), (4.33), (4.35), and (4.36) into Eq. (4.32) gives the strong form of the Bloch eigenvalue problem

$$\nabla \cdot \mathbf{C}_{\mathrm{K}} : \left[\nabla^{\mathrm{S}}\tilde{\mathbf{u}} + \frac{\mathrm{i}}{2}(\boldsymbol{\kappa} \otimes \tilde{\mathbf{u}} + \tilde{\mathbf{u}} \otimes \boldsymbol{\kappa})\right] + \nabla \cdot \mathbf{C}_{\mathrm{C}} : \left[\nabla^{\mathrm{S}}\dot{\tilde{\mathbf{u}}} + \frac{\mathrm{i}}{2}(\boldsymbol{\kappa} \otimes \dot{\tilde{\mathbf{u}}} + \dot{\tilde{\mathbf{u}}} \otimes \boldsymbol{\kappa})\right] = \rho\ddot{\tilde{\mathbf{u}}}. \tag{4.37}$$

Applying the time derivatives, Eq. (4.37) becomes

$$\nabla \cdot \mathbf{C}_{\mathrm{K}} : \left[\nabla^{\mathrm{S}}\tilde{\mathbf{u}} + \frac{\mathrm{i}}{2}(\boldsymbol{\kappa} \otimes \tilde{\mathbf{u}} + \tilde{\mathbf{u}} \otimes \boldsymbol{\kappa})\right] + \gamma\nabla \cdot \mathbf{C}_{\mathrm{C}} : \left[\nabla^{\mathrm{S}}\tilde{\mathbf{u}} + \frac{\mathrm{i}}{2}(\boldsymbol{\kappa} \otimes \tilde{\mathbf{u}} + \tilde{\mathbf{u}} \otimes \boldsymbol{\kappa})\right] = \gamma^2\rho\tilde{\mathbf{u}}. \tag{4.38}$$

Equation (4.38) can be discretized using a numerical method. We will consider the finite element (FE) method [102], but it should be noticed that the following treatment of damping is independent of the specific choice the numerical method. The discretization transforms the continuous Bloch displacement functions to discrete Bloch displacement vectors, yielding

$$\hat{\mathbf{M}}\ddot{\tilde{\mathbf{u}}} + \hat{\mathbf{C}}\dot{\tilde{\mathbf{u}}} + \hat{\mathbf{K}}\tilde{\mathbf{u}} = \mathbf{0}, \tag{4.39}$$

and

$$[\gamma^2\hat{\mathbf{M}} + \gamma\hat{\mathbf{C}} + \hat{\mathbf{K}}]\tilde{\mathbf{u}} = \mathbf{0}, \tag{4.40}$$

respectively. $\hat{\mathbf{M}}$, $\hat{\mathbf{C}}$, and $\mathbf{K}$ now denote the finite element mass, damping, and stiffness matrices. In Eqs. (4.39) and (4.40), the vectors are of size $n_e \times 1$ and each of the matrices is of size $n_e \times n_e$ where n_e denotes the number of FE equations.

For the undamped case, where $\hat{\mathbf{C}} = \mathbf{0}$, we realize that $\gamma = \mathrm{i}\omega$ (hence $\mathbf{u}(\mathbf{x};t) = \tilde{\mathbf{u}}(\mathbf{x})\mathrm{e}^{\mathrm{i}\omega t}$) and subsequently obtain the familiar eigenvalue problem for undamped Bloch wave propagation

$$[\hat{\mathbf{K}} - \omega^2\hat{\mathbf{M}}]\tilde{\mathbf{u}} = \mathbf{0}. \tag{4.41}$$

On the other hand, if the second term in the left-hand-side of Eq. (4.40) is nonzero, this prevents us from generating an eigenvalue problem in the usual way for calculating the band structure.

4.4.1.1 General damping

To enable a formal eigenvalue analysis of a problem exhibiting general damping, we transform Eq. (4.39) into the state-space formulation consistent with Eq. (4.10). In this case, the eigenvalue solution is wave vector-dependent:

$$\lambda_s(\boldsymbol{\kappa}) = -\xi_s(\boldsymbol{\kappa})\omega_s(\boldsymbol{\kappa}) \pm \mathrm{i}\omega_{\mathrm{d},s}(\boldsymbol{\kappa}), \qquad s = 1, \ldots, n_e. \tag{4.42}$$

In the same manner as in the discrete case, we can extract $\xi_s(\boldsymbol{\kappa})$ and $\omega_{\mathrm{d},s}(\boldsymbol{\kappa})$ from Eq. (4.42).

4.4.1.2 Proportional (Rayleigh) damping

As discussed earlier in Sec. 4.3.1.2, a special case for a phononic crystal damping model is proportional damping [63]. We will define the proportional viscous finite element matrix similarly as given in Eq. (4.18), substitute into Eq. (4.39), and subsequently obtain

$$\hat{\mathbf{M}}\ddot{\tilde{\mathbf{u}}} + [p\hat{\mathbf{M}} + q\hat{\mathbf{K}}]\dot{\tilde{\mathbf{u}}} + \hat{\mathbf{K}}\tilde{\mathbf{u}} = \mathbf{0}. \tag{4.43}$$

As we did in the discrete case, we employ the concept of Bloch mode expansion [63, 102] which allows us to linearly transform the model to a set of Bloch generalized coordinates, $\tilde{\mathbf{v}}^{\mathrm{T}}(t) =$

$[\tilde{v}_1(t)\ \ \tilde{v}_2(t)\cdots\tilde{v}_m(t)]$, i.e.,

$$\tilde{\mathbf{u}}(t)_{(n_e\times 1)} = \mathbf{\Phi}_{(n_e\times m)}\tilde{\mathbf{v}}_{(m\times 1)}(t), \tag{4.44}$$

where $\mathbf{\Phi}$ is a Bloch modal matrix. In Eq. (4.44), m denotes the total number of Bloch modes retained in the expansion. We follow the same procedure as in Sec. 4.3.1.2, and utilize the orthogonality condition that the Bloch vectors exhibit with respect to $\hat{\mathbf{M}}$ and $\hat{\mathbf{K}}$ at the current $\boldsymbol{\kappa}$-point to uncouple the governing equations. This is done by substituting Eq. (4.44) into Eq. (4.43) and pre-multiplying all terms by $\mathbf{\Phi}^{\mathrm{H}}$. Returning to Eq. (4.44), only as many Bloch modes m need to be incorporated in the expansion as the number of branches of interest in the damped band diagram that is to be generated. The result is a set of m uncoupled equations

$$\ddot{\tilde{v}}_s + 2\xi_s(\boldsymbol{\kappa})\omega_s(\boldsymbol{\kappa})\dot{\tilde{v}}_s + [\omega_s(\boldsymbol{\kappa})]^2\tilde{v}_s = 0, \quad s = 1,\ldots,m. \tag{4.45}$$

where $\tilde{v}_s$ is the sth Bloch generalized coordinate and $\omega_s(\boldsymbol{\kappa})$ represents the wavenumber-dependent frequency of undamped wave propagation (as in the discrete case). In Eq. (4.45), $\xi_s(\boldsymbol{\kappa})$ is the damping ratio of the sth branch (out of a total of m branches) of the damped band structure at point $\boldsymbol{\kappa}$ and is defined as

$$\xi_s(\boldsymbol{\kappa}) = \frac{1}{2}\left[\frac{p}{\omega_s(\boldsymbol{\kappa})} + q\omega_s(\boldsymbol{\kappa})\right], \quad s = 1,\ldots,m. \tag{4.46}$$

Applying the derivatives in Eq. (4.45) and solving for the roots yields a similar expression as given in Eq. (4.25)

$$\lambda_s(\boldsymbol{\kappa}) = -\xi_s(\boldsymbol{\kappa})\omega_s(\boldsymbol{\kappa}) \pm \omega_s(\boldsymbol{\kappa})\sqrt{\xi_s^2(\boldsymbol{\kappa}) - 1}, \quad s = 1,\ldots,m. \tag{4.47}$$

For the undamped case $[\xi_s(\boldsymbol{\kappa}) = 0]$, the frequency of the sth branch of the original undamped band structure is recovered. For $\xi_s(\boldsymbol{\kappa}) < 1$, the medium is underdamped at $\boldsymbol{\kappa}$ and propagating waves exhibit temporal decay in time. Subsequently,

$$\lambda_s(\boldsymbol{\kappa}) = -\xi_s(\boldsymbol{\kappa})\omega_s(\boldsymbol{\kappa}) \pm \mathrm{i}\omega_{\mathrm{d},s}(\boldsymbol{\kappa}), \quad s = 1,\ldots,m, \tag{4.48}$$

and the wave vector-dependent frequency of damped oscillation is defined as

$$\omega_{\mathrm{d},s}(\boldsymbol{\kappa}) = \omega_s(\boldsymbol{\kappa})\sqrt{1 - \xi_s^2(\boldsymbol{\kappa})}, \quad s = 1,\ldots,m, \tag{4.49}$$

which is essentially the frequency of the sth branch of the damped band structure at point $\boldsymbol{\kappa}$. For $\xi_s(\boldsymbol{\kappa}) > 1$, the medium is overdamped at $\boldsymbol{\kappa}$ and temporal oscillations cannot exist. The medium is critically damped at $\boldsymbol{\kappa}$ when $\xi_s(\boldsymbol{\kappa}) = 1$.

4.4.2 Results

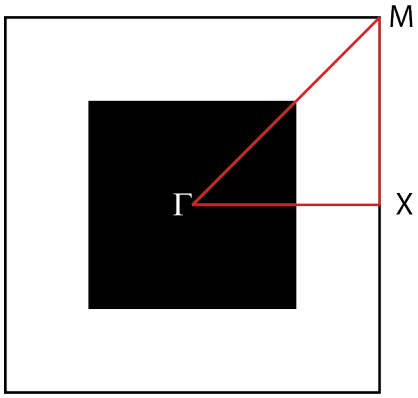

Figure 4.6: Continuous model of phononic crystal with irreducible Brillouin zone enclosed in red.

In this section, we examine the behavior of a continuous model of both a proportionally damped and a generally damped phononic crystal. We use the finite element method to discretize the spatial domain in both cases. For the proportionally damped case we solve Eq. (4.45) and proceed to calculating $\xi_s(\boldsymbol{\kappa})$ and $\omega_{\mathrm{d},s}(\boldsymbol{\kappa})$ by simply post-processing the resulting undamped band structure data using Eqs. (4.46) and (4.49), respectively. For the generally damped case we use the state-space formulation, solve for $\lambda_s(\boldsymbol{\kappa})$, and extract $\xi_s(\boldsymbol{\kappa})$ and $\omega_{\mathrm{d},s}(\boldsymbol{\kappa})$. Both damping-type formulations are applicable to three-dimensional models. However, for ease of exposition we present results for a 2D model under plane strain conditions. In our example model, a square lattice is considered with a bi-material unit cell consisting of a centrally located square inclusion, as shown in Fig. 4.6. The filling ratio is 0.3086. The material phase for the matrix (denoted by subscript "1") is chosen to be compliant and light while the phase for the inclusion (denoted by subscript "2") is stiff and dense. In particular, a ratio of Young's moduli of $E_2/E_1 = 20$ and a ratio of densities of $\rho_2/\rho_1 = 2$ are chosen. A Poisson ratio of $\nu = 0.34$ is assumed for both phases. The unit

cell finite element mesh consists of 9×9 uniformly sized four-node bi-linear quadrilateral elements. The path along the symmetry points, $\Gamma \to X \to M \to \Gamma$, bordering the irreducible Brillouin zone is sampled into ninety-seven $\boldsymbol{\kappa}$-point steps. In the results, we refer to the degree of proportional damping using the scaling parameters p and q. The shear Lamé constant for material phase "1" is denoted μ_1. For the general damping case we perturb a stiffness-proportional damping model by multiplying each of the Lamé constants by a different scalar, thus breaking the proportionality of the damping matrix to the stiffness matrix.

Figure 4.7a,b shows the frequency band structure (restricted to real wave vectors) for the undamped case, where $p, q = 0$, a proportionally damped case with parameters $p = 0$ and $q = 0.05$, and a generally damped case whereby a proportionally damped model with parameters $p_{\text{scaled}} = 0$ and $q_{\text{scaled}} = 0.05$ is perturbed by replacing μ by $\mu_{\text{damp}} = 1.4\mu$ and λ by $\lambda_{\text{damp}} = 0.6\lambda$ in the damping matrix $\mathbf{C}$. The damping ratio corresponding to each mode, as a function of $\boldsymbol{\kappa}$, is shown in Fig. 4.7c,d. We observe that for the proportionally damped case considered the location of the branches in the frequency domain drop with damping, and do so at an increasing rate as the branch number increases. The damping ratio diagram shown in Fig. 4.7c resembles the frequency band structure in shape. Furthermore, the locations of the curves in Fig. 4.7a drop, and in Fig. 4.7c rise, with increase in the value of q (not shown). We also studied the case where $p \neq 0$ and $q = 0$ (not shown). Here, the band structure away from the Γ-point experiences very small shifts, whereas at and near the Γ-point the downward shift in frequencies is dramatic, and this is due to sharp increases in ξ_s within this neighborhood. In fact, with a small increase in p, the value of the damping ratio at and near the Γ-point exceeds unity, i.e., exceeds the critical damping level beyond which there is no temporal oscillations. We therefore focus on a nonzero q while keeping $p = 0$. The response of the considered generally damped case follows a similar trend to the proportionally damped case with deviations in certain regions such as between the M- and Γ-points, especially for the sixth branch. The damping ratio diagram for both cases also differ considerably especially at the high branches. Even though λ_{damp} was decreased at the same rate (40%) as μ_{damp} was increased in the general damping matrix, we observe that the level of overall damping in the

band structure has increased compared to the nominal stiffness-proportionally damped case. This suggests that damping in shear has a more significant effect on the band structure than longitudinal damping. This conclusion is confirmed by considering the opposite case where μ has been replaced by $\mu_{\text{damp}} = 0.6\mu$ and λ by $\lambda_{\text{damp}} = 1.4\lambda$, the results of which are presented in Fig. 4.7b and d.

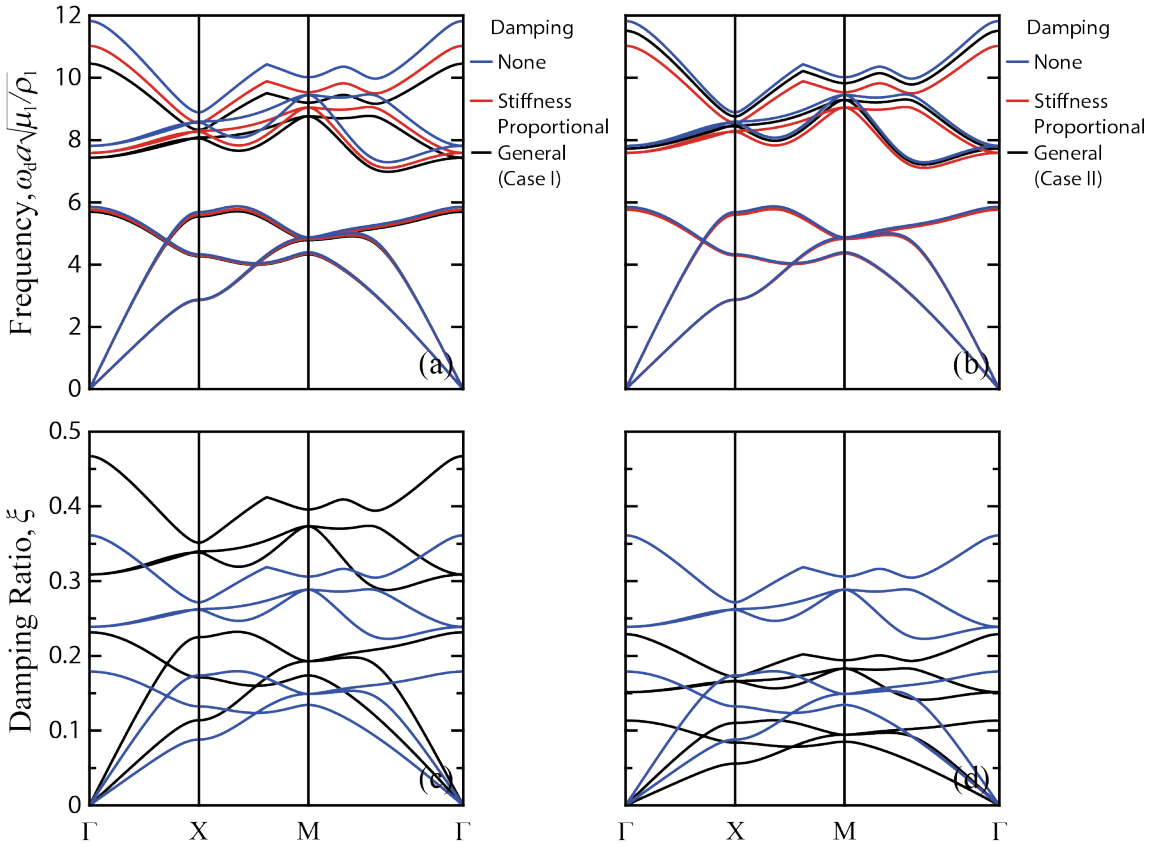

Figure 4.7: Frequency (a,b) and damping ratio (c,d) band structures for.

4.5 Conclusions

We presented a formal treatment of the Bloch wave propagation problem for viscously damped phononic crystals. We first studied an infinite chain consisting of two masses in the unit cell, then generalized to a continuum model of a phononic crystal which was subsequently discretized using the finite element method. We considered both the general damping case and the special case where the damping matrix is proportional to the mass and/or stiffness matrices. In all our analyses

we presented the mathematical formulations governing the application of Bloch theory to a single unit cell, and obtained the frequency band structure as well as the wavenumber- (wave vector-) dependent damping ratio band structure.

Our results show that damping in general alters the shape of the frequency band structure. For the specific case of proportional damping, we observed from the discrete model results that the optical branch is more sensitive to stiffness-proportional damping, while the acoustical branch responds more readily to mass-proportional damping. The band gap shrinks or widens accordingly. These alterations induce both quantitative and qualitative changes to the group velocity dispersion curves. A significant consequence is the possibility of transition of the group velocity corresponding to some branches from positive to negative as a result of damping [63].

Our results also revealed that when the damping is significant it could lead to rather dramatic changes to the frequency band structure (and hence the band gaps). In particular, we observed the branch overtaking phenomenon whereby the higher branches drop at a faster rate than the lower branches, thus allowing for the possibility of a branch overtake. We also observed, in the context of general damping, the phenomenon of a wavenumber (wave vector) band gap whereby in the case considered the acoustical branch experiences a cut-off, that is, it no longer spans the entire first Brillouin zone.

The treatment of damping using modal analysis and state-space transformation is common in the study of the *dynamics of structures* [103–105]. In this paper, and building on our earlier work [63, 102] we have extended the application of these techniques to the study of the *dynamics of materials* within the framework of Bloch theory. Incorporation of damping in this context is necessary as the newly emerging field of phononics – the science of phonons and their manipulation for technological applications – expands to incorporate a broader range of constituent material phases exhibiting different levels of dissipation. Since our formalisms revolve around the use of the damping matrix $\mathbf{C}$, we can fully utilize already established quantitative models of damping in the finite structural dynamics literature [103–105]. Furthermore, the presented formalisms are relevant to the study of Bloch wave propagation in other types of dissipative periodic media such as lossy

photonic crystals [108–110].

Chapter 5

Metadamping: An emergent phenomenon in dissipative metamaterials[4]

5.1 Abstract

Using a generalized form of Bloch's theorem, we derive the dispersion relation of a viscously damped, locally resonant metamaterial modeled as an infinite mass-in-mass lumped parameter chain. For comparison, we obtain the dispersion relation for a statically equivalent Bragg-scattering mass-spring chain that is also viscously damped. For the two chains, we prescribe identical damping levels in the dashpots and compare the damping ratio associated with all propagating Bloch modes. We find that the locally resonant metamaterial exhibits higher dissipation throughout the spectrum which indicates a damping emergence phenomena due to the presence of local resonance. This phenomenon, which we define as "metadamping", provides a new paradigm for the design of material systems that display both high damping and high stiffness. We conclude our investigation by quantifying the degree of metadamping as a function of the long-wave speed of sound in the medium or the static stiffness.

5.2 Introduction

Damping is an intrinsic property of materials and when present in a structural configuration may play a significant role in shaping the structural response. While in certain applications – such as energy harvesting – dissipation is not desired, its maximization is sought in numerous avenues, including vibration suppression, shock resistance,and acoustic absorption. From a design

[4] This chapter is adapted from Hussein and Frazier, *Journal of Sound and Vibration* (2013).

perspective, a highly constraining trade-off in these latter applications is that an increase in the intensity of damping in the materials employed commonly appears at the expense of stiffness,or mechanical load-bearing capacity. For example, elastomeric materials are more dissipative than metallic materials but are much less stiff. Hence, the development of concepts in material design that lead to both high levels of dissipation and stiffness has been an active area of research. Lakes *et al.* [111], for example, demonstrated that composite materials incorporating constituents in a metastable state simultaneously exhibit elevated values of viscoelastic stiffness and damping. Research on shape memory alloys has also presented an example, showing that hysteretic motion of interfaces at the thermoelastic martensitic phase leads to realization of high damping capacity without reduction in overall stiffness [112]. Chung [113] presents a review of other approaches for enhancing damping-stiffness capacity of materials through composite materials engineering.

In this chapter, we propose periodic acoustic metamaterials (AMs) with local resonance properties [8] as a candidate for materials that can be designed to exhibit high levels of dissipation while retaining high stiffness. An underlying principle is that vibration attenuation due to damping is most profound at resonance frequencies, as is well known in the field of structural dynamics. Here we draw an analogy and explore the effect of resonance on dissipation in the context of what we may refer to as "material dynamics". In this setting, we examine the level of dissipation not only near a resonance frequency but across the entire frequency-wavenumber spectrum of the material's dispersion curves.

To assess the degree of dissipation in a locally resonant AM, we first generalize Bloch's theorem to incorporate complex frequencies – which is necessary to allow for proper treatment of temporally attenuating waves. The original form of Bloch's theorem, which was developed for electronic band structure calculation [3], is sufficiently based on real frequencies. Next, we derive the frequency and damping ratio band structures of a damped AM and compare the characteristics of the latter with those of a corresponding statically-equivalent phononic crystal (PC), i.e., another type of periodic material that does not possess local resonances yet has the same long-wave propagation characteristics. In this analysis,we seek to determine the possibility of an "emergence of

damping" in the AM. The concept of emergence in complex systems theory and other disciplines stems from the widely held notion that for certain systems "the whole is greater than the sum of its parts" [114]. Although emergence is usually associated with a lack of predictability, the concept may also be relevant to systems whose properties are predictable in principle, yet unforeseen *a priori* [115]. In relation to chemistry and materials science, often the emerging *whole* stems from the structure while the parts is associated with the composition. From a similar perspective, our aim is to demonstrate emergence in the context of how local resonance within the internal structure, of a material, leads to enhanced dissipation, over all frequencies and wavenumbers, when compared to other materials with equivalent static properties and the same level of prescribed damping. We emphasize that the practical implications of damping emergence are profound since this phenomenon provides a novel paradigm towards the design of materials with both high damping and high stiffness.

5.3 Acoustic metamaterial and phononic crystal: Models and equations of motion

By considering lumped masses, springs, and viscous damping (dashpot) elements, we construct a simple one- dimensional (1D) model of a damped diatomic AM (represented by a "mass-in-mass" configuration [116] as shown in Fig. 5.1a), and for comparison we also examine a corresponding 1D model of a damped diatomic PC (represented by a "mass-and-mass" configuration as shown in Fig. 5.1b). This choice of simple lumped parameter models allows us to focus on the underlying damping emergence phenomenon free from the distraction of irrelevant system complexities. Both models represent a unit cell that is infinitely repeated in both directions.

Considering unit cell periodicity, the set of homogeneous equations describing the motion of each mass in the AM model shown in Fig. 5.1a is obtained as follows (where the AM superscript

is omitted for brevity):

$$m_1\ddot{u}_1^j + c_1(2\dot{u}_1^j - \dot{u}_1^{j-1} - \dot{u}_1^{j+1}) + c_2(\dot{u}_1^j - \dot{u}_2^j) + k_1(2u_1^j - u_1^{j-1} - u_1^{j+1}) + k_2(u_1^j - u_2^j) = 0, \quad (5.1a)$$

$$m_2\ddot{u}_2 + c_2(\dot{u}_2^j - \dot{u}_1^j) + k_2(u_2^j - u_1^j) = 0, \quad (5.1b)$$

where u_α^j is the displacement of mass α in an arbitrary jth unit cell. In general, a unit cell and its neighbors may be identified by $j+n$, where $n = 0, -1, 1$ denotes the present, previous, and subsequent unit cell, respectively. Similarly for the PC model shown in Fig. 5.1b, the equations of motion corresponding to the two masses are (where the PC superscript is omitted for brevity) as follows:

$$m_1\ddot{u}_1^j + (c_1 + c_2)\dot{u}_1^j - c_2\dot{u}_2^j - c_1\dot{u}_2^{j-1} + (k_1 + k_2)u_1^j - k_2u_2^j - k_1u_2^{j-1} = 0, \quad (5.2a)$$

$$m_2\ddot{u}_2 + (c_1 + c_2)\dot{u}_2^j - c_2\dot{u}_1^j - c_1\dot{u}_1^{j+1} + (k_1 + k_2)u_2^j - k_2u_1^j - k_1u_1^{j+1} = 0. \quad (5.2b)$$

5.4 Generalized Bloch's theorem: Derivation of frequency and damping ratio dispersion curves

For each of the system of equations, Eqs. (5.1) and (5.2), we apply the generalized form of Bloch's theorem [63, 77]

$$u_\alpha^{j+n}(\kappa, t) = \tilde{U}_\alpha e^{\mathrm{i}n\kappa a + \lambda t}, \quad \alpha = 1, 2, \quad (5.3)$$

which represents the displacement of mass α in the $(j+n)$th unit cell in the periodic chain, and where $\tilde{U}_\alpha$ is the wave amplitude, a is the unit-cell length, κ is the wavenumber, and λ is a complex frequency function that permits wave attenuation in time. In the limiting case of no damping, $\lambda = \pm\mathrm{i}\omega$, and the usual form of Bloch's theorem is recovered. Substituting Eq. (5.3) into the governing equations for both the AM and the PC yields a characteristic equation of the form

$$\lambda^4 + a\lambda^3 + b\lambda^2 + c\lambda + d = 0, \quad (5.4)$$

where for the AM,

$$a = \frac{(m_1 + m_2)c_2 + 2m_2c_1(1 - \cos\kappa a)}{m_1 m_2}, \tag{5.5a}$$

$$b = \frac{(m_1 + m_2)k_2 + 2(m_2k_1 + c_1c_2)(1 - \cos\kappa a)}{m_1 m_2}, \tag{5.5b}$$

$$c = \frac{2(c_1k_2 + c_2k_1)(1 - \cos\kappa a)}{m_1 m_2}, \tag{5.5c}$$

$$d = \frac{2k_1k_2(1 - \cos\kappa a)}{m_1 m_2}, \tag{5.5d}$$

and for the PC,

$$a = \frac{(m_1 + m_2)(c_1 + c_2)}{m_1 m_2}, \tag{5.6a}$$

$$b = \frac{(m_1 + m_2)(k_1 + k_2) + 2c_1c_2(1 - \cos\kappa a)}{m_1 m_2}, \tag{5.6b}$$

$$c = \frac{2(c_1k_2 + c_2k_1)(1 - \cos\kappa a)}{m_1 m_2}, \tag{5.6c}$$

$$d = \frac{2k_1k_2(1 - \cos\kappa a)}{m_1 m_2}. \tag{5.6d}$$

We note that the form of each of c and d does not vary between the two models. Upon solving Eq. (A.8) for either the AM or the PC, we obtain the general solution

$$\lambda_{1,2} = \frac{1}{2}\left(3a \mp S + \sqrt{18a^2 - 48b - 6\sqrt[3]{4}R - \frac{12\sqrt[3]{2}P}{R} \mp \frac{54(a^3 - 4ab + 8c)}{S}})\right), \tag{5.7}$$

where

$$P = b^2 - 3ac + 12d, \tag{5.8a}$$

$$Q = 2b^3 - 9abc + 27(c^2 + a^2d) - 72bd, \tag{5.8b}$$

$$R = \sqrt[3]{Q + \sqrt{Q^2 - 4P^3}}, \tag{5.8c}$$

$$S = \sqrt{9a^2 - 24b + 6\sqrt[3]{4}R + \frac{12\sqrt[3]{2}P}{R}}. \tag{5.8d}$$

The distinction between the solution of the two systems arises upon the appropriate substitution of a and b as given in Eqs. (5.5) and (5.6), respectively.

The roots we obtain from Eq. (5.7) may also be expressed as

$$\lambda_s(\kappa) = -\xi_s(\kappa)\omega_s(\kappa) \pm \mathrm{i}\omega_{\mathrm{d},s}(\kappa), \quad s = 1, 2, \tag{5.9}$$

where s represents the branch number. Hence from Eqs. (5.7) and (5.9), we can obtain the frequency, $\omega_{\mathrm{d},s}(\kappa)$, and damping ratio, $\xi_s(\kappa)$, relations. Specifically, from the complex solution, $\lambda_s(\kappa)$, we directly extract $\omega_{\mathrm{d},s}(\kappa) = \mathrm{Im}[\lambda_s(\kappa)]$ and $\xi_s(\kappa) = -\mathrm{Re}[\lambda_s(\kappa)]/\mathrm{Abs}[\lambda_s(\kappa)]$ for each of the two dispersion branches.

5.5 Metadamping phenomenon

Now we examine the frequency and damping ratio dispersion curves of both systems for the following parameter ratios: $m_2/m_1 = 5$ and $k_2/k_1 = 1/5$. Furthermore, we set $m_1 = 1$, $\omega_0 = \sqrt{k_2/m_2} = 100$, and $a = 1$. All the parameters here and elsewhere in this work may be read in any consistent system of physical units. To enable proper comparison, we select the value of ω_0^{AM} [critically, keeping $m_{1,2}^{\mathrm{AM}}$ constant and varying $k_{1,2}^{\mathrm{AM}}$ (maintaining $k_2^{\mathrm{AM}}/k_1^{\mathrm{AM}} = 1/5$)] such that $\omega_0^{\mathrm{AM}} \neq \omega_0^{\mathrm{PC}}$ and in such a manner as to render both systems statically equivalent, that is, both systems having the same undamped long-wave sound speed as the wavenumber goes to zero, $c_{\mathrm{st}} = \lim_{\kappa\to 0}[\omega_1(\kappa)/\kappa]$. With the chosen parameters for the PC, $c_{\mathrm{st}} = 83.33$. The AM is set to exhibit the same value of long-wave sound speed when $\omega_0^{\mathrm{AM}} = 40.90$. Concerning the damping prescription, we define $\eta_1 = c_1^{\mathrm{PC}} = c_1^{\mathrm{AM}}$ and $\eta_2 = c_2^{\mathrm{PC}} = c_2^{\mathrm{AM}}$. For the special case of the two dashpots in each system having the same prescribed damping value, we $\eta = \eta_1 = \eta_2$ (i.e., $c_2^{\mathrm{AM}}/c_1^{\mathrm{AM}} = c_2^{\mathrm{PC}}/c_1^{\mathrm{PC}} = 1$).

The first set of results is shown in Fig. 5.2. The left hand side (LHS) of Fig. 5.2a displays the frequency band structure of the AM for three example cases: no damping ($\eta = 0$), low damping ($\eta = 40$), and high damping ($\eta = 80$). The LHS of Figs. 5.2b,c display the damping ratio band structures for the low damping and high damping cases, respectively. In the damping ratio diagrams, we have added a third curve to represent the summation of the damping ratio values for the acoustic and optical branches, i.e., $\xi_{\mathrm{sum}}(\kappa)|_\nu = \xi_1(\kappa)|_\nu + \xi_2(\kappa)|_\nu$, where $\nu = \mathrm{AM}, \mathrm{PC}$. On the right hand side (RHS) of Fig. 5.2, the matching diagrams for the corresponding PC are shown. The results show that there are shifts in the frequency band diagrams (greater in the optical branches) due to the presence of damping, and that these shifts are more profound in the AM. This

behavior manifests itself in a most remarkable manner in the damping ratio diagrams. Despite the static equivalence and equally prescribed value of the viscous damping constant, η, we observe in Figs. 5.2b,c that the AM exhibits higher damping ratio values (i.e., higher dissipation) across the entire Brillouin zone (BZ), for both the acoustic and optical branches. This is an indication of a considerable amplification, or emergence, of dissipation in the AM compared to its PC counterpart. Moreover, this emergence is present for all propagating Bloch modes and not only for modes close to the band gap. Consequently, even though the band gap of the AM might be smaller in width, as in our case, the overall wave attenuation performance when viewed across the entire spectrum is more favorable compared to the PC. This is because outside a band gap, attenuation of propagating modes may only be realized via damping.

To quantify this difference in damping ratio values, we introduce a wavenumber-dependent *damping emergence metric*, $Z_\ell(\kappa) = \xi_\ell(\kappa)|_{\mathrm{AM}} - \xi_\ell(\kappa)|_{\mathrm{PC}}$, where $\ell = 1, 2,$ or sum. In Fig. 3, we show $Z_\ell(\kappa)$, its cumulative value

$$Z_\ell^{\mathrm{cum}}(\theta) = \int_0^\theta Z_\ell(\kappa)\mathrm{d}\kappa, \qquad \ell = 1, 2, \mathrm{sum}; \theta \in [0, \pi] \tag{5.10}$$

and its total value, $Z_\ell^{\mathrm{tot}} = Z_\ell^{\mathrm{cum}}(\pi)$ for our example AM and PC pair – displaying the data for the acoustic branch ($\ell = 1$), the optical branch ($\ell = 2$), and the summation of the two branches ($\ell = \mathrm{sum}$) in Figs. 3a-c, respectively (for $\eta = 40$ on the LHS and $\eta = 80$ on the RHS). The results reveal significantly high values of Z_ℓ^{tot} which we may view as a measure of the intensity of damping emergence. We also observe that $Z_2 > Z_1$ for all values of κ, in line with what we noted above. Fig. 4a shows that the value of Z_ℓ^{tot} varies linearly with the level of damping, η. Here the subfigure terminates when the value of the damping ratio of the AM optical branch is no longer limited to unity (i.e., critical damping) within the BZ. This occurs at $\eta = 165.57$. Fig. 4b focuses on isolating the role of c_1^{AM} versus c_2^{AM} in the creation of damping emergence (considering that only c_2^{AM} is associated with the prescribed damping level of the local resonator in the AM). This is done by varying η_2 while keeping $\eta_1 = 0$ and comparing with the case of varying η_1 while keeping $\eta_2 = 0$. The case of varying η (i.e., varying 1 and 2 simultaneously while keeping them

equal) is also plotted for reference. A more representative reference curve is one that corresponds to varying $\eta/2$, as it directly correlates with the first two curves since the total amount of prescribed damping among the two dashpots is the same for each value of η^*. As expected, it is shown that the impact of c_2^{AM} is higher than that of c_1^{AM}, although not by a significant degree. This suggests that prescribed damping levels even away from local resonators in an AM are bound to influence damping emergence.

Returning to the driving objective of realizing materials that exhibit increased damping without deterioration of static stiffness, we repeat our calculations for a range of c_{st} values. We do so by keeping all the parameters as in the previous example except for ω_0^{PC} and ω_0^{AM}. Changing ω_0^{PC} causes c_{st} to vary, and, in turn, ω_0^{AM} is adjusted accordingly to keep both systems statically equivalent. Throughout this process, the ratio $\omega_0^{\mathrm{AM}} = \omega_0^{\mathrm{PC}}$ stays constant, and hence the relative size and location of the undamped band gap between one system and the other also remains constant. In Fig. 5, we show the relationship between the level of dissipation (i.e., actual damping) versus c_{st} for the AM and the PC. For this purpose, we calculate the total damping ratio over both branches, $\xi_{\mathrm{sum}}^{\mathrm{tot}}$; which we obtain by integration, i.e., $\xi_{\mathrm{sum}}^{\mathrm{tot}} = \xi_{\mathrm{sum}}^{\mathrm{cum}}(\pi)$; where

$$\xi_{\mathrm{sum}}^{\mathrm{cum}}(\theta) = \int_0^{\theta} \xi_{\mathrm{sum}}(\kappa)\mathrm{d}\kappa, \qquad \theta \in [0, \pi]. \tag{5.11}$$

To provide further insight, we calculate an effective static Young's modulus, E_{st}, which we obtain by considering an effective elastic rod, with a cross-sectional area equal to unity. Using the standard rod properties of E, the Young's modulus, ρ, the density, and $c = \sqrt{E/\rho}$, the speed of sound in the rod, we derive $E_{\mathrm{st}} \approx (m_1^{\nu} + m_2^{\nu})c_{\mathrm{st}}^2$ for each of our periodic chains. We clearly observe in Fig. 5 that for a given value of long-wave speed, or effective static Young modulus, the AM exhibits a substantial increase in the value of $\xi_{\mathrm{sum}}^{\mathrm{tot}}$ when compared to the PC. In other words, even though there is still a trade-off between damping and stiffness, the level of dissipation in the AM increases without sacrifice of stiffness. Shaded in gray is the region of damping emergence, or "metadamping region". We note that the level of metadamping (represented by the height of the shaded region) is highest at low levels of c_{st} (i.e., compliant materials) and reduces in value as c_{st} increases to

represent more stiff materials. The intensity of metadamping, or area of the metadamping region, increases with η,or η_1 and η_2 (as we may deduce from Fig. 4 and as elaborately demonstrated in Fig. 6); however, for a given η,or η_1 and η_2, this area may be increased further upon optimization of the periodic chain parameters including the local resonator parameters [117].

5.6 Conclusions

In conclusion, we have demonstrated the concept of damping emergence, or metadamping, due to the presence of local resonance. This finding has far reaching implications on the design of materials for numerous applications that require the reduction, mitigation, or absorption of vibrations, shock, and/or sound. While the analysis has been presented in the context of simple mass-spring-dashpot periodic chains, it can be readily extended to practical realizations of locally resonant acoustic metamaterials. Examples include material structures that utilize: heavy inclusions with compliant coatings [8], soft inclusions [118], split-resonators [119], inertial amplifiers [120], pillars [121,122], holes drilled in a rigid block [72] and suspended masses [123]. The two underlying features needed are (1) the presence of locally resonant elements and (2) the presence of at least one constituent material phase or component that exhibits damping (e.g., by utilizing viscoelastic materials, friction at material interfaces, etc.). It is the combination of these two features that forms a prerequisite for metadamping. As such, other concepts for enhancing damping while retaining stiffness (such as those described in Refs. [111–113]) may be applied in conjunction with the inclusion of local resonators leading to an additive effect. While the perspective in this study has been that metadamping is a desired phenomenon (i.e., for the applications noted above), conversely, there is another category of metamaterial-based applications where metadamping is not desired (such as subwavelength energy harvesting, waveguiding or focusing). For this latter category, however, an awareness and understanding of the phenomenon is necessary for achievement of optimal design. Finally, while the concept of metadamping has been presented in the context of a mechanical problem, in principle it is also applicable to other disciplines in materials physics that involve both resonance and dissipation.

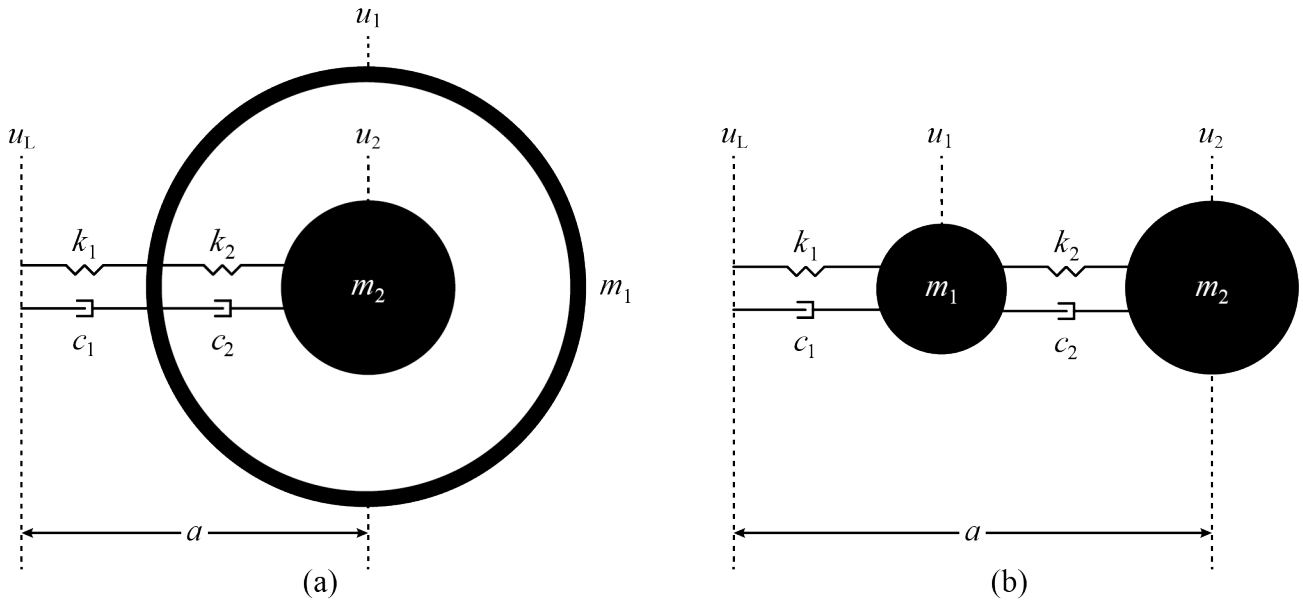

Figure 5.1: Unit cells of statically-equivalent periodic chains consisting of masses, springs and viscous damping (dashpot) elements: (a) acoustic metamaterial (mass-in-mass), (b) phononic crystal (mass-and-mass).

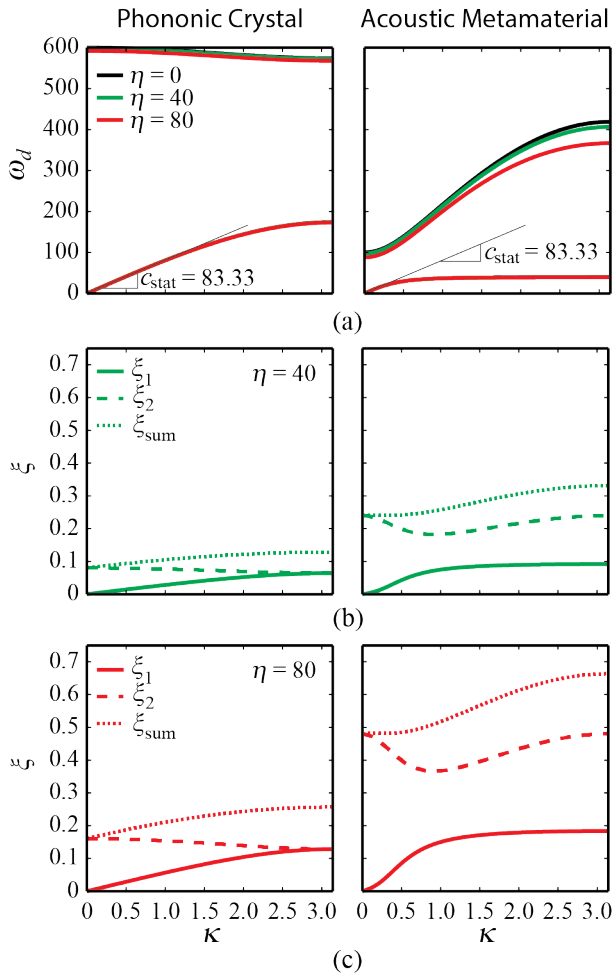

Figure 5.2: (a) Frequency band structure for the acoustic metamaterial and statically equivalent phononic crystal with $\eta = 0, 40,$ and80. The associated damping ratio band structure corresponding to (b) $\eta = 40$ and (c) $\eta = 40$.

Chapter 6

Viscous-to-viscoelastic transition in metamaterial band structure[5]

6.1 Abstract

The dispersive behavior of phononic crystals and metamaterials is influenced by the type and degree of damping present in the constituent materials forming the unit cell. Dissipation arising from viscous damping depends upon the instantaneous modal velocities; whereas in the case of viscoelastic damping, the dissipation is influenced by the past history of motion because the elastic component of the damping adds a storage capacity. Following a state-space framework, we construct a Bloch eigenvalue problem incorporating general viscoelastic damping based on the Zener model. In this approach, the conventional Kelvin-Voigt viscous damping model is recovered as a special case. We examine, in a continuous fashion, the influence of the elastic component of the damping on the band structure of both a phononic crystal and a metamaterial. While viscous damping generally narrows a band gap, the hereditary nature of the viscoelastic conditions reverses this behavior. In the limit of vanishing heredity, the formulation of the viscoelastic equations of motion allows us to analyze the transition between the two regimes. The presented theory also allows us to quantify the increase in the modal dissipation enhancement (metadamping) capacity as the type of damping transitions from viscoelastic to viscous.

[5] This chapter is adapted from a manuscript being prepared for journal submission.

6.2 Introduction

The field of wave propagation in periodic materials has witnessed an explosive increase in activity over the past few decades [124], especially in the category of phononic crystals [43, 45] and acoustic/elastic metamaterials [8], collectively, phononic materials. The appeal of vibration control by design gives impetus to phononic material research. However, despite its physical reality, investigations into the impact of material damping on wave propagation is largely absent in the literature. Nevertheless, discrepancies between theoretical and experimental results have been attributed to energy loss [23]. The theoretical acknowledgment of dissipative effects not only constitutes a more authentic description of the dispersion characteristics of phononic materials, but also provides a means by which the material design process may be guided by the application-specific demand for the maximization (or minimization) of dissipation [125].

Of the studies that consider the treatment of damping, many focus on simulating finite periodic structures [49,51,99]. Dispersion analysis at the unit cell level, on the other hand, provides information on the intrinsic dynamical properties of the medium, which offers insights that are in principle applicable to any finite-structure analysis, regardless of the size, number of cells, boundary conditions, or nature of excitation. In unit cell analysis, wave propagation in a periodic material is fully characterized by the application of Bloch's theorem [3]. The proposition maintains that the wave field in a periodic medium is the product of an amplitude function with the spatial periodicity, $\mathbf{a}$, of the unit cell and a plane wave envelope. In terms of the displacement response, $u(\mathbf{x}, \boldsymbol{\kappa}, t)$, this is expressed as

$$u(\mathbf{x}, \boldsymbol{\kappa}, t) = \tilde{u}(\mathbf{x}) \mathrm{e}^{\mathrm{i}\boldsymbol{\kappa}\cdot\mathbf{x}+\lambda t} \tag{6.1}$$

where $\tilde{\mathbf{u}}(\mathbf{x})$ represents the amplitude function that is periodic across the unit cell domain. Subsequently,

$$u(\mathbf{x}+\mathbf{a}, \boldsymbol{\kappa}, t) = u(\mathbf{x}, \boldsymbol{\kappa}, t) \mathrm{e}^{\mathrm{i}\boldsymbol{\kappa}\cdot\mathbf{a}} \tag{6.2}$$

The wavevector, $\boldsymbol{\kappa}$, and the temporal quantity, λ, modulate the wave envelope in space and time, respectively. In much of the literature, λ is prescribed as an imaginary value, i.e., $\lambda = -\mathrm{i}\omega$,

representing waves that, due to energy dissipation may decay in space but not in time [48, 52, 57, 126].[6] In the laboratory, this scenario is analogous to the harmonic excitation of a corresponding finite periodic structure. In this article, we consider the case where λ is generally a complex number thus the energy loss manifests as temporal attenuation [60, 63, 77, 126]. This treatment is consistent with results obtained from free vibration analysis of a corresponding finite periodic structure. Only in the absence of energy dissipation do the free and harmonic wave conditions yield identical results [124].

A literature synopsis of past studies that investigated dispersion properties of damped periodic materials reveals a variety of approaches in both the manner of modeling the damping and the method of solution. Among the early studies is Mead's calculation of the wave motion phase and attenuation constants for 1D lumped-parameter, chain-like models exhibiting structural damping (i.e., velocity-independent damping forces) [48]. Generally, it is common to incorporate the damping via a complex elastic modulus [49, 61, 62] or a convolution integral expression applied to the elastic modulus [54]. Damping has also been introduced via a complex inertial term [50] and as a stand-alone parameter, or matrix, that multiplies with the velocity vector in the equation of motion [63, 77]. The quality of an adopted damping model improves whenever its performance is compared and calibrated with experimental results [127–129]. Nevertheless, regardless of the choice, any damping model is theoretically acceptable provided the resulting rate of energy dissipation is positive [130–132].

Other than the manner of introducing the damping into the problem, a key classification of damping is in the nature of the dissipation mechanism it describes. Here, we consider two key classes: *viscous damping* and *viscoelastic damping*. Dissipation arising from viscous damping depends upon the instantaneous modal velocities. On the other hand, dissipation arising from viscoelastic damping is influenced by the past history of motion; this is because the elastic component of the damping adds a storage capacity. A viscous damping model is appropriate for material systems where fluid viscosity is the dominant dissipative mechanism, such as in a dashpot or in a

[6] This is in addition to the spatial decay experience resulting from wave interference.

configuration where the material is exposed to a fluid [133]. A viscoelastic model, on its part, is representative of a solid exhibiting material loss, such as in polymers. Non-conservative forces in a viscoelastic model are hereditarily dependent upon the entire history of motion up to and including the present state. Mathematically, this dependence manifests as a convolution integral over kernel functions rather than the instantaneous value of any state variable. The contrast between the viscous and the viscoelastic nature of material damping results in fundamental differences in the dispersion behavior, which is the main focus of this paper.

Another aim of this work is to consider the effect of the type of damping on the dissipative capacity of phononic crystals and metamaterials, particularly the latter. One of the aims of vibration control is to decrease transmission from the environment to a protected structure. This is often attempted through the introduction of an intervening, dissipative material such as rubber. However, dissipative materials generally lack a load-bearing capacity (stiffness) and efforts to combat this deficiency usually sacrifice the damping quality that was the original appeal, revealing an age-old trade-off in materials engineering. The challenge of achieving simultaneously high stiffness and high damping within a material has been addressed in a variety of ways using composites [111–113, 134]. In a recent study of damped phononic materials [125], the concept of *metadamping* was introduced to describe the notion of an amplification of dissipation in locally resonant materials when compared to Bragg-scattering materials of equivalent stiffness and equally prescribed viscous damping. In the present article, using a phononic crystal and metamaterials as Bragg and locally resonant materials, respectively, we investigate the metadamping phenomenon within the framework of both types of damping, viscous and viscoelastic.

The paper is divided into three parts. First, in Sec. 6.3, we introduce the viscous and viscoelastic damping models that form the foundation of the rest of the paper; we discuss their physical attributes as it relates to material deformation and address the non-standard eigenvalue problem that arise from their representation in the equations of motion. Following this discussion, Sec. 6.4 presents wave dissipation in phononic crystals and elastic metamaterials with a focus on the qualitative differences between the viscous and viscoelastic types. In Sec. 6.5, these differences

are explored further to reveal the implications on metadamping. Finally, conclusions are presented in Sec. 6.6.

6.3 State-space Transformation

Damping dependent upon state variables other than the instantaneous displacement or acceleration does not immediately yield a standard eigenvalue problem. In this section, by a state-space transformation of the equations of motion, the standard eigenvalue problem is formulated [77, 78, 132]. In the case of viscous damping, this transformation adopts the familiar Duncan form. For the viscoelastic description, this formulation is extended by the addition of one or more internal variables.

6.3.1 Formulation of Viscous Wave Propagation

Consider the unit cell of a phononic material with spatial periodicity in one, two, or three dimensions. For a material model represented by a lumped-parameter system or by the spatial discretization of a continuum, the equations of motion for a viscously damped unit cell are written compactly in matrix form as

$$\mathbf{M}\ddot{\mathbf{u}} + \mathbf{C}\dot{\mathbf{u}} + \mathbf{K}\mathbf{u} = \mathbf{f}, \tag{6.3}$$

where $\mathbf{M}$, $\mathbf{C}$, and $\mathbf{K}$ are the assembled $n \times n$ mass, damping, and equilibrium stiffness matrices, respectively. While the material properties make the determination of $\mathbf{M}$ and $\mathbf{K}$ relatively straightforward, the coefficients of $\mathbf{C}$ must be extracted from experimental data [128–130]. Often, $\mathbf{C}_j$ is obtained for each material/structural constituent j so that $\mathbf{C}$ is assembled from the individual $\mathbf{C}_j$. The $n \times 1$ vector $\mathbf{u}$ collects the displacement degrees of freedom while the associated nodal forces (applied by neighboring unit cells) are contained within $\mathbf{f}$.

Following [57], we define an $m \times 1$ ($m < n$) condensed displacement vector $\hat{\mathbf{u}}$ containing the minimal set of degrees of freedom including the internal $\mathbf{u}_\mathrm{i}$ and the essential boundary $\mathbf{u}_\mathrm{b}$ displacements. The remaining boundary displacements are obtained from the essential boundary freedoms through the application of the appropriate lattice propagation constant. Thus, exploiting Eq. (6.2),

the condensed set relates to the full set of unit cell displacements according to $\mathbf{u} = \mathbf{T}\hat{\mathbf{u}}$, where $\mathbf{T}$ is the $n \times m$ transformation matrix enforcing the Bloch boundary conditions. For convenience, we adopt the partitioning $\hat{\mathbf{u}} = [\mathbf{u}_\mathrm{i} \;\; \mathbf{u}_\mathrm{b}]^\mathrm{T}$. Given this arrangement, $\mathbf{T}$ may be partitioned into suitably-sized identity matrices $\mathbf{I}$ and diagonal matrices for each propagation direction. For the case of a cubic unit cell with lattice periods a_i $(i = 1, 2, 3)$, $\mathbf{T}$ has the block form

$$\mathbf{T} = \begin{bmatrix} \mathbf{I} & \mathbf{0} \\ \mathbf{0} & \mathbf{I} \\ \mathbf{0} & \mathbf{I}\mathrm{e}^{\mathrm{i}\kappa_1 a_1} \\ \mathbf{0} & \mathbf{I}\mathrm{e}^{\mathrm{i}\kappa_2 a_2} \\ \mathbf{0} & \mathbf{I}\mathrm{e}^{\mathrm{i}\kappa_3 a_3} \\ \mathbf{0} & \mathbf{I}\mathrm{e}^{\mathrm{i}(\kappa_1 a_1 + \kappa_2 a_2)} \\ \mathbf{0} & \mathbf{I}\mathrm{e}^{\mathrm{i}(\kappa_2 a_2 + \kappa_3 a_3)} \\ \mathbf{0} & \mathbf{I}\mathrm{e}^{\mathrm{i}(\kappa_1 a_1 + \kappa_3 a_3)} \\ \mathbf{0} & \mathbf{I}\mathrm{e}^{\mathrm{i}\boldsymbol{\kappa}\cdot\mathbf{a}} \end{bmatrix}. \tag{6.4}$$

Equation (6.3) is written in terms of $\hat{\mathbf{u}}$ as follows:

$$\hat{\mathbf{M}}\ddot{\hat{\mathbf{u}}} + \hat{\mathbf{C}}\dot{\hat{\mathbf{u}}} + \hat{\mathbf{K}}\hat{\mathbf{u}} = \mathbf{0}, \tag{6.5}$$

where

$$\hat{\mathbf{M}} = \mathbf{T}^*\mathbf{M}\mathbf{T}, \tag{6.6a}$$

$$\hat{\mathbf{C}} = \mathbf{T}^*\mathbf{C}\mathbf{T}, \tag{6.6b}$$

$$\hat{\mathbf{K}} = \mathbf{T}^*\mathbf{K}\mathbf{T}, \tag{6.6c}$$

and $\mathbf{T}^*\mathbf{f} = \mathbf{0}$ [135], with $\mathbf{T}^*$ being the conjugate transpose of $\mathbf{T}$. Although, in this work, the Bloch condition is applied through $\mathbf{T}$, alternative formulations for lumped-parameter [78] and discretized [136] systems are suitable.

In general, $\hat{\mathbf{C}}$ is not simultaneously diagonalizable with $\hat{\mathbf{M}}$ and $\hat{\mathbf{K}}$ by the system eigenvectors, and so applying the derivatives in Eq. (6.5) formulates a coupled, non-standard eigenvalue problem

with eigenvalues λ_s and eigenvectors $\hat{\mathbf{u}}_s$ $(s = 1, \ldots, m)$. For such scenarios, Eq. (6.5) is recast into first-order form via a state-space transformation [77]

$$\hat{\mathbf{A}}\dot{\hat{\mathbf{y}}} + \hat{\mathbf{B}}\hat{\mathbf{y}} = \mathbf{0}. \tag{6.7}$$

where

$$\hat{\mathbf{A}} = \begin{bmatrix} \mathbf{0} & \hat{\mathbf{M}} \\ \hat{\mathbf{M}} & \hat{\mathbf{C}} \end{bmatrix}, \tag{6.8a}$$

$$\hat{\mathbf{B}} = \mathrm{diag}\begin{bmatrix} -\hat{\mathbf{M}} & \mathbf{0} \\ \mathbf{0} & \hat{\mathbf{K}} \end{bmatrix}, \tag{6.8b}$$

$$\hat{\mathbf{y}} = \begin{bmatrix} \dot{\hat{\mathbf{u}}} & \hat{\mathbf{u}} \end{bmatrix}^{\mathrm{T}}. \tag{6.8c}$$

Now, assuming the solution $\hat{\mathbf{y}} = \bar{\mathbf{y}}\mathrm{e}^{\gamma t}$, we obtain a standard eigenvalue problem.

For viscous damping, the state-space transformation doubles the size of the original problem. Consequently, the eigenvalue problem that emerges from the substitution of $\hat{\mathbf{y}} = \bar{\mathbf{y}}\mathrm{e}^{\gamma t}$ in Eq. (6.7) has eigenvalues γ_s and eigenvectors $\bar{\mathbf{y}}_s$ $(s = 1, \ldots, 2m)$ that appear in conjugate pairs. Given their orthogonality with respect to the system matrices, the eigenvectors decouple the equations into $2m$ modal equations with complex roots γ_s, and thus effectively represent $2m$ single-degree of freedom systems. Focusing on the member of the conjugate pair with $\mathrm{Im}[\gamma_s] > 0$, we can write

$$\begin{aligned} \gamma_s(\boldsymbol{\kappa}) &= -\xi_s(\boldsymbol{\kappa})\omega_s(\boldsymbol{\kappa}) + \mathrm{i}\omega_s(\boldsymbol{\kappa})\sqrt{1 - \xi_s^2(\boldsymbol{\kappa})} \\ &= -\xi_s(\boldsymbol{\kappa})\omega_s(\boldsymbol{\kappa}) + \mathrm{i}\omega_{\mathrm{d},s}(\boldsymbol{\kappa}), \qquad s = 1, \ldots, m \end{aligned} \tag{6.9}$$

where, in the special case of Rayleigh damping, $\omega_s(\boldsymbol{\kappa})$ is the undamped frequency. From Eq. (6.9), we extract the wavevector-dependent damped frequency $\omega_{\mathrm{d},s}(\boldsymbol{\kappa})$ and damping ratio $\xi_s(\boldsymbol{\kappa})$, respectively:

$$\omega_{\mathrm{d},s}(\boldsymbol{\kappa}) = \mathrm{Im}[\gamma_s(\boldsymbol{\kappa})], \tag{6.10}$$

$$\xi_s(\boldsymbol{\kappa}) = -\frac{\mathrm{Re}[\gamma_s(\boldsymbol{\kappa})]}{\mathrm{Abs}[\gamma_s(\boldsymbol{\kappa})]}. \tag{6.11}$$

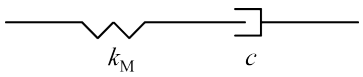

Figure 6.1: Maxwell element composed of a linear elastic spring and viscous dashpot representing, respectively, conservative and non-conservative mechanical processes.

6.3.2 Formulation of Viscoelastic Wave Propagation

For the case of viscous damping presented in Sec. 6.3.1, the non-conservative forces are assumed to depend only on the instantaneous velocities. In practice, this is unique to the situation in which a viscous fluid is the mechanism for dissipation. The dissipative forces within common materials such as polymers, composites, and even metals nonviscously depend on quantities other than the instantaneous velocities. In the linear hereditary theory, energy loss is attributed to the phase lag between the displacement and the applied stress [137]. The label "hereditary" refers to the role of the past history of motion on the current state. While preserving the linearity of the problem, perhaps the most general way of imparting this characteristic to Eqs. (6.3) and (6.5) is through convolution integrals over kernel functions $G(t)$ [133]. With exponentially decreasing kernel functions of the form $G(t) = \mu_1 \mathrm{e}^{-\mu_2 t}$, we rewrite Eq. (6.5) as

$$\hat{\mathbf{M}}\ddot{\hat{\mathbf{u}}} + \sum_{j=1}^{\ell} \hat{\mathbf{C}}_j \int_0^t \mu_{1,j} \mathrm{e}^{-\mu_{2,j}(t-\tau)} \dot{\hat{\mathbf{u}}}(\tau) \mathrm{d}\tau + \hat{\mathbf{K}}\hat{\mathbf{u}} = \mathbf{0}, \tag{6.12}$$

where the summation reflects the possibility of multiple coefficient matrices and kernel functions with relaxation pairs $(\mu_{1,j}, \mu_{2,j})$ being required to accurately describe the behavior. Such a system is described as one of hereditary of degree ℓ. Although, for the Maxwell element of viscoelasticity, the kernel functions are traditionally associated with a stiffness matrix (effectively adding a dissipative capability), in Eq. (6.12), the kernel functions are associated with the damping matrix (effectively adding a storage capability). Figure 1 depicts a Maxwell element as a linear spring and a viscous dashpot in series. The kernel function can be derived as [138]

$$G(t) = k_{\mathrm{M}} \mathrm{e}^{-(k_{\mathrm{M}}/c)t}. \tag{6.13}$$

One may imagine that in the limit $k_{\mathrm{M}} \to \infty$, the viscous dashpot joins a rigid spring such that essentially no mechanical energy is stored by the spring and, instead, is dissipated by the dashpot.

Viscoelastic effects emerge to varying degrees if k_{M} has a finite, non-zero value that permits the storage of a portion of the mechanical energy supplied to the Maxwell element. In the limit $k_{\mathrm{M}} \to 0$, the spring and dashpot effectively disengage and mechanical energy is neither conserved nor dissipated. Multiple Maxwell elements arranged in parallel to an equilibrium spring (Maxwell-Weichert model) may be applied to more accurately describe the material behavior.

In this section, we apply the state-space approach to Eq. (6.12) by introducing a set of internal variables. We develop the state-space matrices using an approach proposed for finite structural dynamics systems [132]; here, we extend it to the analysis of the unit cell problem. The approach is specific to the case in which the magnitude of the relaxation pairs are equal (i.e., $\mu_j = \mu_{1,j} = \mu_{2,j}$). This particular form of the kernel function, possessing a unit area,

$$\int_0^\infty \mu_j \mathrm{e}^{-\mu_j t} \mathrm{d}t = 1, \tag{6.14}$$

allows the direct comparison of the viscous and viscoelastic cases [131]. For the special case of $\ell = 1$ and damping is low such that the damped frequency is approximately equal to the undamped frequency, Ref. [131] describes a method for extracting μ_1 and $\bar{\mathbf{C}}_1$ from experimental data.

First, we equate each convolution integral with an internal variable $\hat{\mathbf{p}}_j$ such that

$$\hat{\mathbf{p}}_j = \int_0^t \mu_j \mathrm{e}^{-\mu_j (t-\tau)} \dot{\hat{\mathbf{u}}}(\tau) \mathrm{d}\tau, \tag{6.15}$$

$$\hat{\mathbf{M}} \ddot{\hat{\mathbf{u}}} + \sum_{j=1}^{k} \hat{\mathbf{C}}_j \hat{\mathbf{p}}_j + \hat{\mathbf{K}} \hat{\mathbf{u}} = \mathbf{0}. \tag{6.16}$$

From the Leibniz integral rule applied to Eq. (6.15), we obtain

$$\begin{aligned} \dot{\hat{\mathbf{p}}}_j &= -\int_0^t \mu_j^2 \mathrm{e}^{-\mu_j (t-\tau)} \dot{\hat{\mathbf{u}}}(\tau) \mathrm{d}\tau + \mu_j \dot{\hat{\mathbf{u}}} \\ &= \mu_j [\dot{\hat{\mathbf{u}}} - \hat{\mathbf{p}}_j]. \end{aligned} \tag{6.17}$$

Substituting Eq. (6.17) into Eq. (6.16) gives

$$\hat{\mathbf{M}} \ddot{\hat{\mathbf{u}}} + \sum_{j=1}^{k} \hat{\mathbf{C}}_j \left[\dot{\hat{\mathbf{u}}} - \frac{1}{\mu_j} \dot{\hat{\mathbf{p}}}_j \right] + \hat{\mathbf{K}} \hat{\mathbf{u}} = \mathbf{0}. \tag{6.18}$$

At this point, incorporating Eq. (6.18) into a state-space format will result in non-square matrices. To produce square and block-symmetric state-space matrices, we formulate an additional equation.

Premultiplying Eq. (6.17) by $\hat{\mathbf{C}}_j$ and dividing by μ_j^2 yields

$$-\frac{1}{\mu_j}\hat{\mathbf{C}}_j\dot{\hat{\mathbf{u}}} + \frac{1}{\mu_j^2}\hat{\mathbf{C}}_j\dot{\hat{\mathbf{p}}}_j + \frac{1}{\mu_j}\hat{\mathbf{C}}_j\hat{\mathbf{p}}_j = \mathbf{0}. \tag{6.19}$$

Finally, adjoining (6.18) and (6.19) may be assembled into the state-space format of Eq. (6.7) where

$$\hat{\mathbf{A}} = \begin{bmatrix} \mathbf{0} & \hat{\mathbf{M}} & \mathbf{0} & \mathbf{0} & \cdots & \mathbf{0} \\ \hat{\mathbf{M}} & \sum_{j=1}^{k}\hat{\mathbf{C}}_j & -\frac{1}{\mu_1}\hat{\mathbf{C}}_1 & -\frac{1}{\mu_2}\hat{\mathbf{C}}_2 & \cdots & -\frac{1}{\mu_k}\hat{\mathbf{C}}_k \\ \mathbf{0} & -\frac{1}{\mu_1}\hat{\mathbf{C}}_1 & \frac{1}{\mu_1^2}\hat{\mathbf{C}}_1 & \mathbf{0} & \cdots & \mathbf{0} \\ \mathbf{0} & -\frac{1}{\mu_2}\hat{\mathbf{C}}_2 & \mathbf{0} & \frac{1}{\mu_2^2}\hat{\mathbf{C}}_2 & \cdots & \mathbf{0} \\ \vdots & \vdots & \vdots & \vdots & \ddots & \vdots \\ \mathbf{0} & -\frac{1}{\mu_k}\hat{\mathbf{C}}_k & \mathbf{0} & \mathbf{0} & \cdots & \frac{1}{\mu_k^2}\hat{\mathbf{C}}_k \end{bmatrix}, \tag{6.20a}$$

$$\hat{\mathbf{B}} = \mathrm{diag}\left[-\hat{\mathbf{M}} \quad \hat{\mathbf{K}} \quad \frac{1}{\mu_1}\hat{\mathbf{C}}_1 \quad \frac{1}{\mu_2}\hat{\mathbf{C}}_2 \quad \cdots \quad \frac{1}{\mu_k}\hat{\mathbf{C}}_k\right], \tag{6.20b}$$

$$\hat{\mathbf{y}} = \left[\dot{\hat{\mathbf{u}}} \quad \hat{\mathbf{u}} \quad \hat{\mathbf{p}}_1 \quad \hat{\mathbf{p}}_2 \quad \cdots \quad \hat{\mathbf{p}}_k\right]^{\mathrm{T}}, \tag{6.20c}$$

and diag[·] contains the elements of a block diagonal matrix.

Upon obtaining the eigenvalues γ_s, there are m conjugate pairs that physically represent the modes of damped wave propagation. The remaining real eigenvalues are non-oscillating. As seen in the above formulation, in the limit $\mu_j \to \infty \; \forall j$, the viscous state-space formulation [Eq. (6.8)] is recovered. That is, high values of μ_j represent more viscous behavior (less dependence on the past history), while low values of μ_j represent more viscoelastic behavior (more dependence on the past history).

6.4 Band Structure of Damped Phononic Materials and the Viscous-to-viscoelastic Transition

6.4.1 Lumped parameter model

The formulations in Eqs. (6.8) and (6.20) are suitable to a finite element discretization of a material continuum; however, for simplicity, to compare the effects of viscous and viscoelastic

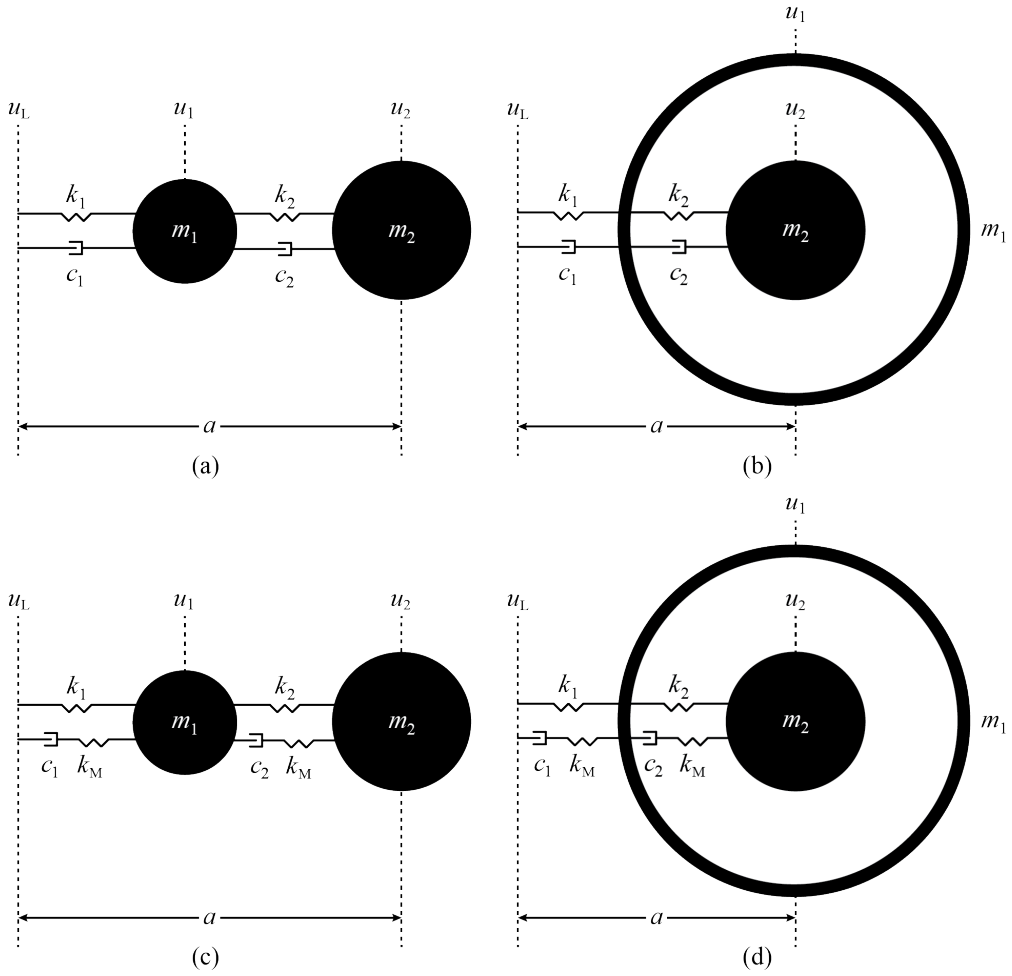

Figure 6.2: Lumped parameter models of a two-mass 1D phononic material unit cell with lattice spacing a with (a,c) the Bragg scattering configuration of a phononic crystal and (b,d) the locally resonant configuration of an elastic metamaterial. In (a,b), damping is represented by a Zener (viscoelastic damping) model; whereas in (c,d) it is represented by a KelvinVoigt (viscous damping) model.

damping on wave propagation in periodic materials, we utilize a simple lumped-parameter material model composed of point masses, linear elastic springs, and viscous dashpots. Furthermore, we examine the results for two archetypal material configurations: phononic crystal (PC) [Fig. 6.2a] and elastic metamaterial (AM) [Fig. 6.2b]. For the purpose of demonstration, the material parameters have the following relations: $m_2/m_1 = r_\mathrm{m} = 3$, $c_2/c_1 = r_\mathrm{c} = 1/2$, and $k_2/k_1 = r_\mathrm{k} = 1$. With these criteria and degrees of freedom organized such that $\mathbf{u} = [u_1 \quad u_2 \quad u_\mathrm{L}]^\mathrm{T}$, $\mathbf{f} = [f_1 \quad f_2 \quad f_\mathrm{L}]^\mathrm{T}$, and $\hat{\mathbf{u}} = [u_1 \quad u_2]^\mathrm{T}$, we write the matrices associated with each unit cell configuration in Fig. 6.2

explicitly. The two material configurations share a common mass matrix.

$$\mathbf{M} = m_2\mathbf{M}_\mathrm{o} = m_2\begin{bmatrix} 1/r_\mathrm{m} & 0 & 0 \\ 0 & 1 & 0 \\ 0 & 0 & 0 \end{bmatrix} \tag{6.21}$$

Specifically, for the phononic crystal:

$$\mathbf{C} = c_2\mathbf{C}_\mathrm{o} = c_2\begin{bmatrix} 1/r_\mathrm{c}+1 & -1 & -1/r_\mathrm{c} \\ -1 & 1 & 0 \\ -1/r_\mathrm{c} & 0 & 1/r_\mathrm{c} \end{bmatrix}, \tag{6.22a}$$

$$\mathbf{K} = k_2\mathbf{K}_\mathrm{o} = k_2\begin{bmatrix} 1/r_\mathrm{k}+1 & -1 & -1/r_\mathrm{k} \\ -1 & 1 & 0 \\ -1/r_\mathrm{k} & 0 & 1/r_\mathrm{k} \end{bmatrix}, \tag{6.22b}$$

$$\mathbf{T} = \begin{bmatrix} 1 & 0 \\ 0 & 1 \\ 0 & \mathrm{e}^{-\mathrm{i}\kappa a} \end{bmatrix}. \tag{6.22c}$$

For the metamaterial:

$$\mathbf{C} = c_2\mathbf{C}_\mathrm{o} = c_2\begin{bmatrix} 1/r_\mathrm{c}+1 & -1 & -1/r_\mathrm{c} \\ -1 & 1 & 0 \\ -1/r_\mathrm{c} & 0 & 1/r_\mathrm{c} \end{bmatrix}, \tag{6.23a}$$

$$\mathbf{K} = k_2\mathbf{K}_\mathrm{o} = k_2\begin{bmatrix} 1/r_\mathrm{k}+1 & -1 & -1/r_\mathrm{k} \\ -1 & 1 & 0 \\ -1/r_\mathrm{k} & 0 & 1/r_\mathrm{k} \end{bmatrix}, \tag{6.23b}$$

$$\mathbf{T} = \begin{bmatrix} 1 & 0 \\ 0 & 1 \\ \mathrm{e}^{-\mathrm{i}\kappa a} & 0 \end{bmatrix}. \tag{6.23c}$$

After applying the transformation matrix, $\hat{\mathbf{M}}$, $\hat{\mathbf{C}}$, and $\hat{\mathbf{K}}$ are the same matrices appearing in

Ref. [78]. Dividing by m_2, the general equations of motion are

$$\hat{\mathbf{M}}_{\mathrm{o}}\ddot{\hat{\mathbf{u}}} + \beta\hat{\mathbf{C}}_{\mathrm{o}}\int_0^t \mu \mathrm{e}^{-\mu(t-\tau)}\dot{\hat{\mathbf{u}}}(\tau)\mathrm{d}\tau + \omega_0^2\hat{\mathbf{K}}_{\mathrm{o}}\hat{\mathbf{u}} = \mathbf{0}, \tag{6.24}$$

where $\beta = c_2/m_2$, which varies with c_2, is a measure of damping intensity and $\omega_0 = \sqrt{k_2/m_2} =$ 150rad/s. To demonstrate the viscoelastic case, we employ only one kernel function.

6.4.2 Phononic crystal versus metamaterial and viscous versus viscoelastic damping

As we examine the frequency and damping ratio dispersion diagrams, the undamped condition, achieved by setting the normalized damping intensity $\beta/\omega_0 = 0$, is represented by a black curve, while light and dark green curves represent the damping conditions $\beta/\omega_0 = 0.1$ and $\beta/\omega_0 = 0.2$, respectively. In particular, the frequency diagrams are normalized with respect to $\omega_0 = 150$rad/s.

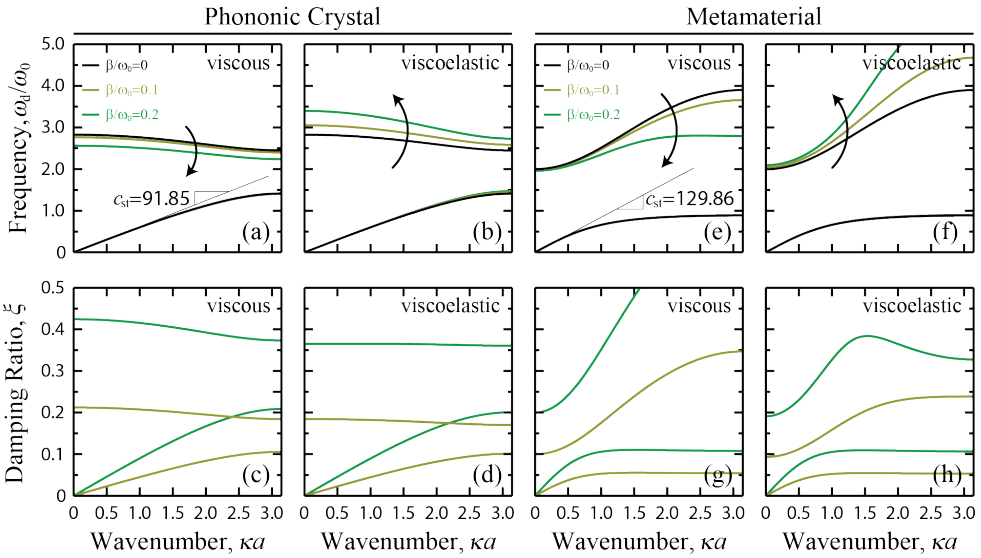

Figure 6.3: Damped dispersion diagrams (top row) of a discrete, two degree-of-freedom phononic crystal (left column) and elastic metamaterial (right column). The undamped, long-wavelength speed of sound, c_{st} is displayed in each frequency diagram. The corresponding damping ratio diagrams (bottom row) are a consequence of a complex temporal frequency in the application of the Bloch condition. All mass, stiffness, and damping parameters are identical between each material model.

Figures 6.3a,c,e,g shows the dispersion diagrams generated by Eqs. (6.7) and (6.8) for the viscous case [i.e., or Eq. (6.20) when all the corresponding kernels are delta functions]. Because the damping force is proportional to the relative velocity (a function of λ) of each degree of freedom, the damping effect is more pronounced at higher frequencies. Also noticeable, energy dissipated by propagating waves manifests as a decrease in propagation frequency across the whole of the wavenumber domain for each branch in Figs. 6.3a,e; which is characteristic of viscous damping. Thus the width of the band gap decreases and the value of the central frequency shifts to lower magnitudes. The corresponding damping ratio diagrams in Figs. 6.3c,g reinforces these findings. Naturally, for sufficiently high β, wavenumbers for which $\xi_s(\kappa) \geq 1$ (not shown) represent non-oscillating modes.

Assuming a single relaxation parameter $\mu = 10^3$ ($k_{\mathrm{M}} \propto \mu$), Figs. 6.3b,d,f,h demonstrate the viscoelastic case. Similar to the viscous case, the effect of damping increases with frequency. On the other hand, the viscoelastic frequency diagrams in Figs. 6.3b,f display unique behavior compared to the viscous case. Under the chosen viscoelastic conditions, both branches show an increase in frequency across the wavenumber domain with this trait emphasized in the second branch. As a consequence, the band gap widens and its central frequency shifts upwards. By introducing a hereditary effect into the damping model, a portion of the mechanical energy that would be dissipated in the viscous case is instead conserved, leading to the increase in frequency and the decrease in damping ratio seen in Figs. 6.3d,h, respectively. This is a manifestation of joining an elastic spring in series with the viscous dashpot, forming a Maxwell element.

6.4.3 Damping zones and transition lines

In Sec. 6.3.2, we emphasized that in the limit $\mu_j \to \infty \; \forall j$, the viscous state-space formulation [Eqs. (6.8)] is recovered. For each material configuration of the models examined in Fig. 6.3, the plots in Fig. 6.4 track the evolution of the viscoelasticly damped band-gap edge frequencies over a range of μ for $\beta/\omega_0 = 0.1$ and $\beta/\omega_0 = 0.2$. The light and dark green dashed horizontal lines indicate the location of the viscously damped edge frequencies for, respectively, these two values

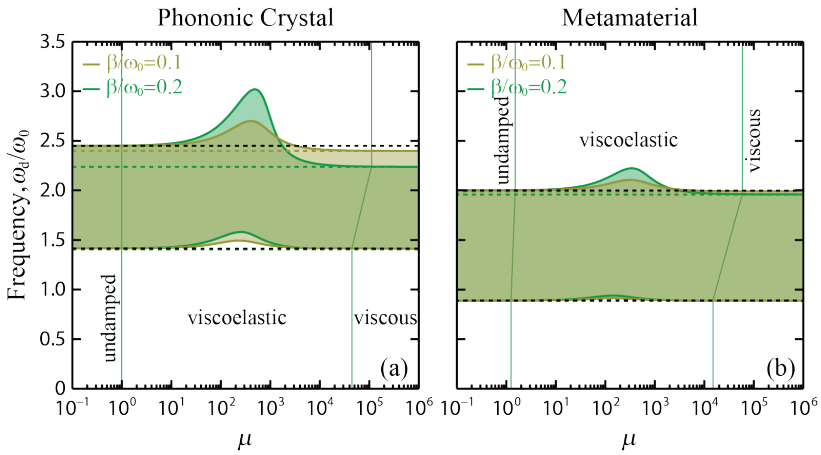

Figure 6.4: Viscoelasticly damped band-gap edge frequencies over the viscoelastic-viscous regime. Dashed, horizontal lines mark the value of the corresponding viscously damped band-gap frequencies.

of damping intensities. The dashed black lines correspond to the undamped case. The maximum viscoelastic effect grows with damping intensity as the storage capability of the Maxwell element is amplified more than the dissipative capacity.

For ease of exposition, since the results are similar between the material types, we focus exclusively on the phononic crystal model to further examine viscoelastic wave propagation. The plots in Fig. 6.5 highlight the viscous-viscoelastic metamorphosis particular to $\beta/\omega_0 = 0.2$ in Fig. 6.4a. Using a Maxwell element with a fixed c and variable k_{M} as a guide, we inspect the damped band-gap edge frequencies for various values of $\mu \propto k_{\mathrm{M}}$. Point A marks the value of μ at which the band-gap edge frequency is 1% over the viscous value and beyond which k_{M} is so stiff that it is effectively a rigid rod and the vast majority of the energy transferred to the Maxwell element (i.e., not stored by the equilibrium springs $k_{1,2}$) is dissipated by the dashpot. In this limiting case, the viscoelastic band structure closely resembles the corresponding viscous band structure. Conversely, point D marks the value of μ at which the band-gap edge frequency is 1% over the undamped value and below which k_{M} is so elastic as to effectively disengage the dashpot so as to deprive the Maxwell element of mechanical influence. As a result, the damped band-gap edge frequencies approach their undamped values and so does the viscoelastic band structure as a whole. Between points A and D,

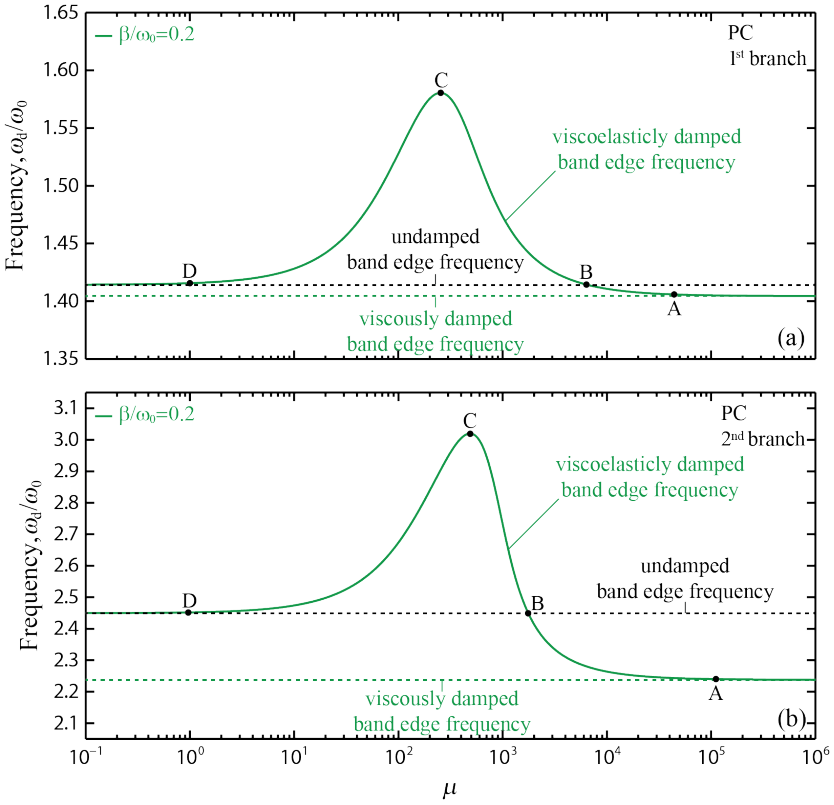

Figure 6.5: Detailed view of viscoelasticly damped band-gap frequencies in Fig. 6.4 ($\beta/\omega_0 = 0.2$).

while dissipation remains present in the Maxwell element, k_{M} is neither too rigid nor too flexible to store a meaningful fraction of mechanical energy. Point B marks the value of μ where the undamped and damped band-gap edge frequencies are equal, as if the spring component of the Maxwell element cancels the damping component, although this equivalence is not necessarily true universally over the entire wavenumber domain. At point C, the energy storage capability reaches its zenith and the damped band-gap edge frequency achieves the greatest separation above its viscously damped counterpart.

In Fig. 6.5, it is apparent that points A–D do not coincide between the two branches, softening thus rendering the transition between the contrast between the viscous and viscoelastic behavior frequency dependent. To better distinguish the two two damping regimes, we identify essentially viscous damping as that for which the viscoelastic band structure ω_{VE} is, on average, within 1% of the viscous band structure ω_{V} as obtained from matrices of Eq. (6.8). Similarly,

with the undamped band structure ω_{U} as a reference, we separate the qualitatively undamped and viscoelastic regions. Mathematically, the relevant criteria may be stated as follows:

$$\phi_1 = \frac{1}{mC}\sum_{s=1}^{m}\oint\left(\frac{\omega_{\mathrm{VE},s}}{\omega_{\mathrm{U},s}}-1\right)\mathrm{d}\boldsymbol{\kappa} \qquad \begin{cases} \phi \le 0.01 & \text{undamped} \\ \phi > 0.01 & \text{viscoelastic} \end{cases} \tag{6.25a}$$

$$\phi_2 = \frac{1}{mC}\sum_{s=1}^{m}\oint\left(\frac{\omega_{\mathrm{VE},s}}{\omega_{\mathrm{V},s}}-1\right)\mathrm{d}\boldsymbol{\kappa} \qquad \begin{cases} \phi \le 0.01 & \text{viscous} \\ \phi > 0.01 & \text{viscoelastic} \end{cases} \tag{6.25b}$$

where C is the path length of the irreducible Brillouin zone (IBZ). In the present case, assuming a lattice spacing of $a = 1$, then $C = \pi$.

Figures 6.6a,b show the variation of $\phi_{1,2}$ as a function of μ for a set of damping intensities, specifically, $\beta/\omega_0 = \{0.05, 0.10, 0.15, 0.20\}$. Typically, $\phi_{1,2}(\mu)$ displays a single maximum at $\mu = \mu_{\mathrm{peak}}$ where the viscoelastic band structure has the greatest disagreement with the relevant undamped or viscous band structure. In Fig. 6.6a, for $\mu < \mu_{\mathrm{peak}}$, $_1$ approaches zero as ω_{VE} better approximates ω_{U}. Detailed in the inset, the undamped-to-viscoelastic transition occurs at $\mu = \mu_{\mathrm{trans}}$, where $\phi_1(\mu_{\mathrm{trans}}) = 0.01$. As the prescribed damping intensity β/ω_0 increases, it is observed that μ_{trans} shifts to ever lower values. Above μ_{peak}, the function converges to negative values as ω_{VE} descends below the undamped band structure to approach ω_{V}. Using ϕ_2, Fig. 6.6b shows the transition of the band structure from viscoelastic to the viscous condition. In Fig. 6.6b, as β/ω_0 increases, the slope of ϕ_2 for $\mu > \mu_{\mathrm{peak}}$ becomes steeper such that the transition to viscous behavior becomes more abrupt. At the higher damping intensities presented in Fig. 6.6c, μ_{trans} indicates the increasing abrupt transition as it moves closer to μ_{peak}. Below μ_{peak}, the opposite occurs and ever smaller values of are required to trigger the transition to the undamped regime.

Figure 6.6c combines the results of Figs. 6.6a,b to define the viscoelastic region over a range of damping levels. The transitions to viscoelastic behavior from the respective undamped and viscously damped conditions are indicated. Below $\beta/\omega_0 \approx 0.016$, $\phi_{1,2} \le 0.01\ \forall\mu$ and so, following our criteria, no clear distinction between the three damping scenarios exists. However, given that undamped and viscous qualities reside on either side of μ_{peak}, it may serve as a boundary between the two regimes in this otherwise ambiguous damping region. At $\beta/\omega_0 \approx 0.016$, the viscous-

viscoelastic transition is established when first $\phi_{1,2}(\mu_{\text{peak}}) = 0.01$ and $\mu_{\text{trans}} = \mu_{\text{peak}}$. Generally, for ϕ_1 and ϕ_2, these points do not coincide but converge with transition criteria more demanding than the present 1%.

Strikingly, for constant β/ω_0, an overly damped, non-propagating dispersion branch [$\omega_{\text{d},s}(\boldsymbol{\kappa}) = 0$ for all or a subset of $\boldsymbol{\kappa}$] in the viscous region may become a propagating branch in the viscoelastic region as a result of the amplification of k_{M} with decreased μ. This amplification leads to a second interesting result. Under viscous circumstances, if $\mathbf{K} = \mathbf{0}$, wave propagation is impossible; however, with the storage capability of the Maxwell element, this is not necessarily true under viscoelastic conditions. Increasing $\mathbf{C}$ or decreasing μ may amplify k_{M} to the extent of supporting oscillation and, thus, wave propagation in the phononic material. With $\mathbf{K} = \mathbf{0}$ and the appropriate kernel function, we model a viscoelastic fluid [137], not a viscoelastic solid. For our phononic crystal, the viscoelastic fluid domain is indicated in Fig. 6.6b.

6.5 Metadamping: Enhancement of modal dissipation

To combat potentially damaging dynamic loads, it is desirable for an engineering material to possess a high damping capacity while maintaining a load-bearing capability (stiffness). However, for classic materials, an advantage in one of these traits comes at the expense of the other. For example, the load-bearing capability of steel is exploited in many engineering applications although its damping capacity is unremarkable; on the contrary, polymers such as rubber excel at dissipating energy but possess little stiffness. The challenge of achieving simultaneously high stiffness and high damping within a material has been met in a variety of ways. Chung [113] sought the optimal combination of dissipative and stiff elements forming a composite. Van Humbeek [112] explored the conditions (amplitude, frequency, etc.) for which metal alloys with highly dissipative martensitic phases achieved superior damping and stiffness. Lakes *et al* [111] demonstrated the efficacy of embedding negative-stiffness inclusions within a supporting matrix to generate a material with extreme damping and stiffness. Meaud *et al* [48] designed a hierarchical microstructure that displayed significantly higher stiffness than conventional polymers while maintaining high damping. In a recent

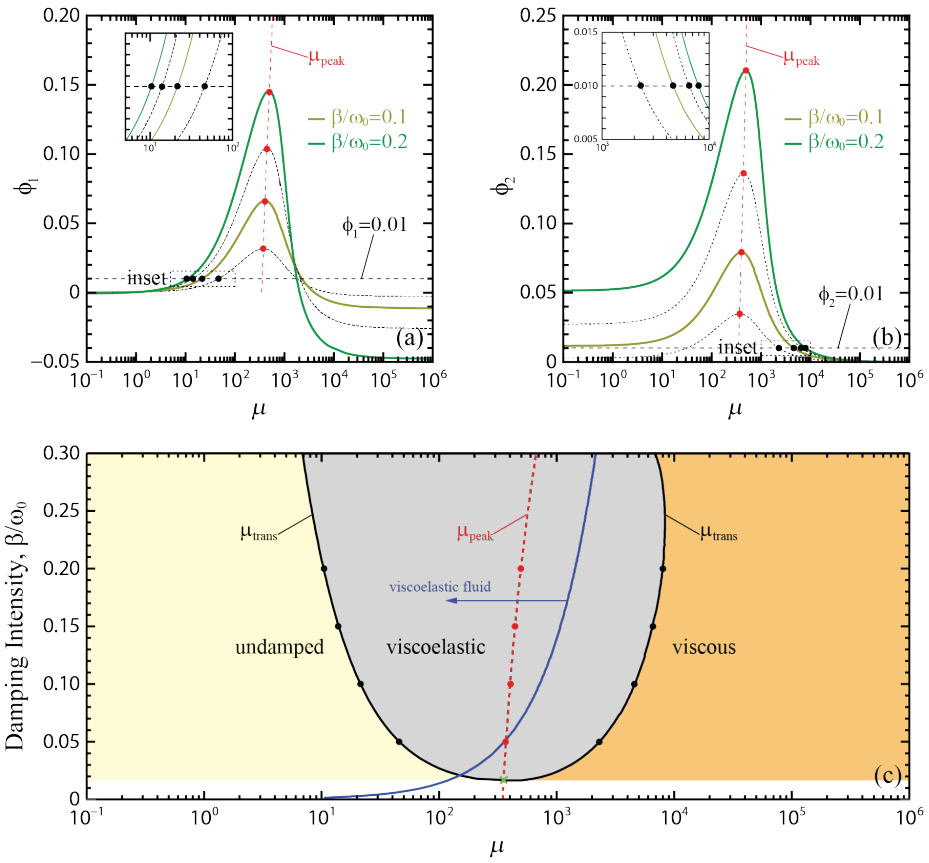

Figure 6.6: The fractional deviation of the viscoelastic band structure ω_{VE} from the (a) undamped band structure ω_{U} and (b) viscous band structure ω_{V}. Particular to the damping intensity, ω_{VE} transitions to either ω_{U} or ω_{V} at a specific $\mu = \mu_{\mathrm{trans}}$. With $\mu_{\mathrm{trans}} < \mu_{\mathrm{peak}}$, $\phi_1(\mu_{\mathrm{trans}}) = 0.01$ marks the undamped-viscoelastic transition. Similarly, with $\mu_{\mathrm{trans}} > \mu_{\mathrm{peak}}$, the viscous-viscoelastic transition occurs when $\phi_2(\mu_{\mathrm{trans}}) = 0.01$. (c) A map distinguishing the three phases of ω_{VE}. The viscoelastic fluid domain indicates where wave propagation is possible even with $\mathbf{K} = \mathbf{0}$.

study [125], the concept of metadamping was introduced to describe the phenomenon of damping emergence that may arise in an acoustic/elastic metamaterial. Specifically, when compared to a statically equivalent phononic crystal with identically prescribed damping, a metamaterial may exhibit higher dissipation levels across many, if not all, modes of wave propagation. This phenomenon has implications for the design of highly dissipative materials that maintain (or do not sacrifice) mechanical load-bearing capacity. Previously, metadamping has been demonstrated for viscous conditions [125]. In this Section, we utilize our material models to illuminate the metadamping phenomenon in viscoelastic circumstances.

Given that the total mass of each configuration in Fig. 6.2 is the same, static equivalence is achieved when, in the absence of dissipation, the long-wavelength sound speed, $c_{\mathrm{st}} = \lim_{|\boldsymbol{\kappa}|\to 0}(\omega_1(\boldsymbol{\kappa})/|\boldsymbol{\kappa}|)$, of each material is also in agreement. At present, as indicated in Figs. 6.3a,e, $c_{\mathrm{st}}^{\mathrm{PC}} = 91.85$ and $c_{\mathrm{st}}^{\mathrm{AM}} = 129.86$. While maintaining r_k, the two long-wavelength sound speeds may be brought into agreement by strengthening the springs of the phononic crystal such that ω_0 is configuration-specific (i.e., $\omega_0^{\mathrm{PC}} \neq \omega_0^{\mathrm{AM}}$). Alternatively, the same goal can be achieved by weakening the springs of the metamaterial. The damping ratio diagrams may then be used to compare the damping capacity of each material configuration. For this purpose, we calculate the total damping ratio over both branches,

$$\xi_{\mathrm{tot}}^{\nu} = \sum_{s=1}^{m} \oint \xi_{\mathrm{s}}^{\nu}(\boldsymbol{\kappa}) \mathrm{d}\boldsymbol{\kappa} \qquad \nu = \mathrm{PC}, \mathrm{AM} \tag{6.26}$$

where the integration is over the IBZ boundaries.

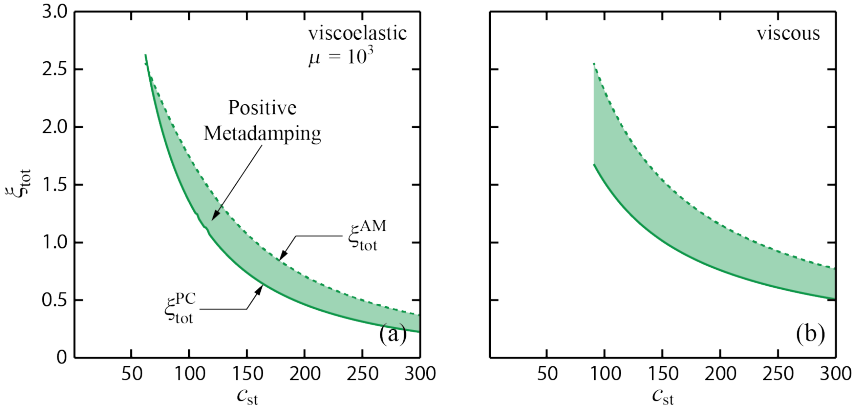

Figure 6.7: Total damping ratio over both branches for the phononic crystal (solid) and metamaterial (dashed) over a range of c_{st} values for (a) the viscoelastic condition and (b) the viscous condition. The total damping ratio of each configuration is displayed for comparison until the overdamped condition ($\xi > 1$) is attained.

For $\beta/\omega_0 = 0.2$, the diagrams in Fig. 6.7 illustrate the variation of ξ_{tot} over a range of c_{st}. In each plot, the dashed curve corresponding to $\xi_{\mathrm{tot}}^{\mathrm{AM}}$ and the solid curve of $\xi_{\mathrm{tot}}^{\mathrm{PC}}$ enclose a positive metadamping region (i.e., $(\xi_{\mathrm{tot}}^{\mathrm{AM}} - \xi_{\mathrm{tot}}^{\mathrm{PC}}) > 0$). A typical feature of each plot is the downward slope of ξ_{tot}^{ν} as c_{st} increases, a result of the material becoming stiffer. The metadamping region is bounded on the left by a minimum value of c_{st} for which dissipative wave propagation is still

possible for both configurations over the entire boundary of the IBZ. Below this value of c_{st}, the elastic metamaterial is overdamped and, because Eq. 6.11 limits the damping ratio to $\xi \leq 1$, a fair comparison of $\xi_{\mathrm{tot}}^{\mathrm{PC}}$ and $\xi_{\mathrm{tot}}^{\mathrm{AM}}$ can no longer be made. Inspecting each frame in Fig. 6.7 reveals the effect of viscoelasticity on the metadamping region. Naturally, the metadamping region diminishes and favors the lower left of the diagram as the damping condition becomes more viscoelastic and heredity mitigates the dissipation of mechanical energy.

Figure 6.8 shows the sensitivity of the metadamping phenomenon to the relevant material parameters. As increased heredity effectively transforms the viscous dampers into elastic springs in Fig. 6.8a, the metadamping region simultaneously descends the ξ_{tot}-axis and collapses. Metadamping results from the concentration of strain energy, a task at which the elastic metamaterial, with the aid of the internal resonator, outperforms the phononic crystal. In general, as illustrated in Fig. 6.8b,c,d, decreasing r_{m} or increasing the coupling between m_1 and m_2 through one or a combination of $r_{\mathrm{c}} \to \infty$ and $r_{\mathrm{k}} \to \infty$ diminishes the role of the internal resonator and curtails the metadamping phenomenon. The metamaterial resembles more the phononic crystal as r_{m} decreases. Manipulating the ratio of damping viscosities r_{c} bestows the metamaterial resonator with more/less influence over the emergent phenomenon. Smaller storage ratios are indicative of a decreased ability for the metamaterial resonator to cache the energy of oscillation and, thus, the dissipative element of the resonator expresses greater influence. Consequently, smaller storage ratios promote the emergence of the metadamping phenomenon.

Until now, metadamping has been demonstrated with the aid of a locally resonant material possessing a dipole resonance. However, locally resonant material designs featuring monopolar [29] and quadripolar [27, 30] resonances appear in the literature. This motivates a study of what effect the type of resonance has on the material damping capacity. Continuing with the one-dimensional lumped parameter models used thus far, in Fig. 6.9, we present the unit cell of an elastic metamaterial similar to that of Ref. [139] (although with damping elements) and supporting a monopole resonance. Four rigid, massless truss members connect the unit cell microstructure. While the mass and transformation matrices are the same as those defined in Eqs. (6.21) and

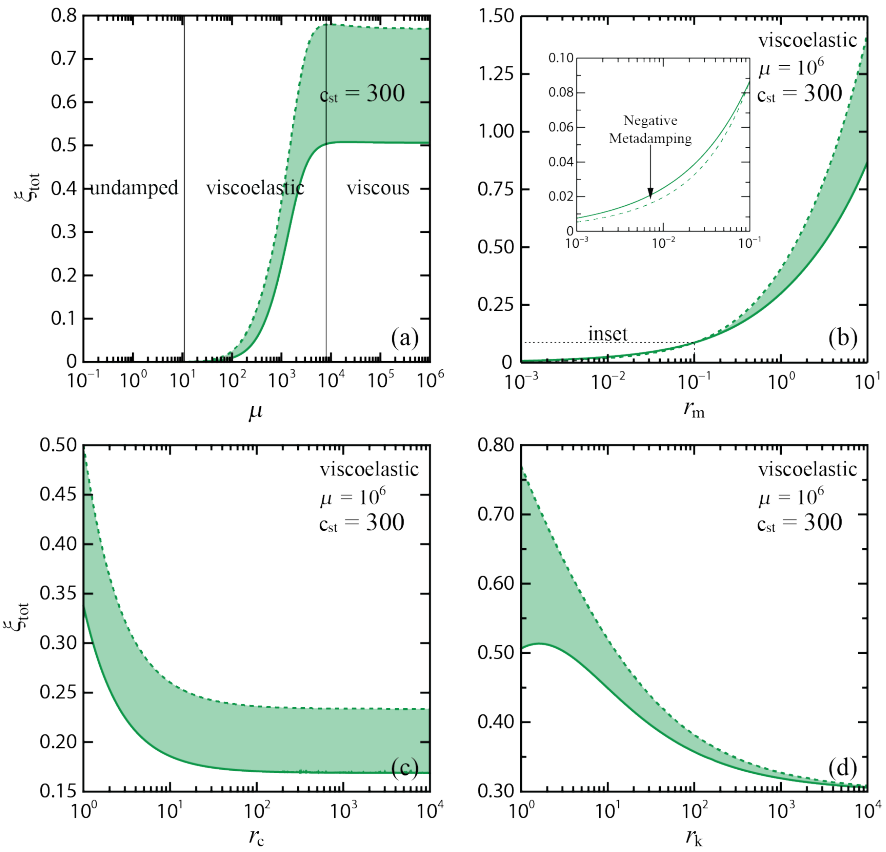

Figure 6.8: Variation of the metadamping phenomenon with material parameters r_m, r_c, and r_k affecting the influence of the metamaterial internal resonator and μ affecting the influence of heredity. Damping intensity held constant at $\beta/\omega_0 = 0.2$. Except where plainly contradictory, $r_m = 3$, $r_c = 1/2$, and $r_k = 1$. A negative metadamping ($\xi_{tot}^{AM} < \xi_{tot}^{PC}$) region emerges as $r_m \to 0$.

(6.23c), respectively, the corresponding damping and stiffness matrices for the unit cell in Fig. 6.9 are given by Eq. (6.27) where $\delta = (a/D)^2$.

$$\mathbf{C} = c_2\mathbf{C}_o = c_2\begin{bmatrix} 1/r_c + \delta/2 & \sqrt{\delta} & -(1/r_c + \delta/2) \\ \sqrt{\delta}/2 & 1 & -\sqrt{\delta}/2 \\ -(1/r_c + \delta/2) & -\sqrt{\delta} & 1/r_c + \delta/2 \end{bmatrix} \tag{6.27a}$$

$$\mathbf{K} = k_2\mathbf{K}_o = k_2\begin{bmatrix} 1/r_k + \delta/2 & \sqrt{\delta} & -(1/r_k + \delta/2) \\ \sqrt{\delta}/2 & 1 & -\sqrt{\delta}/2 \\ -(1/r_k + \delta/2) & -\sqrt{\delta} & 1/r_k + \delta/2 \end{bmatrix} \tag{6.27b}$$

The band structure associated with the monopolar metamaterial has features similar to the

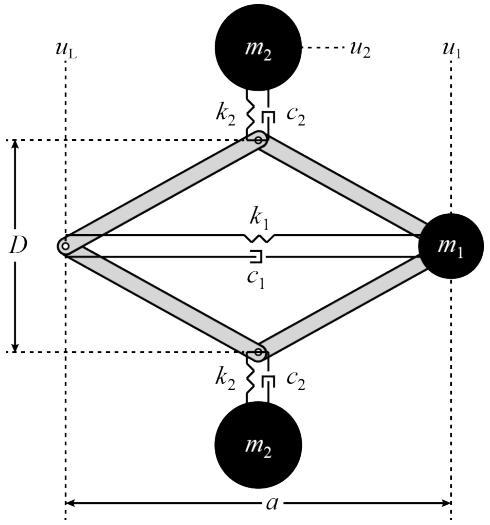

Figure 6.9: Lumped parameter model of a two-phased 1D phononic material unit cell with local monopolar resonance.

dipolar metamaterial and will not be shown here. In addition, the conclusions reached earlier in this section regarding the effects of viscoelasticity, energy concentration, and coupling on the metadamping phenomenon still hold. For simplicity, we consider the viscous case in the metadamping plot in Fig. 6.10. Here the total damping ratio associated with the phononic crystal, elastic metamaterial with dipole resonance (DP), and elastic metamaterial with monopole resonance (MP) ($\delta = 1$) are compared over a range of c_{st}. Monopole responses have a higher degree of symmetry than those of the dipole which permits a greater concentration of mechanical energy. With the application of damping, this superior ability to pool mechanical energy results in greater damping amplification for the monopole metamaterial than the dipole metamaterial and phononic crystal. Extending this reasoning to quadrupole and higher-order resonances, it is expected that the metadamping region will generally narrow with the increased order of the resonance. More work is needed to confirm this.

6.6 Conclusions

In this article, viscous and viscoelastic descriptions of material damping are used to model dissipative wave propagation in two archetypal phononic materials: an elastic metamaterial and

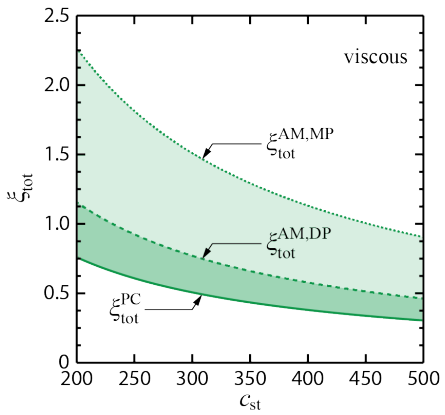

Figure 6.10: Total damping ratio over both branches for the phononic crystal (solid), metamaterial with dipole resonance (dashed), and metamaterial with monopole resonance (dotted) over a range of c_{st} values for the viscous condition.

a phononic crystal. The viscous assumption (characteristic of fluids) regards the instantaneous velocity to be the only relevant state variable in the determination of the damping force, while the viscoelastic condition [characteristic of polymeric solids and (to a lesser extent) metals] accounts for the whole time history of motion through convolution integrals over exponentially decreasing kernel functions associated with the damping matrix. Following [132], the viscoelastic equations of motion are recast into a standard eigenvalue problem by an extended state-space transformation which acquires the familiar Duncan form of viscous damping when all kernels are delta functions. We observe viscous damping to decrease the propagating frequency and thereby contract the band structure; however, the hereditary effect of viscoelastic damping mitigates this response. By regarding viscoelasticly damped band-gap frequencies within 1% of their viscously damped values as representative of essentially viscous behavior, we define a viscous-viscoelastic transition. Plotted over a parameter space of damping and kernel decay constants, the transition traces a bow shape as increasingly narrow kernel functions are required to trigger the viscous-viscoelastic transition at higher damping intensities. Similar to [125], we found the influence of dissipation to be greatly affected by the configuration of the material through which a wave propagates. In localizing mechanical energy, the damping capacity of elastic metamaterials (locally resonant materials) is, in general, amplified when compared to statically equivalent phononic crystals (Bragg-scattering materials).

Among the locally resonant materials, those with monopolar resonance yield greater amplification over their counterparts with dipolar resonance. The hereditary effect of viscoelasticity lessens this effect, as does increased coupling between the matrix and inclusions. The consequences of these findings extend to the design of materials for elastic/acoustic vibration reduction, mitigation, and absorption purposes.

Chapter 7

Conclusions

The studies taken up in this dissertation are directed toward an understanding of dissipative wave propagation in phononic materials for improved performance prediction and extending the application space. To this end, methods from structural dynamics analysis were extended to the wave propagation problem at the material level to reveal the impact of dissipation on the band diagram and the dynamic effective properties. The results inspire a phononic-based solution to a long-standing materials problem. The purpose of this chapter is to recapitulate the main findings and to suggest some future research directions.

7.1 Summary

The native control of acoustic/elastic waves opens phononic materials to many applications in engineering where noise reduction and vibration isolation is desirable. In addition, their dynamic effective properties are central to the realization of advanced concepts, including cloaking and super-resolution imaging devices. Bloch's theorem forms the theoretical foundation of phononic material analysis, yielding the frequency band diagram, which summarizes much of the wave propagation characteristics and provides insight into the performance of the phononic structure in its practical engineering form. Material damping inevitably leads to dissipation of the wave energy; however, due to the variety of damping mechanisms and the complexity of damping models, among other reasons, much of the theoretical literature assumes conservative systems. This assumption negatively impacts the predictability of implemented phononic material designs and foregoes damping

as a design parameter/objective. To address each of these issues, this dissertation extends the models and analysis techniques originally developed in the context of vibration in finite structures to wave propagation in phononic materials.

Chapter 1 introduces phononic materials and indicates where the dissertation fits within the relevant literature. Phononic materials are shown to consist of fundamental structural elements called "unit cells" that repeat periodically in one-, two-, or three spatial dimensions. This internal structuring affects the propagation of acoustic/elastic waves in a manner described by Bloch's theorem, opening phononic materials to vibration control applications in engineering. The chapter shows how the frequency band diagram, the result of a unit cell analysis, describes the wave propagation characteristics of a phononic material and how its results relate to the dynamics of the corresponding structure. Phononic materials are divided into two subcategories—phononic crystals and metamaterials—and advanced applications (i.e., beyond vibration control) are highlighted for each classification. Metamaterials have especially remarkable applications due to their unnatural dynamic effective properties which may include negative density and modulus. The chapter concludes with a literature review pertaining to the subject of dissipative wave propagation in damped phononic materials, placing this dissertation within it and identifying the dissertation objectives as improved predictability of phononic material performance and damping as a design parameter/objective.

A review of the literature highlights the prevalence of studies investigating dissipative wave propagation from the perspective of waves at prescribed frequencies. Free waves have received far less attention and only from the propagating modes of the band diagram. Chapter 2 constructs the complete band diagram (propagating and non-propagating modes) for free waves and compares this to the corresponding complete diagram for prescribed waves. In the absence of energy dissipation, the two band diagrams are the same. For prescribed waves, material damping hinders the transmission of energy between subsequent unit cells, resulting in spatial attenuation throughout the spectrum. For free waves, energy dissipation lowers the propagation frequency resulting in a more compact band diagram. Free waves also experience a temporal decay in amplitude whose

normalized rate, the damping ratio, is expressed in its own diagram. Damped phononic structures will inhabit both impact and harmonic loading environments where the complete band diagram for free and prescribed waves, respectively, will provide insight into the structure's performance. The chapter also examines the correlation between the response of infinite periodic phononic materials and their finite counterpart.

Chapter 3 presents a parallel study on phononic material performance from the perspective of the effective properties that emerge dynamically from damped phononic materials due to the motion of the internal structure. Following a homogenization procedure, a dynamic effective density and modulus are determined, and, unique to the literature, in the case of damped phononic materials, a dynamic effective viscosity. The dynamic effective viscosity provides a means of quantifying damping in composite materials while taking into account inertia effects. The conventional viscoelastic correspondence principle does not account for inertia effects and, thus, is restricted to low frequencies. As suggested by the disparate band diagrams of free and frequency-prescribed waves presented in Ch. 2, these properties are sensitive to the type of wave propagation. For free waves, the dynamic effective properties remain positive and real-valued except for the frequency region of the band gap where propagation is forbidden. For frequency-prescribed waves, the effective properties, are complex at every frequency. These dynamic effective properties, especially the viscosity parameter, are of significance to advanced phononic applications such as acoustic superresolution imaging and acoustic cloaking whose performance depends on precise dynamic effective properties.

Focusing on free waves, the remaining chapters (Chs. 4, 5, and 6) consider discrete models (lumped or discretized continuum) and extend structural dynamics methods for vibration in generally damped structures to wave propagation in generally damped phononic materials. Chapter 4, using a state-space transformation, demonstrates the band diagram phenomena of branch-overtaking and branch cut-off unique to free waves. Using an extended state-space transformation, Ch. 6 continuously tunes the frequency band diagram from the undamped to the viscously damped regimes with an intervening viscoelastic domain. The two damping cases, the viscous and viscoelas-

tic regimes, respectively, reflect material damping mechanisms stemming from motion involving a fluid and relaxation processes in polymers/metals. Thus, phononic materials of a variety of compositions are represented.

As a dimensionless measure of the amplitude decay rate, the damping ratio diagram introduced in Ch. 2 may be used to compare the damping capacity of phononic materials with differing internal structure. Chapter 5 highlights the strategic design of phononic materials for engineering applications where high damping is desired without sacrificing load-bearing capacity as is common for conventional materials/composites. The damping capacity of two metamaterials, distinguished by monopolar and dipolar resonance, and a reference phononic crystal are compared. Taking advantage of the increased dissipation associated with resonance, the metamaterials show an enhanced damping capacity over the phononic crystal, a phenomenon referred to as "metadamping". Moreover, the uniform force distribution of the monopole resonance outperforms the directional force distribution of the dipole resonance. The metadamping effect addresses the long-standing challenge of realizing a material with simultaneously high stiffness and damping capacity. For an additive effect, metadamping may be integrated with other damping enhancement methods (e.g., material/mechanical instabilities, hierarchical internal structuring, etc.).

7.2 Future Research Directions

The studies conducted in this dissertation have shown the impact of energy dissipation on wave propagation in phononic materials which improves the prediction of their performance. The same qualitative behavior can be expected to appear in practice. Opportunities to design for extreme damping have also been highlighted. The following are potential avenues of research emerging from this dissertation.

- *Experimental Verification*: The models in this dissertation deliver qualitative results of dissipative wave propagation that, in a broad sense, are expected to arise in practical implementations. There is a need for experimental verification to further refine the models

and direct future theoretical investigations in synergistic manner.

- *Material/Geometric Nonlinearities*: Throughout the dissertation, the material models have been linear which facilitated the derivation of close-form solutions for the dispersion relations. However, certain materials, such as muscle tissue, demonstrate a nonlinear damping response. In general, nonlinear effects are triggered by large deformation [140]. Particular lattice constructions, may display a strong amplitude dependence [42]. Such systems present an opportunity to realized a wide, tunable range of effective properties. These to factors motivate the use of more complex damping models and extending the linear dynamic homogenization procedure to the nonlinear regime.

- *Harnessing Instabilities*: Fabricating shape memory alloy (SMA) nanolattices with combined elastic buckling and metadamping could lead to enhanced dissipation for sensitive microelectromechanical systems (MEMS). The austenite-martensite phase transition in SMAs represents a material instability marked by energy dissipation [112]. Moreover, a significant size effect has been reported whereby the nanoscale samples demonstrate an enhanced damping capacity compared to the bulk [141]. Meza *et al* [142] constructed recoverable ceramic nanolattices following a unit cell design methodology that exchanges brittle fracture for elastic shell buckling, a mechanical instability.

- *Minimizing Loss* Many proposed phononic material designs for constructing super-resolution imaging lenses involve a highly dissipative local resonance effect. Dissipation erodes the performance of the device. The resonance effect is insensitive to the lattice configuration of the resonating bodies, however, the overall dissipation may be affected. Considering prescribed waves, the homogenization procedure will elucidate the effect of resonator orientation on dissipation.

Bibliography

[1] Liang-fu Lou. Introduction to Phonons and Electrons. World Scientific Publishing Co., 2003.

[2] Gaston Floquet. Sur les équations différentielles linéaries à coefficients périodiques. Annales de lEcole Normale Supérieur, 12:47–88, 1883.

[3] Felix Bloch. Über die quantenmechanik der elektronen in kristallgittern. Zeitschrift für Physik, 52:555–600, August 1929.

[4] W. Kohn, J. A. Krumhansl, and Erastus H. Lee. Variational methods for dispersion relations and elastic properties of composite materials. Journal of Applied Mechanics, 39:327–336, June 1972.

[5] Léon Brillouin. Wave propagation in periodic structures : electric filters and crystal lattices. Dover Publications, New York, 2nd edition, 1953.

[6] G. Sen Gupta. Natural flexural waves and the normal modes of periodically-supported beams and plates. Journal of Sound and Vibration, 13:89–101, September 1970.

[7] Jakob Søndergaard Jensen. Phononic band gaps and vibrations in one- and two-dimensional massspring structures. Journal of Sound and Vibration, 266:1053–1078, October 2003.

[8] Zhengyou Liu, Xixiang Zhang, Yiwei Mao, Y. Y. Zhu, Zhiyu Yang, C. T. Chan, and Ping Sheng. Locally resonant sonic materials. Science, 289:1734–1736, September 2000.

[9] R. Sainidou, N. Stefanou, and A. Modinos. Formation of absolute frequency gaps in three-dimensional solid phononic crystals. Physical Review B, 66:212301, December 2002.

[10] Yong Xiao, Brian R. Mace, Jihong Wen, and Xisen Wen. Formation and coupling of band gaps in a locally resonant elastic system comprising a string with attached resonators. Physics Letters A, 375:1485–1491, March 2011.

[11] C. T. Sun, J. D. Achenbach, and G. Herrmann. Time-harmonic waves in a stratified medium propagating in the direction of the layering. Journal of Applied Mechanics, 35:408–411, June 1968.

[12] Erastus H. Lee and Wei H. Yang. On waves in composite materials with periodic structure. SIAM Journal on Applied Mathematics, 25:492–499, November 1973.

[13] D. J. Mead. Wave propagation in continuous periodic structres: research contributions from Southampton, 19641995. Journal of Sound and Vibration, 190:495–524, February 1996.

[14] Eric Tassilly. Propagation of bending waves in a periodic beam. International Journal of Engineering Science, 25:85–94, 1987.

[15] Yan Pennec, Bahram Djafari-Rouhani, J. O. Vasseur, A. Khelif, and Pierre A. Deymier. Tunable filtering and demultiplexing in phononic crystals with hollow cylinders. Physical Review E, 69:046608, April 2004.

[16] Roy H. Olsson, III, Simon X. Griego, Ihab El-Kady, Mehmet Su, Yasser Soliman, Drew Goettler, and Zayd Leseman. Ultra high frequency (UHF) phononic crystal devices operating in mobile communication bands. In Ultrasonics Symposium (IUS), 2009 IEEE International, pages 1150–1153, September 2009.

[17] Roy H. Olsson, III and I. El-Kady. Microfabricated phononic crystal devices and applications. Measurement Science & Technology, 20:012002, January 2009.

[18] B. Liang, X. S. Guo, J. Tu, D. Zhang, and J. C. Cheng. An acoustic rectifier. Nature Materials, 9:989–992, December 2010.

[19] Xue-Feng Li, Xu Ni, Liang Feng, Ming-Hui Lu, Cheng He, and Yan-Feng Chen. Tunable unidirectional sound propagation through a sonic-crystal-based acoustic diode. Physical Review Letters, 106:084301, February 2011.

[20] N. Boechler, G. Theocharis, and C. Daraio. Bifurcation-based acoustic switching and rectification. Nature Materials, 10:665–668, September 2011.

[21] Francisco Cervera, L. Sanchis, J. V. Sánchez-Pérez, R. Martínez-Sala, C. Rubio, F. Meseguer, C. López, D. Caballero, and José Sánchez-Dehesa. Refractive acoustic devices for airborne sound. Physical Review Letters, 88:023902, December 2001.

[22] Suxia Yang, John H. Page, Zhengyou Liu, M. L. Cowan, C. T. Chan, and Ping Sheng. Focusing of sound in a 3D phononic crystal. Physical Review Letters, 93:024301, July 2004.

[23] Alexey Sukhovich, Li Jing, and John H. Page. Negative refraction and focusing of ultrasound in two-dimensional phononic crystals. Physical Review B, 77:014301, January 2008.

[24] Nicholas X. Fang, Dongjuan Xi, Jianyi Xu, Muralidhar Ambati, Werayut Srituravanich, Cheng Sun, and Xiang Zhang. Ultrasonic metamaterials with negative modulus. Nature Materials, 5:452–456, June 2006.

[25] Shanshan Yao, Xiaoming Zhou, and Gengkai Hu. Experimental study on negative effective mass in a 1D mass-spring system. New Journal of Physics, 10:043020, April 2008.

[26] Z. Yang, Jun Mei, Min Yang, N. H. Chan, and Ping Sheng. Membrane-type acoustic metamaterial with negative dynamic mass. Physical Review Letters, 101:204301, November 2008.

[27] Yun Lai, Ying Wu, Ping Sheng, and Zhao-Qing Zhang. Hybrid elastic solids. Nature Materials, 10:620–624, June 2011.

[28] Jensen Li and C. T. Chan. Double-negative acoustic metamaterial. Physical Review E, 70:055602, November 2004.

[29] Yiqun Ding, Zhengyou Liu, Chunyin Qiu, and Jing Shi. Metamaterial with simultaneously negative bulk modulus and mass density. Physical Review Letters, 99:093904, August 2007.

[30] Xianyu Ao and C. T. Chan. Negative group velocity from resonances in two-dimensional phononic crystals. Waves in Random and Complex Media, 20:276–288, March 2010.

[31] X. N. Liu, G. K. Hu, G. L. Huang, and C. T. Sun. An elastic metamaterial with simultaneously negative mass density and bulk modulus. Applied Physics Letters, 98:251907, June 2011.

[32] Vladimir Fokin, Muralidhar Ambati, Cheng Sun, and Xiang Zhang. Method for retrieving effective properties of locally resonant acoustic metamaterials. Physical Review B, 76:144302, October 2007.

[33] Muralidhar Ambati, Nicholas Fang, Cheng Sun, and Xiang Zhang. Surface resonant states and superlensing in acoustic metamaterials. Physical Review B, 75:195447, May 2007.

[34] Xianyu Ao and C. T. Chan. Far-field image magnification for acoustic waves using anisotropic acoustic metamaterials. Physical Review E, 77:025601, February 2008.

[35] Steven A. Cummer and David Schurig. One path to acoustic cloaking. New Journal of Physics, 9:45, March 2007.

[36] Shu Zhang, Chunguang Xia, and Nicholas X. Fang. Broadband acoustic cloak for ultrasound waves. Physical Review Letters, 106:024301, January 2011.

[37] Huanyang Chen and C. T. Chan. Acoustic cloaking in three dimensions using acoustic metamaterials. Applied Physics Letters, 91:183518, November 2007.

[38] M. Brun, S. Guenneau, and A. B. Movchan. Achieving control of in-plane elastic waves. Applied Physics Letters, 94:061903, February 2009.

[39] Mohamed Farhat, Sebastien Guenneau, and Stefan Enoch. Ultrabroadband elastic cloaking in thin plates. Physical Review Letters, 103:024301, July 2009.

[40] Nicolas Stenger, Manfred Wilhelm, and Martin Wegener. Experiments on elastic cloaking in thin plates. Physical Review Letters, 108:014301, January 2012.

[41] Pai Wang, Filippo Casadei, Sicong Shan, James C. Weaver, and Katia Bertoldi. Harnessing buckling to design tunable locally resonant acoustic metamaterials. Physical Review Letters, 113:014301, July 2014.

[42] Neel Nadkarni, Chiara Daraio, and Dennis M. Kochmann. Dynamics of periodic mechanical structures containing bistable elastic elements: From elastic to solitary wave propagation. Physical Review E, 90:023204, August 2014.

[43] Michael M. Sigalas and Eleftherios N. Economou. Elastic and acoustic wave band structure. Journal of Sound and Vibration, 158:377–382, October 1992.

[44] Michael M. Sigalas and Eleftherios N. Economou. Band structure of elastic waves in two dimensional systems. Solid State Communications, 86:141–143, February 1993.

[45] Manvir Singh Kushwaha, Peter Halevi, Leonard Dobrzynski, and Bahram Djafari-Rouhani. Acoustic band structure of periodic elastic composites. Physical Review Letters, 71:2022–2025, September 1993.

[46] Eli Yablonovitch. Inhibited spontaneous emission in solid-state physics and electronics. Physical Review Letters, 58:2059–2062, May 1987.

[47] Sajeev John. Strong localization of photons in certain disordered dielectric superlattices. Physical Review Letters, 58:2486–2489, June 1987.

[48] D. J. Mead. A general theory of harmonic wave propagation in linear periodic systems with multiple coupling. Journal of Sound and Vibration, 27:235–260, March 1973.

[49] M. P. Castanier and C. Pierre. Individual and interactive mechanisms for localization and dissipation in a mono-coupled nearly-periodic structure. Journal of Sound and Vibration, 168(3):479–505, December 1993.

[50] R. S. Langley. On the forced response of one-dimensional periodic structures: vibration localization by damping. Journal of Sound and Vibration, 178:411–428, December 1994.

[51] I. E. Psarobas. Viscoelastic response of sonic band-gap materials. Physical Review B, 64:012303, June 2001.

[52] Rayisa P. Moiseyenko and Vincent Laude. Material loss influence on the complex band structure and group velocity in phononic crystals. Physical Review B, 83:064301, February 2011.

[53] D. J. Thompson. A continuous damped vibration absorber to reduce broad-band wave propagation in beams. Journal of Sound and Vibration, 311:824–842, April 2008.

[54] B. Merheb, Pierre A. Deymier, M. Jain, M. Aloshyna-Lesuffleur, S. Mohanty, A. Berker, and R. W. Greger. Elastic and viscoelastic effects in rubber/air acoustic band gap structures: A theoretical and experimental study. Journal of Applied Physics, 104:064913, September 2008.

[55] Joo Hwan Oh, Yoon Jae Kim, and Yoon Young Kim. Wave attenuation and dissipation mechanisms in viscoelastic phononic crystals. Journal of Applied Physics, 113:106101, March 2013.

[56] James M. Manimala and C. T. Sun. Microstructural design studies for locally dissipative acoustic metamaterials. Journal of Applied Physics, 115:023518, January 2014.

[57] Farhad Farzbod and Michael J. Leamy. Analysis of Bloch's method in structures with energy dissipation. Journal of Vibration and Acoustics, 133:051010, September 2011.

[58] M. Collet, M. Ouisse, Massimo Ruzzene, and M. N. Ichchou. Floquet-Bloch decomposition for the computation of dispersion of two-dimensional periodic, damped mechanical systems. International Journal of Solids and Structures, 48:2837–2848, October 2011.

[59] W. G. Cady. Theory of longitudinal vibrations of viscous rods. Physical Review, 19:1–6, January 1922.

[60] Subrata Mukherjee and E. H. Lee. Dispersion relations and mode shapes for waves in laminated viscoelastic composites by finite difference methods. Computers & Structures, 5:279–285, December 1975.

[61] Rudolf Sprik and Gerard H. Wegdam. Acoustic band gaps in composites of solids and viscous liquids. Solid State Communications, 106:77–81, April 1998.

[62] Xin Zhang, Zhengyou Liu, Jun Mei, and Youyan Liu. Acoustic band gaps for a two-dimensional periodic array of solid cylinders in viscous liquid. Journal of Physics: Condensed Matter, 15:8207–8212, November 2003.

[63] Mahmoud I. Hussein. Theory of damped Bloch waves in elastic media. Physical Review B, 80:212301, December 2009.

[64] W. Voigt. Ueber die Beziehung zwischen den beiden Elasticitätsconstanten isotroper Körper. Annalen der Physik, 274:573–587, September 1889.

[65] A. Reuss. Berechnung der Fließgrenze von Mischkristallen auf Grund der Plastizitätsbedingung für Einkristalle. Zeitschrift für Angewandte Mathematik und Mechanik, 9:49–58, February 1929.

[66] Z. Hashin and S. Shtrikman. A variational approach to the theory of the elastic behaviour of multiphase materials. Journal of the Mechanics and Physics of Solids, 11:127–140, March 1963.

[67] James G. Berryman. Long-wavelength propagation in composite elastic media I. Spherical inclusions. The Journal of the Acoustical Society of America, 68:1809–1819, December 1980.

[68] Jun Mei, Zhengyou Liu, Weijia Wen, and Ping Sheng. Effective mass density of fluid-solid composites. Physical Review Letters, 96:024301, January 2006.

[69] Sia Nemat-Nasser and Ankit Srivastava. Negative effective dynamic mass-density and stiffness: micro-architecture and phononic transport in periodic composites. AIP Advances, 1:041502, December 2011.

[70] Massimo Ruzzene, Fabrizio Scarpa, and Francesco Soranna. Wave beaming effects in two-dimensional cellular structures. Smart Materials and Structures, 12:363–372, April 2003.

[71] Mahmoud I. Hussein, Gregory M. Hulbert, and Richard A. Scott. Dispersive elastodynamics of 1D banded materials and structures: design. Journal of Sound and Vibration, 307:865–893, November 2007.

[72] J. Zhu, J. Christensen, J. Jung, L. Martin-Moreno, X. Yin, L. Fok, X. Zhang, and F. J. Garcia-Vidal. A holey-structured metamaterial for acoustic deep-subwavelength imaging. Nature Physics, 7:52–55, November 2010.

[73] Daniel Torrent and José Sánchez-Dehesa. Acoustic metamaterials for new two-dimensional sonic devices. New Journal of Physics, 9, September 2007.

[74] Y. P. Zhao and P. J. Wei. The band gap of 1D viscoelastic phononic crystal. Computational Materials Science, 46:603–606, September 2009.

[75] Yaozong Liu, Dianlong Yu, Honggang Zhao, Jihong Wen, and Xisen Wen. Theoretical study of two-dimensional phononic crystals with viscoelasticity based on fractional derivative models. Journal of Physics D: Applied Physics, 41:065503, February 2008.

[76] Wenqiang Wang, Jidong Yu, and Zhiping Tang. General dispersion and dissipation relations in a one-dimensional viscoelastic lattice. Physics Letters A, 373:5–8, December 2008.

[77] Mahmoud I. Hussein and Michael J. Frazier. Band structure of phononic crystals with general damping. Journal of Applied Physics, 108:093506, November 2010.

[78] Mahmoud I. Hussein and Michael J. Frazier. Damped Phononic Crystals and Acoustic Metamaterials. In Pierre A. Deymier, editor, Acoustic Metamaterials and Phononic Crystals, chapter 6. Springer, January 2013.

[79] Mahmoud I. Hussein, Gregory M. Hulbert, and Richard A. Scott. Dispersive elastodynamics of 1D banded materials and structures: analysis. Journal of Sound and Vibration, 289:779–806, February 2006.

[80] Mahmoud I. Hussein, Michael J. Frazier, and Mohammad H. Abedinnasab. Microdynamics of Phononic Materials. In Shaofan Li and Xin-Lin Gao, editors, Handbook of Micromechanics and Nanomechanics, chapter 1. Pan Stanford Publishing, May 2013.

[81] John William Strutt Rayleigh. The Theory of Sound, volume 1. London: Macmillan and Co., 1877.

[82] Suxia Yang, John H. Page, Zhengyou Liu, M. L. Cowan, C. T. Chan, and Ping Sheng. Ultrasound Tunneling through 3D Phononic Crystals. Physical Review Letters, 88:104301, February 2002.

[83] M. J. Beran and J. J. McCoy. Mean field variation in random media. Quarterly of Applied Mathematics, 28:245–258, July 1970.

[84] John R. Willis. The overall elastic response of composite materials. Journal of Applied Mechanics, 50:1202–1209, December 1983.

[85] Diener, G. and Hürrich, A. and Weissbarth, J. Bounds on the non-local effective elastic properties of composites. Journal of the Mechanics and Physics of Solids, 32:21–39, 1984.

[86] John R. Willis. Dynamics of Composites. In P. Suquet, editor, Continuum Micromechanics, chapter 5, pages 265–290. Springer Vienna, 1997.

[87] A. L. Shuvalov, A. A. Kutsenko, A. N. Norris, and O. Poncelet. Effective Willis constitutive equations for periodically stratified anisotropic elastic media. Proceedings of the Royal Society of London A: Mathematical, Physical and Engineering Sciences, 467:1749–1769, January 2011.

[88] A. N. Norris, A. L. Shuvalov, and A. A. Kutsenko. Analytical formulation of three-dimensional dynamic homogenization for periodic elastic systems. Proceedings of the Royal Society of London A: Mathematical, Physical and Engineering Sciences, 468:1629–1651, February 2012.

[89] Sia Nemat-Nasser, John R. Willis, Ankit Srivastava, and Alireza V. Amirkhizi. Homogenization of periodic elastic composites and locally resonant sonic materials. Physical Review B, 83:104103, March 2011.

[90] Sia Nemat-Nasser and Ankit Srivastava. Overall dynamic constitutive relations of layered elastic composites. Journal of the Mechanics and Physics of Solids, 59:1953–1965, July 2011.

[91] Ankit Srivastava and Sia Nemat-Nasser. Overall dynamic properties of three-dimensional periodic elastic composites. Proceedings of the Royal Society of London A: Mathematical, Physical and Engineering Sciences, 468:269–287, September 2011.

[92] G. Nagai, J. Fish, and K. Watanabe. Stabilized nonlocal model for dispersive wave propagation in heterogeneous media. Computational Mechanics, 33:144–153, January 2004.

[93] Mahmoud I. Hussein and Gregory M. Hulbert. Mode-enriched dispersion models of periodic materials within a multiscale mixed finite element framework. Finite Elements in Analysis and Design, 42:602–612, January 2006.

[94] Steven A. Cummer, Bogdan-Ioan Popa, David Schurig, David R. Smith, John Pendry, Marco Rahm, and Anthony Starr. Scattering theory derivation of a 3D acoustic cloaking shell. Physical Review Letters, 100:024301, January 2008.

[95] Mahmoud I. Hussein, Sedat Biringen, Osama R. Bilal, and Alec Kucala. Flow stabilization by subsurface phonons. Proceedings of the Royal Society of London A: Mathematical, Physical and Engineering Sciences, 471, April 2015.

[96] Zhengyou Liu, C. T. Chan, and Ping Sheng. Analytic model of phononic crystals with local resonances. Physical Review B, 71:014103, January 2004.

[97] Graeme W. Milton and John R. Willis. On modifications of Newton's second law and linear continuum elastodynamics. Proceedings of the Royal Society of London A: Mathematical, Physical and Engineering Sciences, 463:855–880, January 2007.

[98] Michael M. Sigalas, Manvir Singh Kushwaha, Eleftherios N. Economou, Maria Kafesaki, Ioannis E. Psarobas, and Walter Steurer. Classical vibration modes in phononic lattices: theory and experiment. Zeitschrift für Kristallographie, 220:765–809, September 2005.

[99] Y. Yong and Y. K. Lin. Propagation of decaying waves in periodic and piecewise periodic structures of finite length. Journal of Sound and Vibration, 129:99–118, February 1989.

[100] P. W. Mauriz, M. S. Vasconcelos, and E. L. Albuquerque. Acoustic phonon power spectra in a periodic superlattice. Physica Status Solidi B, 243:1205–1211, March 2006.

[101] Chang-Yong Lee, Michael J. Leamy, and Jason H. Nadler. Frequency band structure and absorption predictions for multi-periodic acoustic composites. Journal of Sound and Vibration, 329:1809–1822, May 2010.

[102] Mahmoud I. Hussein. Reduced Bloch mode expansion for periodic media band structure calculations. Proceedings of the Royal Society of London A: Mathematical, Physical and Engineering Sciences, 465:2825–2848, September 2009.

[103] Leonard Meirovitch. Principles and Techniques of Vibrations. Prentice Hall, 1997.

[104] Jr. Craig, Roy R. and Andrew J. Kurdila. Fundamentals of Structural Dynamics. John Wiley, 2nd edition, 2006.

[105] T. K. Caughey and M. E. J. O'Kelly. Classical normal modes in damped linear dynamic systems. Journal of Applied Mechanics, 32:583–588, September 1965.

[106] Mahmoud I. Hussein, Karim Hamza, Gregory M. Hulbert, Richard A. Scott, and Kazuhiro Saitou. Multiobjective evolutionary optimization of periodic layered materials for desired wave dispersion characteristics. Structural and Multidisciplinary Optimization, 31:60–75, January 2006.

[107] Mahmoud I. Hussein, Karim Hamza, Gregory M. Hulbert, and Kazuhiro Saitou. Optimal synthesis of 2D phononic crystals for broadband frequency isolation. Waves in Random and Complex Media, 17:491–510, October 2007.

[108] V. Kuzmiak and A. A. Maradudin. Distribution of electromagnetic field and group velocities in two-dimensional periodic systems with dissipative metallic components. Physical Review B, 58:7230–7251, September 1998.

[109] Christian Engström and Markus Richter. On the Spectrum of an Operator Pencil with Applications to Wave Propagation in Periodic and Frequency Dependent Materials. SIAM Journal on Applied Mathematics, 70:231–247, May 2009.

[110] Aaswath Raman and Shanhui Fan. Photonic band structure of dispersive metamaterials formulated as a Hermitian eigenvalue problem. Physical Review Letters, 104:087401, February 2010.

[111] Roderic S. Lakes, T. Lee, A. Bersie, and Y. C. Wang. Extreme damping in composite materials with negative-stiffness inclusions. Nature, 410:565–567, March 2001.

[112] Jan Van Humbeeck. Damping capacity of thermoelastic martensite in shape memory alloys. Journal of Alloys and Compounds, 355:58–64, June 2003.

[113] D. D. L. Chung. Structural composite materials tailored for damping. Journal of Alloys and Compounds, 355:216–223, June 2003.

[114] Jeffrey Goldstein. Emergence as a Construct: history and issues. Emergence, 1:49–72, March 1999.

[115] Pier Luigi Luisi. Emergence in chemistry: chemistry as the embodiment of emergence. Foundations of Chemistry, 4:183–200, October 2002.

[116] H. H. Huang, C. T. Sun, and G. L. Huang. On the negative effective mass density in acoustic metamaterials. International Journal of Engineering Science, 47:610–617, April 2009.

[117] Michele Zilletti, Stephen J. Elliott, and Emiliano Rustighi. Optimisation of dynamic vibration absorbers to minimise kinetic energy and maximise internal power dissipation. Journal of Sound and Vibration, 331:4093–4100, May 2012.

[118] Gang Wang, Xisen S. Wen, Jihong-H. Wen, Lihui-H. Shao, and Yaozong-Z. Liu. Two-dimensional locally resonant phononic crystals with binary structures. Physical Review Letters, 93:154302, October 2004.

[119] A. B. Movchan and S. Guenneau. Split-ring resonators and localized modes. Physical Review B, 70:125116, September 2004.

[120] Cetin Yilmaz, Gregory M. Hulbert, and Noboru Kikuchi. Phononic band gaps induced by inertial amplification in periodic media. Physical Review B, 76:054309, August 2007.

[121] Yan Pennec, Bahram Djafari-Rouhani, H. Larabi, J. O. Vasseur, and A. C. Hladky-Hennion. Low-frequency gaps in a phononic crystal constituted of cylindrical dots deposited on a thin homogeneous plate. Physical Review B, 78:104105, September 2008.

[122] Tsung-Tsong Wu, Zi-Gui Huang, Tzu-Chin Tsai, and Tzung-Chen Wu. Evidence of complete band gap and resonances in a plate with periodic stubbed surface. Applied Physics Letters, 93:111902, September 2008.

[123] Liao Liu and Mahmoud I. Hussein. Wave motion in periodic flexural beams and characterization of the transition between Bragg scattering and local resonance. Journal of Applied Mechanics, 79:011003, November 2011.

[124] Mahmoud I. Hussein, Michael J. Leamy, and Massimo Ruzzene. Dynamics of phononic materials and structures: historical origins, recent progress, and future outlook. Applied Mechanics Reviews, 66:040802, May 2014.

[125] Mahmoud I. Hussein and Michael J. Frazier. Metadamping: An emergent phenomenon in dissipative metamaterials. Journal of Sound and Vibration, 332:4767–4774, September 2013.

[126] Erik Andreassen and Jakob Søndergaard Jensen. Analysis of phononic bandgap structures with dissipation. Journal of Vibration and Acoustics, 135:041015, June 2013.

[127] A. Srikantha Phani and Jim Woodhouse. Viscous damping identification in linear vibration. Journal of Sound and Vibration, 303:475–500, June 2007.

[128] A. Srikantha Phani and Jim Woodhouse. Experimental identification of viscous damping in linear vibration. Journal of Sound and Vibration, 319:832–849, August 2008.

[129] Sondipon Adhikari and A. Srikantha Phani. Experimental identication of generalized proportional viscous damping matrix. Journal of Vibration and Acoustics, 131:011008, January 2009.

[130] Sondipon Adhikari and Jim Woodhouse. Identification of Damping: Part 1, Viscous Damping. Journal of Sound and Vibration, 243:43–61, May 2001.

[131] Sondipon Adhikari and Jim Woodhouse. Identification of Damping: Part 2, Non-viscous Damping. Journal of Sound and Vibration, 243:63–88, May 2001.

[132] N. Wagner and Sondipon Adhikari. Symmetric state-space method for a class of nonviscously damped systems. AIAA Journal, 41:951–956, May 2003.

[133] Jim Woodhouse. Linear damping models for structural vibration. Journal of Sound and Vibration, 215:547–569, August 1998.

[134] Julien Meaud, Trisha Sain, Bongjun Yeom, Sei Jin Park, Anna Brieland Shoultz, Gregory M. Hulbert, Zheng-Dong Ma, Nicholas A. Kotov, A. John Hart, Ellen M. Arruda, and Anthony M. Waas. Simultaneously high stiffness and damping in nanoengineered microtruss composites. ACS Nano, 8:3468–3475, March 2014.

[135] Farhad Farzbod and Michael J. Leamy. Analysis of Blochs method and the propagation technique in periodic structures. Journal of Vibration and Acoustics, 133:031010, March 2011.

[136] Mahmoud I. Hussein, Nagi Elabbasi, and Liao Liu. Finite element analysis of wave propagation in periodic Euler-Bernoulli beams, November 2009.

[137] C. W. Bert. Material damping: An introductory review of mathematic measures and experimental technique. Journal of Sound and Vibration, 29:129–153, July 1973.

[138] Yuan-Cheng Fung and Pin Tong. Classical and Computational Solid Mechanics. World Scientific Publishing Co., Singapore, 2001.

[139] H. H. Huang and C. T. Sun. Theoretical investigation of the behavior of an acoustic metamaterial with extreme Young's modulus. Journal of the Mechanics and Physics of Solids, 59:2070–2081, July 2011.

[140] Romik Khajehtourian and Mahmoud I. Hussein. Dispersion characteristics of a nonlinear elastic metamaterial. AIP Advances, 4:124308, December 2014.

[141] Jose San Juan, Maria L. Nó, and Christopher A. Schuh. Nanoscale shape-memory alloys for ultrahigh mechanical damping. Nature Nanotechnology, 4:415–419, June 2009.

[142] Lucas R. Meza, Satyajit Das, and Julia R. Greer. Strong, lightweight and recoverable three-dimensional ceramic nanolattices. Science, 345:1322–1326, September 2014.

Appendix A

Waves in Phononic Materials

A.1 Mode Shapes

In addition to the eigenvalue, γ, Eq. (2.17) yields the eigenvector (state vector), $\mathbf{y}(x_{\mathrm{L}}^1)$, containing the displacement and stress at the left boundary of the unit cell. With this result, we present the following procedure for calculating the displacement and stress mode shapes in a 1D phononic material.

To have a fixed frame of reference, we designate the position of the left boundary of the unit cell at $x = x_{\mathrm{L}}^1 = 0$. Given that $\mathbf{C}_j(0) = \mathbf{I}$, according to Eq. (2.11), the eigenvector computed from Eq. (2.17) can expressed as:

$$\mathbf{y}(x_{\mathrm{L}}^1) = \mathbf{B}_1\mathbf{a}_1. \tag{A.1}$$

Thus, the amplitude vector for the left end of the unit cell is easily determined:

$$\mathbf{a}_1 = \mathbf{B}_1^{-1}\mathbf{y}(x_{\mathrm{L}}^1). \tag{A.2}$$

Utilizing the transfer matrix, $\mathbf{T}_1$, we are able to relate $\mathbf{y}(x_{\mathrm{L}}^2)$ to $\mathbf{y}(x_{\mathrm{L}}^1)$ as

$$\mathbf{y}(x_{\mathrm{L}}^2) = \mathbf{T}_1\mathbf{y}(x_{\mathrm{L}}^1) = \mathbf{B}_2\mathbf{C}_2(x_{\mathrm{L}}^2)\mathbf{a}_2 \tag{A.3}$$

from which we obtain the amplitude vector for the left end of the second layer of a unit cell in terms of the computed eigenvector

$$\mathbf{a}_2 = [\mathbf{B}_2\mathbf{C}_2(x_{\mathrm{L}}^2)]^{-1}\mathbf{T}_1\mathbf{y}(x_{\mathrm{L}}^1). \tag{A.4}$$

With the aid of Eq. (2.15), this process may be extended to any layer j of a unit cell of n layers,

$$\mathbf{a}_j = [\mathbf{B}_j \mathbf{C}_j(x_{\mathrm{L}}^{(j)})]^{-1} \mathbf{T}_{j-1} \cdots \mathbf{T}_0 \mathbf{y}(x_{\mathrm{L}}^1) \tag{A.5}$$

where $\mathbf{T}_0 := \mathbf{I}$.

Once all $\mathbf{a}_j$ have been determined, the portion of the displacement and stress mode shapes within each layer in the first unit cell can be computed from Eq. (2.11). Furthermore, Bloch's theorem, as formulated in Eq. (2.16), may be used to compute the displacement and stress mode shapes over as many subsequent unit cells as desired. A full mode shape is realized when the displacement/stress profile spans a complete wavelength, $2\pi/\kappa_{\mathrm{R}}$, noting that the periodicity of the wave mode shape is related to the periodicity of the medium through the phase multiplier $\mathrm{e}^{\mathrm{i}\kappa a}$.

A.2 Damped Vibration in 1D Phononic Structures

In subsection 2.3.2, the transfer matrix method implements successive matrix operations $\mathbf{T}_j$ and enforces continuity conditions to relate the boundary states $u(x_{\mathrm{L}}^1)$ and $\sigma(x_{\mathrm{L}}^1)$ across each layer j of a phononic crystal unit cell. Bloch's theorem and the cumulative transfer matrix (the product of the successive matrix operations) $\mathbf{T}$, formulate an eigenvalue problem from which the eigenvalues establish the dispersion relations and the eigenvectors (the boundary states) may be used to develop mode shapes. For an infinite periodic material, such as a phononic crystal, Bloch's theorem imposes periodic boundary conditions. However, for a periodic structure of finite dimension, the boundary conditions are known *a priori*, allowing for the determination of structural dynamic characteristics using only the cumulative transfer matrix. Here, we formulate the equations for the natural frequencies and frequency response of a finite phononic structure.

A.2.1 Natural Frequencies

For each layer j of the unit cell, we solve Eq. (2.6) for the two $\kappa_s^{(j)}$ solutions

$$\kappa_s^{(j)} = \pm\lambda_s \sqrt{\frac{\rho^{(j)}}{E^{(j)} + \lambda_s \eta^{(j)}}}, \qquad s = 1, 2, \ldots, m \tag{A.6}$$

which we substitute into Eq. (2.14) and ultimately Eq. (2.15). Naturally, for a phononic structure composed of M unit cells of n layers, we have

$$\mathbf{y}(x_{\mathrm{R}}^{nM}) = \mathbf{V}\mathbf{y}(x_{\mathrm{L}}^{1}) \tag{A.7}$$

where $\mathbf{V}(\lambda_s) = \mathbf{T}^M$. For a free-free structure, $\sigma(x_{\mathrm{L}}^1) = \sigma(x_{\mathrm{R}}^{nM}) = 0$, and so $V_{21}(\lambda_s)u(x_{\mathrm{L}}^1) = 0$. However, since $u(x_{\mathrm{L}}^1) \neq 0$,

$$V_{21}(\lambda_s) = 0 \tag{A.8}$$

is the secular equation whose m solutions λ_s simultaneously deliver the damped natural frequencies $\omega_{\mathrm{d},s} = \mathrm{Im}[\lambda_s]$ and damping ratios $\xi_s = \mathrm{Re}[\lambda_s]/|\lambda_s|$. The associated discretized real-valued wavenumbers are

$$\kappa_s = \frac{s\pi}{Ma}. \tag{A.9}$$

A.2.2 Frequency Response and Attenuation

With the exception of the determination of $\kappa^{(j)}$ and the choice of boundary conditions, the development of the frequency response function mirrors that which formulated Eq. (A.8) in A.2.1. In the present case, $\kappa^{(j)}$ is determined by Eq. (2.5) and Eq. (A.7) is constructed with $\mathbf{V}(\omega)$. For a fixed-free structure with a harmonic excitation at the free end, one possible set of boundary conditions is $u(x_{\mathrm{L}}^1) = 0$, $\sigma(x_{\mathrm{L}}^1, t) = \Sigma_{\mathrm{L}}^1 \mathrm{e}^{\mathrm{i}\omega t}$ (steady-state response), and $\sigma(x_{\mathrm{R}}^{nM}, t) = \Sigma_{\mathrm{R}}^{nM}\mathrm{e}^{\mathrm{i}\omega t}$ (forcing). Consequently, $\Sigma_{\mathrm{R}}^{nM}\mathrm{e}^{\mathrm{i}\omega t} = V_{22}(\omega)\Sigma_{\mathrm{L}}^1\mathrm{e}^{\mathrm{i}\omega t}$, which we manipulate into the frequency response function

$$\left|\frac{\Sigma_{\mathrm{L}}^1}{\Sigma_{\mathrm{R}}^{nM}}\right| = |V_{22}(\omega)|^{-1}. \tag{A.10}$$

Using Eq. (A.10), we may also determine the attenuation that occurs over the span of the periodic structure. With Σ_{R}^{nM} as a reference, we write the stress amplitude at the fixed end in terms of that at the free end, $\Sigma_{\mathrm{L}}^1 = \Sigma_{\mathrm{R}}^{nM}\mathrm{e}^{\mathrm{i}\kappa Ma}$. However, recognizing that $\kappa = \kappa_{\mathrm{R}} + \mathrm{i}\kappa_{\mathrm{I}}$, this relation may be expressed as $\Sigma_{\mathrm{L}}^1 = \Sigma_{\mathrm{R}}^{nM}\mathrm{e}^{\mathrm{i}\kappa_{\mathrm{R}}Ma}\mathrm{e}^{-\kappa_{\mathrm{I}}Ma}$. By taking the absolute value of the ratio of stresses as in Eq. (A.10), we arrive at

$$\left|\frac{\Sigma_{\mathrm{L}}^1}{\Sigma_{\mathrm{R}}^{nM}}\right| = \mathrm{e}^{-\kappa_{\mathrm{I}}Ma}. \tag{A.11}$$

Finally, we divide the natural logarithm of Eq. (A.11) by the negative of the structure dimension $\ell = Ma$ to complete the derivation.

$$\kappa_{\mathrm{I}} = -\frac{1}{\ell}\ln\left|\frac{\Sigma_{\mathrm{L}}^{1}}{\Sigma_{\mathrm{R}}^{nM}}\right| \tag{A.12}$$